

# Laminar Flame Propagation in a Stratified Charge

by

Youngchul Ra

B. S., Mechanical Engineering  
Seoul National University, 1992

M. S., Mechanical Engineering  
Seoul National University, 1994

Submitted to the Department of Mechanical Engineering  
in Partial Fulfillment of the Requirements for the Degree of

Doctor of Philosophy

at the

MASSACHUSETTS INSTITUTE OF TECHNOLOGY


August 1999

[September 1999]

© Massachusetts Institute of Technology

All rights reserved

Signature of Author



Department of Mechanical Engineering  
August 23, 1999

Certified by

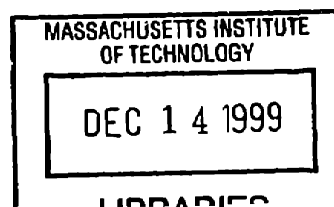


Wai K. Cheng  
Professor of Mechanical Engineering  
Thesis Supervisor

Accepted by



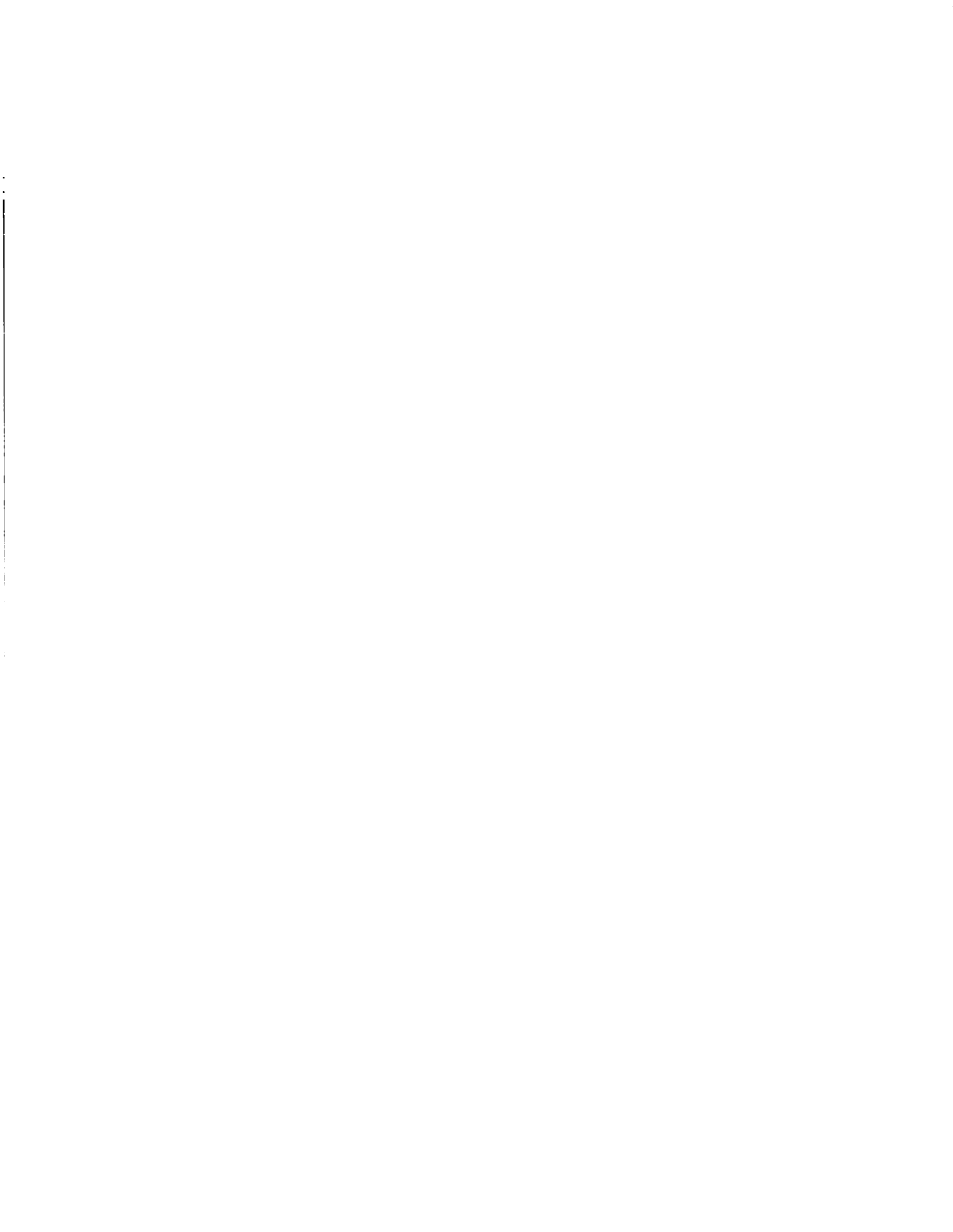
Ain A. Sonin  
Chairman, Department Committee on Graduate Students



ARCHIVES



**(This page was intentionally left blank)**



# **Laminar Flame Propagation in a Stratified Charge**

by

Youngchul Ra

Submitted to the Department of Mechanical Engineering  
on August 23, 1999 in Partial Fulfillment of the Requirements for  
the Degree of Doctor of Philosophy

## **Abstract**

The propagation of laminar flame from a rich or stoichiometric mixture to a lean mixture in a stratified methane-air charge was investigated experimentally and numerically. Emphasis was on the understanding of the flame behavior in the transition region; in particular, on the mechanism of burning velocity enhancement in this region.

In the experimental setup, mixtures of two different equivalence ratios were separated by a soap bubble in a spherical constant volume combustion vessel. The richer mixture inside the bubble was ignited by a focused laser beam. The flame development was observed by Schlieren technique and flame speeds were measured by heat release analysis of the pressure data. An one-dimensional, time-dependant numerical simulation of the flame propagation in a charge with step-stratification was used to interpret the experimental results.

Both the experimental and numerical studies showed that the instantaneous flame speed depended on the previous flame history. Thus a 'strong'(with mixture equivalence ratio close to stoichiometric) flame can sustain propagation into finite regions of substantially lean equivalence ratio. Both thermal and chemical effects were crucial for explaining the mechanism of the flame speed enhancement in the transition period.

Because of the presence of this 'back-support' effect, the usual concept of specifying the burning velocity as a function of the end gas state is inadequate for a stratified charge. A simple correlation for instantaneous flame velocity based on the local burned gas temperature is developed.

Thesis Supervisor: Wai K. Cheng

Title: Professor of Mechanical Engineering

## **Acknowledgment**

I give thanks to God for having allowed me a prestigious chance that I might not deserve, shown me a valuable life that I never have lived, keeping me on His way, and led me to be who I am now.

I am also indebted to many people for the help and encouragement that I have received since my arrival here. Special gratitude goes to my advisor, Prof. Wai K. Cheng for his thoughtful support and supervision in my study at MIT. Prof. A. F. Ghoniem, Prof. T. Q. Qiu, Dr. A. M. Dean, Prof. J. B. Heywood and other faculty members who gave me their precious advice and comments on my thesis can not be omitted from the list of names who deserve my great appreciation. I would like to thank all members of Sloan Automotive Lab and Korean friends and colleagues at MIT. Just their being my friends and colleagues was even so helpful for me to manage a successful life here.

I am more grateful to brothers and sisters of First Korean Church in Cambridge than anyone else for helping me build my faith and their willingness to give hands whenever I need them

It can not be too much to express my gratitude for the overflowing love and concern that my parents, sisters, bother-in-law and my wife Hee Sun have shown to me. Their presence gave me strength to get over all adversities that I confronted. I give great thanks to my family and want to say I love you all from the bottom of my heart. This thesis is to be dedicated to my family as a small fruit of my effort in final times of student.

## Table of Contents

	Page
Title Page.....	1
Abstract.....	3
Acknowledgement.....	4
Table of Contents.....	5
List of Tables.....	7
List of Figures.....	8
<b>CHAPTER I Introduction.....</b>	<b>12</b>
1 Background.....	12
2 Objective.....	16
<b>CHAPTER II Experimental Methodology.....</b>	<b>18</b>
1 Apparatus and procedure.....	18
1.1 Constant volume combustion chamber.....	18
1.2 Mixture preparation.....	18
1.3 Charge Stratification.....	19
1.4 Ignition.....	19
1.5 Pressure Measurement.....	20
1.6 Flame visualization.....	20
2 Data analysis.....	20
2.1 Thermodynamics of combustion.....	20
2.2 Laminar burning velocity.....	23
2.3 Boundary layer correction.....	23
2.4 Test conditions.....	24
<b>CHAPTER III Numerical simulation.....</b>	<b>25</b>
1 Governing equations.....	25
2 Transport coefficients.....	26
3 Chemical kinetics.....	27
4 Computation program.....	27
5 Calculational domain and input values.....	28

6	Charge stratification function.....	28
7	Cases of calculation.....	29
<b>CHAPTER IV Results and discussion.....</b>		<b>30</b>
1	Experimental results.....	30
1.1	Burning of homogeneous charge.....	30
1.2	Burning of stratified charge.....	30
1.2.1	Laminar flame speed behavior.....	31
1.2.2	Equivalence ratio difference effects.....	33
1.2.3	The extension of lean propagation limit.....	34
2	Numerical results and discussion.....	36
2.1	Homogeneous charge burning.....	36
2.2	Stratified charge burning.....	37
2.2.1	Comparisons of the dynamic profiles of the stratified charge burning and the homogeneous charge burning.....	37
2.2.2	Comparisons of burning velocity.....	39
2.2.3	Characteristics of the stratified charge burning.....	41
2.2.4	Equivalence ratio difference effects.....	43
2.2.5	Calculation of pocket burning.....	44
3	Correlation of the burning velocity of stratified charge.....	45
<b>CHAPTER V Summary and conclusions.....</b>		<b>46</b>
<b>Reference.....</b>		<b>48</b>



## List of Tables

		Page
Table 1	Kinetic scheme of methane-air reaction.....	51
Table 2	Correlation of burning velocity with burned gas temperature in stratified charge burning.....	54
Table 3	Coefficient equations for the generalized form of the correlation of the burning velocity and burned gas temperature in stratified charge burning.....	54

## List of Figures

	Page
Figure 2.1 Schematic diagram of the constant volume combustion vessel.....	55
Figure 2.2 Schematic diagram of the mixture preparation setup.....	56
Figure 2.3 Photo of a bubble at the center of the combustion vessel.....	57
Figure 2.4 Schematic diagram of the experimental setup.....	58
Figure 3.1 Domain of numerical calculation.....	59
Figure 4.1 Pressure trajectories of the burning of homogeneous charges (experiment).....	60
Figure 4.2 Burning velocity profiles of the homogeneous charges (experiment).....	60
Figure 4.3 Pressure trajectories of the burning of the mixture in bubble. Mixture : propane + air. Equivalence ratio: $\phi_1=1.0$ , $\phi_2=0$ (air only).....	61
Figure 4.4 Laminar flame behavior in stratified charge burning. Equivalence ratio: $\phi_1=1.0$ , $\phi_2=0.55$ . (a) velocity w.r.t. time, (b) velocity w.r.t. flame radius, (c) velocity w.r.t. unburned gas temperature.....	62
Figure 4.5 Laminar flame behavior in the stratified charge. Equivalence ratio $\phi_1=1.0$ , $\phi_2=0.52$ . (a) velocity w.r.t. time, (b) velocity w.r.t. flame radius, (c) velocity w.r.t. unburned gas.....	63
Figure 4.6 Time history of the stratified charge burning. Equivalence ratio: $\phi_1=1.0$ , $\phi_2=0.55$ . (a) Temperature profiles of the unburned and burned gas of the lean mixture and the burned gas of the rich mixture, (b) Profiles of pressure and flame radius, (c) Profiles of burned mass, burned mass fraction and boundary layer thickness.....	64
Figure 4.7 Pressure trajectories of the stratified charges with various rich mixtures (experiment). Equivalence ratio: $\phi_1=0.6 \sim 1.3$ , $\phi_2=0.55$ ; $\phi_{hg}=0.55$ .....	65
Figure 4.8 Burning velocity profiles of the stratified charge with various rich mixtures (experiment). Equivalence ratio: $\phi_1=0.6 \sim 1.3$ , $\phi_2=0.55$ ; $\phi_{hg}=0.55$ .....	65
Figure 4.9 Pressure trajectories of the stratified charge with various rich mixtures (experiment). Equivalence ratio: $\phi_1=0.6 \sim 1.3$ , $\phi_2=0.52$ .....	66
Figure 4.10 Burning velocity profiles of the stratified charge with various rich mixtures (experiment). Equivalence ratio: $\phi_1=0.6 \sim 1.3$ , $\phi_2=0.52$ .....	66

Figure 4.11	Pressure trajectories of the stratified charge with various rich mixtures (experiment). Equivalence ratio: $\phi_1=0.7 \sim 1.3$ , $\phi_2=0.6$ ; $\phi_{hg}=0.6$ .....	67
Figure 4.12	Burning velocities profiles of the stratified charge with various rich mixtures (experiment). Equivalence ratio: $\phi_1=0.7 \sim 1.3$ , $\phi_2=0.6$ ; $\phi_{hg}=0.6$ .....	67
Figure 4.13	The effect of equivalence ratio difference on the burning velocity enhancement. The second order curves are fitted to the experimental data.....	68
Figure 4.14	Pressure trajectories of the stratified charge with various lean mixtures. Equivalence ratio: $\phi_1=1.0$ , $\phi_2=0.5 \sim 0.7$ .....	69
Figure 4.15	Burning velocity profiles of the stratified charge with various lean mixtures. Equivalence ratio: $\phi_1=1.0$ , $\phi_2=0.5 \sim 0.7$ .....	69
Figure 4.16	Pressure trajectories of the stratified charge for various size of region 1.....	70
Figure 4.17	Pressure trajectories of homogeneous charge burning (numerical simulation).....	71
Figure 4.18	Burning velocity profile of homogeneous charge burning (numerical simulation)..	71
Figure 4.19	Comparison of calculated burning velocity with experimental result and literature data.....	72
Figure 4.20	Dynamic profiles of temperature in homogeneous charge burning. Equivalence ratio: $\phi_{hg}=0.3$ . At lapsed time (a) 0.3 ms, (b) 6.6 ms, (c) 45 ms, (d) 105 ms.....	73
Figure 4.21	Dynamic profiles of gas temperature in stratified charge burning. Equivalence ratio: $\phi_1=1.0$ , $\phi_2=0.5$ . At lapsed time (a) 5 ms, (b) 8 ms, (c) 10 ms, (d) 20 ms, (e) 100 ms.....	74
Figure 4.22	Dynamic profiles of gas temperature in homogeneous charge burning. Equivalence ratio: $\phi_{hg}=0.5$ . At lapsed time (a) 25 ms, (b) 50 ms, (c) 100ms.....	75
Figure 4.23	Dynamic profiles of the mole fraction of major species in stratified charge burning. Equivalence ratio: $\phi_1=1.0$ , $\phi_2=0.5$ At lapsed time (a) 0 ms, (b) 5 ms, (c) 8 ms, (d) 20 ms, (e) 100 ms.....	76
Figure 4.24	Dynamic profiles of the mole fraction of major species in homogeneous charge burning. Equivalence ratio: $\phi_{hg}=0.5$ . At lapsed time (a) 25 ms, (b) 50 ms, (c) 100 ms. .....	77
Figure 4.25	Dynamic profiles of radical mole fraction in stratified charge burning. Equivalence ratio: $\phi_1=1.0$ , $\phi_2=0.5$ At lapsed time (a) 5 ms, (b) 8 ms, (c) 10 ms, (d) 20 ms, (e) 100 ms.....	78

Figure 4.26	Dynamic profiles of radical mole fraction in homogeneous charge burning. Equivalence ratio: $\phi_{hg}=0.5$ . At lapsed time (a) 25 ms, (b) 50 ms, (c) 100 ms.....	79
Figure 4.27	Comparison of pressure profiles between stratified case and homogeneous case. Equivalence ratio: stratified charge: $\phi_1=1.0, \phi_2=0.5$ , homogeneous charge: $\phi_{hg}=0.5$ . (a) pressure w.r.t. time, (b) pressure w.r.t. unburned gas temperature.....	80
Figure 4.28	Comparison of burning velocity between stratified and homogeneous cases. Plot of evolution with respect to time. Equivalence ratio: stratified charge: $\phi_1=1.0, \phi_2=0.5$ , homogeneous charge: $\phi_{hg}=0.5$ .. .....	81
Figure 4.29	Comparison of burning velocity w.r.t. unburned gas temperature between stratified and homogeneous cases. Plot of evolution with respect to unburned gas temperature. Equivalence ratio: stratified charge: $\phi_1=1.0, \phi_2=0.5$ , homogeneous charge: $\phi_{hg}=0.5$ .. .....	82
Figure 4.30	Comparison of burned gas temperature between stratified and homogeneous cases. Plot of evolution with respect to unburned gas temperature. Equivalence ratio: stratified charge: $\phi_1=1.0, \phi_2=0.5$ , homogeneous charge: $\phi_{hg}=0.5$ .. .....	83
Figure 4.31	Profile of the rate of chemical energy production in stratified charge burning. (Gas temperature profile is included for comparison) Equivalence ratio: $\phi_1=1.0, \phi_2=0.5$ , at time 50 ms.....	84
Figure 4.32	Reaction characteristics of major species in stratified charge burning. At time=10 ms, unburned gas temperature = 387 K, equivalence ratio: $\phi_1=1.0, \phi_2=0.5$ . (a) distinction of flame zone, (b) concentration of species, (c) net rate of change, (d)rate of change by diffusion, (e) rate of change by chemical reaction, (f) rate of change by hydrodynamics.....	85
Figure 4.33	Reaction characteristics of radicals in stratified charge burning. At time10 ms, unburned gas temperature = 387 K, equivalence ratio: $\phi_1=1.0, \phi_2=0.5$ . (a) concentration of species, (b) net rate of change, (c) rate of change by diffusion, (d) rate of change by chemical reaction, (e) rate of change by hydrodynamics.....	88
Figure 4.34	Reaction characteristics of major species in homogeneous charge burning. At time=134 ms, unburned gas temperature = 387 K, equivalence ratio: $\phi=0.5$ . (a) distinction of flame zone, (b) concentration of species, (c) net rate of change, (d) rate of change by diffusion, (e) rate of change by chemical reaction, (f) rate of change by hydrodynamics.....	91
Figure 4.35	Reaction characteristics of radicals in homogeneous charge burning. At time=134 ms, unburned gas temperature = 387 K, equivalence ratio: $\phi=0.5$ . (a) concentration of species, (b) net rate of change, (c) rate of change by diffusion, (d) rate of change by chemical reaction, (e) rate of change by hydrodynamics.....	94

Figure 4.36	Comparison of peak radical mole fraction at flame zone w.r.t unburned gas temperature between stratified case and homogeneous case. Equivalence ratio: stratified charge: $\phi_1=1.0$ , $\phi_2=0.5$ , homogeneous charge: $\phi=0.5$ ...	97
Figure 4.37	Comparison of the evolution of peak mole fraction at flame zone between stratified case and homogeneous case. Equivalence ratio: stratified charge: $\phi_1=1.0$ , $\phi_2=0.5$ , homogeneous charge: $\phi=0.5$ ....	97
Figure 4.38	Pressure trajectories of the stratified charge with various rich mixtures (numerical simulation). Equivalence ratio: $\phi_1=0.5\sim 1.4$ , $\phi_2=0.4$ ; $\phi_{hg}=0.4$ .....	98
Figure 4.39	Burning velocity profiles of the stratified charge with various rich mixtures (numerical simulation). Equivalence ratio: $\phi_1=0.5\sim 1.4$ , $\phi_2=0.4$ ; $\phi_{hg}=0.4$ .....	98
Figure 4.40	Comparison of lapsed time of burning between stratified case and homogeneous case. Burned mass = 20 % of the initial mass of lean mixture. Equivalence ratio: stratified charge: $\phi_1=1.0$ , $\phi_2=0.35 \sim 0.8$ , homogeneous charge: $\phi=0.35 \sim 0.8$ .....	99
Figure 4.41	Burning of lean pocket in stoichiometric mixture. The pocket starts 0.4 cm away from the left wall. Equivalence ratio of lean mixture = 0.1, Pocket width=1.2 cm. (a) burning velocity vs. time (b) burning velocity vs. unburned gas temperature (c) pressure vs. time (d) pressure vs. unburned gas temperature (e) burned gas temperature vs. time (f) burned gas temperature vs. unburned gas temperature....	100
Figure 4.42	Correlation of burning velocity with burned gas temperature in stratified charge burning. Equivalence ratio : rich mixture : $\phi_1=1.0$ , lean mixture : $\phi_2=0.5$ . The homogeneous burning case of $\phi_h=0.5$ is included for comparison.....	101
Figure 4.43	Correlation of burning velocity with burned gas temperature in stratified charge burning. Equivalence ratio : rich mixture : $\phi_1=0.6 \sim 1.0$ , lean mixture : $\phi_2=0.4$ . The homogeneous burning case of $\phi_h=0.4$ is included for comparison.....	102

## CHAPTER I Introduction.

### 1 Background.

This thesis reports on the study of flame propagation in a combustible mixture with a non-uniform equivalence ratio distribution. The practical applications that motivates such a fundamental study is described in the following.

In the past few decades, combustion in lean mixtures has been an important topic in the field of internal combustion engines. Under lean operating conditions, there is substantial improvement of fuel economy through thermodynamic effects, and through the reduction of throttling loss, as well as improvement of thermal stress characteristics of the combustor hardware. The excess oxygen also reduces the hydrocarbons and carbon monoxide emissions. While there is  $\text{NO}_x$  reduction due to the lower combustion temperature [1-3], the three way catalyst for  $\text{NO}_x$  treatment does not work in the presence of excess oxygen because it requires strict fueling control in order to remain within the rather narrow fuel-air equivalence ratio operating range of the catalyst, which is near stoichiometry. However, together with substantial development in the lean  $\text{NO}_x$  catalyst technology, SI engine operating under lean condition is an attractive option [1].

Two different air-fuel mixture strategies have been developed for implementation of lean burn systems; homogeneous charge[4] and stratified charge. The charge stratification then can be classified into two concepts; charge stratification with one region of combustion chamber at a different equivalence ratio from the other region [5-7] and charge stratification with fuel-air mixture in one region and air only as a buffer in the other [8-11]. Generally in engine configurations, the former model includes stratification using prechamber method and axial or vertical stratification by swirling or tumble motion of mixture, while the latter includes stratification by direct injection of fuel into combustion chamber. It is notable that, in all configurations, though, non-uniformity in charge equivalence ratio will exist because of imperfect mixing in the homogeneous design and diffusion in the stratified designs.

With lean homogeneous charge engines, much effort has been applied to the ignition of excess air mixtures. As the mixture is leaned from stoichiometry, the minimum ignition energy required for combustion initiation increases, thus a specialized lean mixture ignition system may be required to achieve consistent initiation of the combustion reaction. For example, multiple ignition sources have been an effective tool in reducing the spark advance requirement and combustion duration, and in increasing the lean misfire limit of lean burn engines. Together with a number of compact geometry combustion chamber in order to reduce heat losses, high flow velocity and turbulence have been applied in order to improve the combustion rates in many homogeneous lean systems.

Since stratified charge engines can combine the best features of the spark ignition engines and the diesel; direct control of the ignition process and high compression ratio for efficiency and minimum pumping work, a number of researches have been done on charge stratification and the method of its realization in engines or laboratory combustion chambers.

Various prechamber approaches are examples of physical construction to achieve charge stratification. Goto et al.[12] designed an lean burn engine with pre-combustion chamber to accomplish lower  $\text{NO}_x$  and high efficiency. In their engine configuration, the high temperature, high pressure burnt gas of near stoichiometric mixture from the pre-combustion chamber serves as flame initiator for lean mixture in the main chamber, via supplying sufficient heat and radicals. They achieved improved combustion fluctuation, thus improved engine-speed fluctuation at an excess air ratio exceeding 2.0

Direct cylinder injection along with control of injection timing is another method of stratification. Fuel injection into prechambers, piston bowls, or directly into open chambers in combination with combustion chamber swirl has allowed direct injected stratified charge engines to operate at very lean air-fuel ratios. Injection parameters such as fuel penetration, droplet size, injection duration and spray angle have had a significant impact on mixture stratification and consequently an exhaust emission for these systems[10,11].

Axial stratification generated by swirling motion of mixtures through swirl control valve, and vertical stratification formed by the tumble motion of mixtures through one of

the intake ports of a dual valve engine, are also used for mixture preparation in the lean burn stratified charge engines [13,14].

Combustion quality is dependent on a number of parameters. Among them, laminar burning velocity is one of the key parameters to express the rate of laminar burning of premixtures. The importance of the laminar burning velocity, furthermore, can be extended into the regime of turbulent combustion, through the application of laminar flamelet concepts to turbulent burning velocities [2,15].

The theoretical definition of the laminar burning velocity is the velocity, relative to the unburned gas, with which a plane, one dimensional flame front travels along the normal to its surface. It is the eigenvalue of the one dimensional flame equation. Unfortunately, although its theoretical definition is simple, the same cannot be said of its practical measurement. There have been lots of methods of measurement suggested such as tube method, nozzle method, flat flame burner method, counter flow burner method, particle track method, soap bubble method, constant volume vessel method, etc[16-19]. Also, great efforts have been made to predict laminar burning velocity by numerical calculations based on chemical kinetic models, as the capability of computational tools improves[20-24].

A number of flame speed data by various techniques have been compared by Andrew et al. [25] in terms of the effect of method of measurement on the pressure and temperature dependence of burning velocity. Among them, constant volume combustion vessel has been regarded to give good possibility for the accurate measurement of flame speed in the range of high pressure and temperature [18,25,26], and thus has been used in many studies.

Due to the great effort made so far in order to obtain accurate data of burning velocities for various fuel-air mixtures, the behavior of laminar flame speed has been well established, and many successful analytic expressions to predict the burning velocities in lean hydrocarbon-air mixture at various pressures and temperatures, have been suggested, some of which were proposed by Muller et al.[22,23], Bradley et al.[27], and Metghalchi et al.[18,26] in terms of such parameters as inner layer temperature (where the slope of temperature profile is maximum), unburned and burnt gas temperature, mass fraction of fuel in unburned gas, volumetric heat release rate, etc.



Though the expressions are very convenient to use, they can be applied only to the burning of homogeneous mixtures because all the data were obtained at homogeneous conditions. For example, the burnt gas temperature in the expression of Muller et al. was determined as the adiabatic flame temperature of the homogeneous mixtures at chemical equilibrium. In engine combustion, the lean operation limit has also been determined based on the successful flame propagation in homogeneous mixtures ignited by a spark plug. However, when flame propagates from a rich mixture to a lean mixture, the flame behavior in the lean mixture is affected by the prior burning of the rich mixture. Therefore, the subsequent flame after the transition propagates at a different speed from that of a homogeneous mixtures at the same equivalence ratio. Since there exists non-uniformity in charge equivalence ratio because of imperfect mixing in the homogeneous design and diffusion in the stratified designs, this argument can be applied easily to the conditions encountered in practical combustion environment.

In order to idealize the problem, consider a case in which a flame is spark ignited in a stoichiometric charge. It then propagates and encounters a step change in equivalence ratio, which is lean. The flame propagation in the interfacial region and subsequent leaner region will be affected by the prior condition of the burned gas as well as by the condition of the end gas in terms of its composition and thermodynamic state.

The condition of the burned gas has two effects; there are thermal effects due to heat transfer to unburned gas, and the chemical effects due to the radical supply to the flame front. Since the burned gas temperature increases with the equivalence ratio changing from lean to stoichiometry, the burned gas of the rich mixture in a stratified charge can transfer more heat to the lean unburned gas than the burned gas of a lean homogeneous charge. Similar arguments can be applied to species diffusion in the stratified charge configuration. Especially, due to the importance of the [H] and [OH] radicals in the overall hydrocarbon-air reaction scheme, it is reasonable to expect that increase of supply of [H] and [OH] radicals to flame front by burnt gas of rich mixture should significantly increase the burning intensity. The importance of the [H] and [OH] radicals in the overall hydrocarbon-air

reaction was well observed in the studies on the effects of hydrogen addition on the burning of hydrocarbon-air mixtures by Yu et al. [28], Bell et al. [29], and Refael et al. [21].

The burned gas effects from the previous stoichiometry will last for a finite time which is called relaxation time here; then the flame loses the memory of its previous experience eventually as flame propagates further into leaner region. In a practical point of view, this relaxation time is very important. Consider an imperfectly mixed charge, the flame may burn through in the relaxation time an overly lean eddy that would otherwise burn partially and slowly, or not burn at all. Thus combustion robustness is improved and unburned hydrocarbons are reduced.

There have been some studies related to the flame propagation in stratified charges : Murase et al. [30] observed that the burned gas in pulsed combustion jet was effective for initiation of combustion in very lean mixtures. Kesler et al. [31] observed that dispersing combustion gases originated from the homogeneous charge flame kernel throughout whole combustion chamber by means of gas jet induced into a combustion chamber from outside, was an efficient way to simulate and control lean mixture burning in quiescent and turbulent environment, and to extend lean operating limit. Moriyoshi et al. [32] showed experimentally that combustion of very lean mixture in stratified charge condition with gradient in equivalence ratio can be enhanced through increased overall burning speed. Furuno et al. [33] have focused on the effect of rich mixture volume on combustion duration and  $\text{NO}_x$  emissions in the burning of locally stratified charge mixture under the same total equivalence ratio in a combustion vessel. They observed that the magnitude of the  $\text{NO}_x$  emissions does not increase as the rich mixture volume increase up to a critical volume but the combustion duration shortens remarkably.

However some of these studies were lack in experimental repeatability and there was no systematic analysis of the effect of charge stratification, with no other parameters involved, on the enhancement of flame propagation speed and the extension of lean operating limit.

## 2 Objective.

The present study focused on the flame propagation phenomena in stratified charges of different equivalence ratios in order to determine the mechanism of flame speed enhancement in the transition process. Both experimentation and calculations were carried out in order to understand the flame speed behavior in a step change in equivalence ratio. Experiments were conducted in a spherical constant volume combustion chamber and therefore give results that are valid over an elevated range of unburned gas temperature and pressures. Numerical calculation for one dimensional, unsteady phenomena with detailed chemical kinetics were done to be compared with and to help interpret experimental results.

In chapter II, the experimental methodology is briefly specified, which is followed by computational procedure in chapter III. The experimental and computational results will be shown and discussed in chapter IV, and finally this study will be summarized and concluded in chapter V.

## CHAPTER II Experimental methodology.

### 1. Apparatus and procedure.

#### 1.1 Constant volume combustion chamber.

Constant volume combustion chambers of various shape have been used for many flame speed studies [18, 26, 27]. Among them, a spherical vessel is geometrically simple, thus data are easily analyzed. A schematic diagram of the constant volume combustion chamber used for the present study is shown in Fig. 2.1. It has an inside diameter of 152.4 *mm* and was designed to withstand a pressure of up to 340 bar. There are three ports on the surface of the combustion vessel. Two ports are located on the top and the top-side of the vessel in order to be used as inlet and outlet of the fresh charges and burned gases. The other port is for a pressure transducer and located on the bottom-side of the vessel. A stainless steel tube of 3.175 *mm* in diameter is extended from the top inlet port to the center of the combustion vessel, through which a mixture is introduced into the vessel. The combustion vessel is optically accessible through quartz windows of 50.8 *mm* in diameter which are fit on opposite side of the combustion vessel. The flat windows protrude approximately 4 *mm* into the combustion chamber and would not substantially alter the spherical geometry of the vessel. A hole of 16 *mm* in diameter heading to the center of the combustion chamber is located on the side of the vessel, on the same horizontal plane as that of the flat windows. A lens set is installed in the hole through which laser beam passes.

#### 1.2 Mixture preparation.

Figure 2.2 shows the schematic diagram of the mixture preparation setup. The amount of the fuel and air needed to make a charge was checked by measuring the pressures inside the mixing chamber using the *MKS* vacuum gauge and the pressure gauge *PG3*. After the fuel and air were well mixed in the mixing chamber, the charge was moved to the chamber *Ch1* or chamber *Ch2*. The charge filling into the combustion vessel was controlled by two

precise control valves *CV1* and *CV2* while the pressure inside the combustion vessel was being monitored up to initial pressure of the experiment by pressure gauge *PG2*. The burnt gas in the combustion vessel and the residual gas in the manifold were evacuated by the vacuum pump. The ranges of the pressure gauge *MKS* and *PG1*(same as *PG2* and *PG3*) are 1000 torr and 10 bar in absolute pressure, respectively.

### 1.3 Charge stratification.

In order to realize the charge stratification with step change in equivalence ratio, a soap bubble was used to separate the charge of two different equivalence ratio within the vessel (Fig. 2.1). This method was developed by Toyota Motor Co. [34]. The combustion chamber was filled with the lean mixture  $M_2$  through the top-side port, and then the richer mixture  $M_1$  was introduced through the stainless tube connected to the top port in order to form a bubble of diameter  $D_b$  at the center of the combustion vessel. The bubble confined the richer region from an outer region of leaner charge. The volume ratio of mixture  $M_1$  to mixture  $M_2$  was about 0.1~0.2 % depending on the bubble size. The bubble material of about 4.5 mg was put on the tip of the tube before the introduction of the richer mixture  $M_1$  which blows the bubble. The mixture  $M_1$  in the richer region was at equivalence ratio  $\phi_1$ , while the mixture  $M_2$  in the leaner region was at  $\phi_2$ . Figure 2.3 shows the picture of the bubble formed at the center of the combustion chamber.

### 1.4 Ignition.

The charge  $M_1$  was ignited by a pulsed laser beam focused at the center of the bubble through the lens set on the side of the combustion vessel(Fig 2.1). The original laser beam from frequency-doubled DCR1 Nd-YAG laser of Quanta-Ray was selected by a dichroic mirror so that green beam of 532 nm in wave length could be used. The measured energy level of the laser beam before the focusing lens set was up to 300 mJ with a 7 ns pulse width which was sufficient to make a break-down in the air at the center of the combustion vessel when the vessel was filled with air only. The beam pulse was triggered to

synchronize with the pressure measurements. The ignition by laser can avoid the variation of spark energy and the quenching of flame kernel at early stage of the combustion of the mixture  $M_1$  by electrodes of the conventional capacitive discharge ignition system.

### 1.5 Pressure measurement.

Pressure was measured with a Kistler Model 6123 piezoelectric pressure transducer which was installed on the inner surface of the combustion vessel. The signal from the pressure transducer was transferred to a PC via a charge amplifier and data acquisition hardware. The acquisition frequency and the duration were 20 *kHz* and 2 seconds, respectively. The schematic diagram of the experimental setup is shown in Fig. 2.4.

### 1.6 Flame visualization

Schlieren technique was used to capture the flame propagation in the early stage of the combustion [35]. The setup for this experiment is shown in Fig. 2.4. It consists of one spherical mirror of 1500 *mm* focal length, one convex lens of 500 *mm* focal length, and 350 W mercury lamp as light source. The Schlieren picture of the flame propagation was monitored by a high speed CCD video camera which is capable of taking 3000 frames per second. A framing rate of 1000 or 2000 frames per second was used. The cross-section of the beam which passes the test section is a circle of 50.8 *mm* in diameter.

## 2 Data analysis

### 2.1 Thermodynamics of combustion

The thermodynamic model employed to analyze the combustion process in the combustion chamber is based on the following assumptions.

1. The unburned gas is initially at rest and has uniform temperature and composition.
2. The effect of the existence of the bubble is negligible.
3. The thickness of the reaction zone is negligible.
4. The burned gas of mixture  $M_1$  is uniform and stays at a chemically frozen state after the completion of burning of the mixture  $M_1$ , at which the composition is fixed and

is the same as the equilibrium composition at the completion of combustion of mixture  $M_1$ .

5. The burned gas of the mixture  $M_1$  is isolated, thus there is no heat transfer and species diffusion between the burned gas of the mixture  $M_1$  and the burned gas of the mixture  $M_2$ .
6. The gas within the combustion chamber consists of a burned gas of the mixture  $M_1$ , a burned fraction  $x$  of mixture  $M_2$  at local thermodynamic and chemical equilibrium and an unburned fraction  $1-x$  of mixture  $M_2$  at local thermodynamic equilibrium but with fixed chemical composition.
7. The pressure is independent of position and a function of time only.
8. The reaction front is smooth and spherical.
9. Buoyancy effect is negligible.
10. Charge stratification by gravity is negligible.
11. All species are treated as ideal gas.
12. Thermal radiation heat loss from the flame is neglected.

Since the calculation of burning velocity is performed for the pressure traces after the burning of the mixture  $M_1$  is completed, data analysis consists of two parts: part one is the calculation, when the combustion of mixture  $M_1$  is completed, of the final pressure to which the gases within the combustion chamber attains and the equilibrium composition of the burned gas of the mixture  $M_1$ . Part two is the analysis of the burning of the mixture  $M_2$ .

Under above assumption, the equations for conservation of mass, energy and volume are

mass conservation

$$M = m_1 + m_{2,u} + m_{2,b} = \frac{p}{R^o} \left( \frac{V_{1,b} W_{1,b}}{T_{1,b}} + \frac{V_{2,u} W_{2,u}}{T_{2,u}} + \frac{V_{2,b} W_{2,b}}{T_{2,b}} \right) \quad (2.1)$$

energy conservation

$$E = M e = m_1 e_{1,b}(T_{1,b}) + m_{2,u} e_{2,u}(T_{2,u}) + m_{2,b} e_{2,b}(T_{2,b}) \quad (2.2)$$

volume conservation

$$V_C = V_1 + V_2 = V_{1,b} + V_{2,u} + V_{2,b} \quad (2.3)$$

The equations for isentropic compression of the burned gas of the mixture  $M_1$  and the unburned gas of the mixture  $M_2$  are

$$\int_{T_o}^{T_{1,b,i}} \frac{C_{p1,b}}{T} dT - \int_{p_o}^{p_i} \frac{R^o}{pW_{1,b}} dp = \int_{T_o}^{T_{1,b}} \frac{C_{p1,b}}{T} dT - \int_{p_o}^p \frac{R^o}{pW_{1,b}} dp \quad (2.4)$$

and

$$\int_{T_o}^{T_{2,u,i}} \frac{C_{p2,u}}{T} dT - \int_{p_o}^{p_i} \frac{R^o}{pW_{2,u}} dp = \int_{T_o}^{T_{2,u}} \frac{C_{p2,u}}{T} dT - \int_{p_o}^p \frac{R^o}{pW_{2,u}} dp \quad (2.5)$$

and the equation of state for the burned gas of the mixture  $M_1$  is

$$pV_{1,b} = m_1 R^o T_{1,b} / W_{1,b} \quad (2.6)$$

,where

$M$  = total mass of gas in the combustion chamber

$E$  = energy of gas in the combustion chamber

$V_C$  = volume of the combustion chamber

$p$  = pressure

$V$  = volume of gas

$T$  = temperature

$m$  = mass of gas

$e$  = energy per unit mass

$W$  = molecular weight

$R^o$  = universal gas constant

$C_p$  = specific heat at constant pressure

and the subscripts denote

1 = mixture  $M_1$

2 = mixture  $M_2$

$u$  = unburned gas

$b$  = burned gas



- $o$  = reference value
- $s$  = at the beginning of burning of the mixture  $M_2$
- $i$  = initial value

## 2.2 Laminar burning velocity.

Using Eqs. (2.1)-(2.6) and the measured pressure data, laminar burning velocity can be calculated from the definition

$$S_u = \frac{m_2}{A_f \rho_{2,u}} \frac{dx}{dt} = \frac{1}{A_f \rho_{2,u}} \frac{d}{dt} \left( \frac{pV_{2,b}W_{2,b}}{R^o T_{2,b}} \right) \quad (2.7)$$

,where

$\rho_{2,u}$  = density of unburned gas of the mixture  $M_2$

$A_f = 4 \pi r_f^2$

$r_f = [3V_f/4\pi]^{1/3}$

$V_f = V_1 + V_{2,b} = V_C - V_{2,u}$

In the evaluation of Eq. (2.7), the burned gas properties are computed using an approximation to thermodynamic properties of various species from NASA program[1] and a program to calculate the equilibrium composition adopted from Ref. 36, and unburned gas properties are computed using thermodynamic data from JANAF table [40] for the individual species in the mixture. From the visualization results of the early stage of combustion, no significant buoyant rise or departure from the spherical symmetry was observed under the conditions studied except for the partial burning or unignited cases, even though some distortion was seen on the flame front when the flame propagated through the interface between the mixture  $M_1$  and the mixture  $M_2$ . Wrinkling of the flame front when the flame passes the interface formed by bubble was observed to vary run by run mostly due to the different amount of the bubble material, however it was stabilized after the flame entered the lean mixture  $M_2$ .

## 2.3 Boundary layer correction.

Boundary layer correction was done after the first calculation of adiabatic values of physical variables. Using the equations as followings for the displacement thickness of boundary layer of unburned gas [26], the variables were corrected, and then the calculation of the burning velocity was performed.

$$\delta_u \approx \left( \frac{4\alpha_i \tau_f}{\pi} \right)^{1/2} \left( \frac{p_i}{p} \left( 1 - \frac{p_i}{p} \right) \right)^{1/2} \left( \left( \frac{p}{p_i} \right)^{(\gamma_u - 1)/\gamma_u} - 1 \right) \quad (2.8)$$

,where  $\alpha_i = k/\rho c_p$  is thermal diffusivity at initial condition and  $\tau_f = p/(dp/dt)$  is the characteristic time for pressure increase. For the boundary layer thickness of the burned gas, simple boundary layer growth equation was used.

$$\delta_b = 3.64 \sqrt{\alpha_b t} \quad (2.9)$$

It was found for mixtures near stoichiometry that the thickness of boundary layer on the wall of unburned gas side was less than 1 mm and the heat transfer from the unburned gas to the wall due to the temperature gradient was very small compared to that due to the thermal radiation from the flame [41]. However, for lean mixtures near propagation limit, the boundary layer thickness grows sufficiently because of the low burning velocity, therefore, boundary layer correction becomes important.

#### 2.4 Test conditions.

Experiments were made with methane and air as fuel and oxidizer, respectively. The combination of equivalence ratio of mixture  $M_1$  and  $M_2$  covered the rich and lean limit of ignitability by spark, but the overall equivalence ratio of gas within the combustion vessel was very close to that of leaner mixture, because of the volume ratio between the mixture  $M_1$  and the mixture  $M_2$ . The equivalence ratio of the rich mixture and the lean mixture ranged  $\phi_1 = 0.6 \sim 1.4$  and  $\phi_2 = 0.5 \sim 0.7$ , respectively. The initial temperature and pressure were set at 295 K and 1 atm.

## CHAPTER III Numerical simulation.

One dimensional flame propagation in an enclosure was solved numerically in Cartesian coordinates instead of spherical coordinates using a computer program with hydrodynamics, transport and detailed chemical kinetics. Though the spherical coordinates were best fit to the geometry of the experimental setup, a simplification was made to the problem mainly due to calculational easiness and availability of the computer program. However, when the flame thickness is small compared to the radius of the curvature of the flame front, the calculational results still could be validated to help interpret the experimental results, which is to be dealt with in next chapters.

### 1 Governing Equations.

The governing equations for time dependent profiles of the temperature, velocity, and species concentrations were calculated by solving numerically the general one-dimensional conservation equation in the cartesian coordinates, as follows:

#### A. continuity

$$\frac{D\rho}{Dt} = -\rho \frac{\partial v}{\partial x} \quad (3.1)$$

,where

$$\frac{D}{Dt} = \frac{\partial}{\partial t} + v \frac{\partial}{\partial x} \quad (3.2)$$

#### B. conservation of species concentration

$$\frac{Dc_i}{Dt} = -c_i \frac{\partial v}{\partial x} + \sum_k R_{i,k} - \frac{\partial F_i^c}{\partial x} \quad (3.3)$$

,where

$$F_i^c = -\rho D_i \frac{\partial c_i}{\partial x} \quad (3.4)$$

#### C. conservation of momentum

$$\frac{Dv}{Dt} = -\frac{1}{\rho} \frac{\partial(P+Q)}{\partial x} \quad (3.5)$$

,where

$$Q = -\lambda \frac{\partial v}{\partial x} \quad (3.6)$$

D. conservation of energy

$$\frac{DT}{Dt} = \frac{1}{C_v} \left\{ -\sum_i \sum_k \varepsilon_i R_{i,k} - (P+Q) \frac{\partial v}{\partial x} - \frac{\partial F^\varepsilon}{\partial x} + \sum_i \varepsilon_i \frac{\partial F_i^c}{\partial x} \right\} \quad (3.7)$$

,where

$$F^\varepsilon = \sum_i h_i F_i^c - \alpha^T C_p \frac{\partial T}{\partial x} \quad (3.8)$$

$$C_v = \sum_i c_i \frac{\partial \varepsilon_i}{\partial T} \quad (3.9)$$

In the Eqs. (3.1)~(3.9),  $\rho$  is the mass density,  $c_i$  is the concentration of species  $i$ ,  $v$  is flow velocity,  $R_{i,k}$  is the rate of change of species  $i$  by reaction  $k$ ,  $F_i^c$  is the flux of species  $i$  by diffusion,  $P$  and  $Q$  are the hydrostatic pressure and the viscous force,  $T$  is the temperature in the zone,  $C_v$  is the average specific heat at constant volume process in the zone,  $\varepsilon_i$  is the internal energy density of species  $i$  in the zone,  $F^\varepsilon$  is the flux of energy by conduction and species diffusion.

## 2 Transport Coefficients.

A rigorous method for estimation of the transport coefficient has been adopted. The binary diffusion coefficient was calculated from correction factors based on Chapman-Enskog theory using Lennard-Jones potential [36], namely,

$$D_{ij} = 5.9543 \times 10^{-6} \frac{\sqrt{T^3 (1/M_i + 1/M_j)}}{P \sigma_{ij}^2 \Omega_{D_{ij}}} \quad (3.10)$$

$$\sigma_{ij} = \frac{1}{2} (\sigma_i + \sigma_j) \quad (3.11)$$

, where  $T$  is in Kelvin,  $P$  is in pascals  $\sigma$  is collision diameter and  $\Omega$  is a dimensionless

correction factor (collision integral). The numerical values for  $\sigma$  and  $\Omega$  were taken from Ref. 35 for the initial temperature of the calculation and were assumed to be constant for the entire calculation of the flame propagation of the mixture. The effective diffusion coefficient for each species in the mixture was calculated from a formula as follows [2]:

$$D_i = \frac{1 - X_i}{\sum_{j \neq i} \frac{X_j}{D_{ij}}}, \quad i = 1, \dots, N - 1 \quad (3.12)$$

, where  $X_i$  is mole fraction of species  $i$ .

Since Eq. (3.12) can be used properly at best for  $N-1$  species, the binary diffusion coefficient  $D_{NN}$  was used for  $N^{\text{th}}$  species which was present in excess. The thermal diffusivity of the mixture was calculated from the mass diffusivity by assuming that the Lewis number of the mixture is equal to 1.1. The Fifth-order polynomial fits in  $T$  to the JANAF data was used for the specific heat at constant pressure [36].

### 3 Chemical kinetics.

A reduced kinetic scheme with 24 species and 57 reactions for methane-air combustion, as listed in Table 1, was employed in the calculation. The scheme which is based on the  $C_2$  scheme of Egolfopoulos et al. [19] with 22 species and 40 reactions, consists of formation and consumption reactions of  $CH_4$ ,  $CH_3$ ,  $CH_2$ ,  $HC$ ,  $CO$ ,  $HCO$ ,  $HCCO$ ,  $C_2H_2$ ,  $C_2H_3$ ,  $C_2H_4$ ,  $C_2H_5$ ,  $C_2H_6$ ,  $CH_2O$ ,  $CH_3O$ ,  $CH_2CO$ ,  $HO_2$ , chain propagation and branching reactions, and recombination and dissociation reactions.

### 4 Computation program.

The computer code HCT was used to simulate the flame propagation in a one dimensional constant volume chamber. The code was developed by the Livermore National Laboratory for one-dimensional, time dependent calculations with hydrodynamics, transport and detailed chemical kinetics. It employs Lagrange and Eulerian calculations, and dynamic rezoning to concentrate in area of high temperature gradients. The original code was modified to enhance the calculational stability and to calculate necessary output data for

post-processing.

## 5 Computational domain and input values

The calculational domain is shown in Fig. 3.1. The total dimension of calculation was 3 *cm*, which was divided into a rich region of 0.4 *cm* and a lean region of 2.6 *cm*. Ignition was initiated by a heated region of thickness 0.012 *cm* located at the wall of the rich mixture side in the domain. Into this region energy was deposited for  $t_{ig} = 63 \mu s$ , using a function, as following,

$$S(x) = S_o \frac{1}{1 + \exp\left(\frac{x}{x_o}\right)} \quad (3.13)$$

,where  $S_o = 11700 \text{ callcm}^3 s$  and  $x_o = 0.012 \text{ cm}$ .

The total energy deposition to the gases in the domain was 26 *mJ* and the maximum value of source energy was  $5850 \text{ callcm}^3\text{-s}$ . The ratio of the deposited energy to the heating value of stoichiometric methane-air mixture in this region was 0.513.

Boundary conditions for the calculation are no heat conduction and species diffusion at boundaries, so the gradients of temperature and species mole fraction are set to zero at boundaries.

## 6 Charge stratification function.

Besides the initial temperature and pressure, the initial spatial distribution of the mixture equivalence ratio can be varied. For example, step function for ideal step change in equivalence ratio, ramp function for gradient in fuel concentration, sinusoidal function for periodic change in equivalence ratio, single rectangular wave or gaussian function for pocket distribution of equivalence ratio, and so forth. In this study, the step change in equivalence ratio, especially from the rich region to the lean region, was employed in order to simplify the problems so that the effect of stratification can be figured out as clearly as possible. The forms of the function to represent the step change in the HCT program was chosen as follows by considering the easiness in its implementation as well as the physical

validity [36]. For the step change of concentration from  $C_1$  to  $C_2$ , the following representation was used.

$$C(x) = C_1 f(x) + C_2 [1 - f(x)] \quad (3.14)$$

$$f(x) = \frac{1}{1 + \exp\left(\frac{x - x_o}{x_s}\right)} \quad (3.15)$$

, where  $x_o$  is the location of step change, and  $x_s$  is the span of the variation. As it can be known from Eqs. (3.14) and (3.15), at  $x$  far less than  $x_o$ , the function value approaches  $C_1$ , while at  $x$  far larger than  $x_o$ , the function value approaches  $C_2$ .

In addition to the step distribution, a single rectangular wave shape in equivalence ratio distribution was used in the calculation of flame propagation across a locally isolated lean region within an stoichiometric mixture. With the equivalence ratio of rich mixture fixed at stoichiometry, the depth and width of the rectangular wave shape were expected to model the size of the lean mixture in the pocket and equivalence ratio difference from stoichiometry, respectively.

## 7 Cases of Calculation.

First, the calculations for homogeneous charges were done to compare the results with the available literature data, thus validating the kinetic scheme used in the calculations. For the calculation of stratified charges, the equivalence ratio of rich region ranged from  $\phi_1 = 0.5$  to  $\phi_1 = 1.4$ , while lean region was set at from  $\phi_2 = 0.1$  to  $\phi_2 = 0.8$ , depending on the cases. By changing the equivalence ratio of the lean region, the lean propagation limits of the mixture with charge stratification can be determined. The cases of pocket burning were limited to the equivalence ratio combination under which the flame of the rich gas in step stratification did not propagate through the lean region and extinguished eventually.

## CHAPTER IV Results and Discussion.

### 1 Experimental results

Measurements of the burning velocity of methane-air mixtures with and without charge stratification were made as a function of equivalence ratio with fixed initial temperature and pressure at 295 K and 1 atm, respectively.

#### 1.1 Burning of Homogeneous Charge

Figure 4.1 and 4.2 show the pressure trajectories versus time and the burning velocity versus unburned gas temperature in the burning of homogeneous charges for various equivalence ratios, respectively. The ignition occurred at 50 ms point on time axis for all cases. It is seen that the flame speed increases steadily from the beginning, as unburned gas temperature increases. Since the mixtures of  $\phi = 0.55$  and 0.6 burn very slowly, the boundary layer on the wall of combustion chamber has grown substantially, thus large fraction of the mixture burns under the influence of boundary layer. In the boundary layer where heat is transferred to the wall of the combustion chamber, the burning velocity decreases and the slope of pressure rise becomes less than that of the core mixture as flame approaches the wall. The apparent kink points at about 260 ms for  $\phi = 0.6$  case and 310 ms for  $\phi = 0.55$  case on the pressure curves mean that the flame front meets the boundary layer.

The lean limit of ignitability by laser in the present study was measured to be  $\phi = 0.55$ , which is a little higher than the literature value of  $\phi = 0.46\sim 0.52$ [37, 38]. The cases of  $\phi = 0.55$  and 0.6 are to be compared with the stratified charge cases later.

#### 1.2 Burning of Stratified Charge.

In order to check the validity of the separation of mixture by a bubble and successful ignition of the mixture by laser, the trajectories of pressure rise of the burning of stoichiometric mixture in the bubble of various size with air only in outer zone were measured, as shown in Fig. 4.3 As the gas in the bubble burns, pressure rises up to a final value which depends on the bubble size, then stays constant until it starts to drop very slowly due to the heat loss to the chamber wall(not shown in the figure). The initial slopes



of pressure rising of each curve are all same because it is the function of equivalence ratio only in present study.

### 1.2.1 The laminar flame speed behavior.

The laminar flame behavior in the burning of a stratified charge is shown in Fig. 4.4. The rich mixture within the bubble is stoichiometric and the outer lean mixture is of  $\phi = 0.55$ . As mentioned before,  $\phi = 0.55$  is the limit of ignitability by laser for homogeneous charges. It is also notable that the amount of rich mixture is so small that the overall equivalence ratio of the mixtures is about the same as the equivalence ratio of the leaner mixture; the overall equivalence ratio of the stratified charge with stoichiometric and  $\phi = 0.55$  mixtures is  $\bar{\phi} = 0.55041$  for the bubble size of 15 mm in diameter. In the figure, the velocity data traces begin after the completion of the stoichiometric mixture and stop when the flame front meets the boundary layer on the wall of combustion chamber, which is the region of interest in present study.

Substantial transition effects can be seen at the early stage of combustion of the lean mixture through the enhanced flame speed compared to the homogeneous burning case. The flame speed drops quickly at the beginning from high value (which may be the flame speed of rich mixture in the bubble) and approaches to a minimum value at the end of transition, and then increases as flame propagates further. From the Fig. 4.4 (a) and (b), the transition length and time, which are called the 'flame speed relaxation length' and 'flame speed relaxation time', are about 2 cm and 59 ms, respectively, which are much larger than the diffusion layer length and time scale of burning of the diffusion layer. Using the binary diffusion coefficient between air and methane and the burning time of rich mixture in the bubble, the diffusion layer length can be calculated to be

$$l \approx \sqrt{Dt} \approx \sqrt{0.252 \times 0.01} = 4.74 \times 10^{-2} \text{ cm} \quad (4.1)$$

and the time to burn through this diffusion layer by the flame speed of lean homogeneous charge is

$$t \approx l + S_{L,h} \approx 4.74 \times 10^{-2} + 5 \approx 10 \text{ ms} . \quad (4.2)$$

In Fig. 4.4 (c), the laminar flame speed of homogeneous charge was plotted with the

stratified charge case for comparison. The transition of the flame behavior can be clearly identified here. The curve of stratified charge overlaps the curve of homogeneous charge over a certain temperature which may be the unburned gas temperature at the end of transition in stratified charge burning. These effects also can be shown for the stratified charge of stoichiometric mixture and a leaner mixture than the ignitability limit. Figure 4.5 shows (a) the laminar flame speed versus time, (b) flame radius, and (c) unburned gas temperature of the burning of the stratified charge with stoichiometric and  $\phi=0.52$  mixtures. Even though the mixture of  $\phi = 0.52$  is not ignitable as a homogeneous charge condition, it can be burned through with the help of burned gas of richer mixture which is the stoichiometric mixture in this case.

This flame behavior implies that there is a memory of previous flame history lasting for a while, i.e. a strong flame can sustain itself when it is propagating into a leaner region at least for the relaxation time. This gives a chance that a strong flame can burn through pockets of lean mixtures, as well as the overall burning time can be shortened due to enhanced flame speed. What is more, because of this 'back-support' effects[42], the usual concept of specifying the flame speed as a function of the end gas state is inadequate.

Figure 4.6. shows the time history of (a) the unburned and burned gas temperature of the lean mixture and the burned gas temperature of the rich mixture assuming that the two burned gas regions do not mix, (b) the flame radius and the pressure within the chamber, and the burned mass, (c) the mass fraction of burned gas and the thickness of boundary layer of the stratified charge of stoichiometric and  $\phi = 0.55$  mixture. The substantial difference of the burned gas temperature between the rich mixture and the lean mixture is seen apparently.

In the heat release analysis, it was assumed that the burned gas from the stoichiometric mixture in the bubble does not mix with that from the lean mixture. In reality there are transport processes between the two regions. Neglecting those processes in the data analysis, however, should not substantially change the flame speed data. It is this transport of heat and radicals from the stoichiometric burned gas that is responsible for the enhancement of the flame speed (compared to the homogeneous lean mixture case). These effects will be examined in more details in the numerical results.

As it can be seen in Fig. 4.6 (c), the boundary layer has grown substantially at the later part of combustion due to the slow burning velocity. The fraction of burned mass is substantially less than one when flame front touches the boundary layer, which means that a large amount of unburned gas remains in the boundary layer.

### 1.2.2 Equivalence ratio difference effects.

Various combinations of mixture equivalence ratios were experimented to observe the effect of equivalence ratio difference on the flame speed enhancement of lean mixture. Figures 4.7 and 4.8 show the pressure trajectories and laminar flame speeds of the stratified charge with the lean mixture at  $\phi = 0.55$  and various richer mixtures. The richer mixtures were initially confined in the bubble. The size of the bubbles used for all cases was approximately 15 mm. In the early stage of combustion, the flame speed enhancement by the burned gas of the richer mixture in the transition period varied depending on the equivalence ratio of the richer mixture in a stratified charge. The enhancement effect is noticeable even at a value of  $\phi = 0.6$  for the richer mixture. This result can be explained by the reason that since the flame speed variation becomes more sensitive to equivalence ratio with decreasing equivalence ratio from stoichiometry, the flame speed of the  $\phi = 0.6$  mixture is much higher than that of the  $\phi = 0.55$  mixture; thus the  $\phi = 0.6$  mixture can offer substantial back support to the  $\phi = 0.55$  mixture.

Note that, in the range of the richer equivalence ratio of about 0.9~1.3, all pressure curves tend to collapse on one trajectory(Fig. 4.7). This means that no more benefit of decreasing of overall burning time can be obtained from the stratified charge burning over a certain value of equivalence ratio difference. However the enhancement of flame speed is still shown mostly due to the density variation between the mixtures of different equivalence ratio, though the amount of the burning velocity enhancement becomes less(Fig. 4.8).

The pressure and flame speed data at a lower(0.52) and higher(0.6) values of  $\phi_2$  are shown in Fig. 4.9~4.12. Note that at  $\phi_2=0.52$ , the mixture could not be ignited. The flame speed enhancement by the back support of the rich mixtures in these cases are similar to

that of the  $\phi = 0.55$  case. In Fig. 4.13, the enhancement ratio was plotted with respect to equivalence ratio difference for various lean mixtures. The enhancement ratio is defined as a normalized index to indicate the extent of the enhancement of the burning velocity compared a reference velocity, which was calculated as the burning velocity difference between the stratified case and the homogeneous case at the same unburned gas temperature divided by the burning velocity of the homogeneous case. The burning velocities of the homogeneous and stratified charge cases were the values at the unburned gas temperature of 297 K. For the case of  $\phi = 0.52$  in Fig.13, the reference burning velocity was extrapolated from the burning velocities of the homogeneous mixtures of  $\phi = 0.55$  and  $\phi = 0.6$ . For a given lean mixture the enhancement ratio increases with the increase of equivalence ratio difference, but the slope of the curve shows a saturating trend in all three cases. The enhancement effect becomes larger as the lean mixture in a stratified charge becomes leaner, which can be figured out through higher slope of the curve.

### 1.2.3 The extension of lean propagation limit.

Two different approaches have been suggested to characterize the “flammability limit” respectively by Spalding and Law and Egolfopoulos [39]: loss-based theory and chain-based approach. These characterization are based on the thermal and chemical aspects of the flame behavior. In the loss-based theory, the heat loss from the reaction zone exceeds the chemical heat generation and causes the extinction of the flame. Flammability limit is thus defined as the point where the heat loss is greater than the chemical heat generation. The chain-based approach is based on that the competition between branching and termination reactions must be important for flames close to the flammability limit. The results obtained from calculations using this approach show that at the flammability limit, the normalized sensitivity of the rate of the chain termination is equal to that of the branching reaction rate. Both approaches imply that an increase in the heat addition to the reaction zone by heat transfer from other source, or an increase in branching reaction intensity due to change in radical transport can cause the balancing point to shift, thus extending the flammability limit. Although the term “flammability limit” has been extensively used to describe the failure of a flame to propagate in mixtures beyond a certain

concentration, its definition is somewhat ambiguous when applied to an unsteady flame propagation with variation of temperature and pressure as in the present study because it is basically defined for steady state and for constant conditions. So the term “propagation limit” will be used here instead of “flammability limit”, depending on whether a flame can sustain itself and burn through the mixtures in an enclosure.

Because the flame in the lean charge is affected by the prior burned gas of the rich mixture for a finite time of the transition (the relaxation time), the rich mixture may be used as ‘back supporter’ to extend the propagation limit of the lean mixtures. In order to measure the lean limit of propagation with the help of the burned gas of the rich mixture, flame propagations from a stoichiometric mixture within a bubble of about 15 mm in diameter into various lean mixtures were observed.

Figures 4.14 and 4.15 show the pressure trajectories and laminar flame speed of stratified charges with stoichiometric and various lean mixtures. The propagation limit could be extended to equivalence ratio  $\phi = 0.5$  at which the flame propagated at least half way of the combustion chamber, thus substantial pressure rise could be measured. For the mixtures of  $\phi = 0.45$ , the flame from the stoichiometric mixture did not propagate in the mixture that no more substantial pressure rise than by the burning of stoichiometric mixtures was observed.

It is notable, however, that, for the non-ignitable mixtures stratified with a richer mixture, the amount of richer mixture affects the extent of burning in lean region. In Fig. 4.16, the pressure profiles of burning of stratified charges with various bubble sizes are shown. The larger amount of rich mixture leads to the higher maximum pressure and the longer burning time of lean mixture. Since the pressures at the completion of burning of the rich mixture are all negligible compared to the subsequent pressure rise, the change of unburned gas temperature by isentropic compression at that point is also negligible. It will be shown later in the simulation study that for a given lean mixture, the flame speed is a function of the burned gas temperature. Because the larger bubble had a larger burned mass, the burned gas temperature can be sustained for a larger period as the flame propagates into the lean mixture; thus the larger bubble provides a more extensive period of back-support.

## 2 Numerical results and discussion.

A numerical simulation of the propagation of an unsteady, one-dimensional methane-air flame from a rich mixture into a lean mixture with step change stratification in equivalence ratio was done using the computer code HCT. The code was implemented on a Silicon Graphics Irix machine. The propagation use an adaptive grid with automatic rezoning to resolve regions of high temperature gradients. The total number of zones used in the calculational domain was 60 for most cases, and 80 for the few cases in which more precise data were needed for calculate the change of species concentration and flux around the flame.

### 2.1 Homogeneous charge burning.

Figure. 4.17 and 4.18 show some results of numerical calculations for burning homogeneous mixtures of equivalence ratio  $\phi = 1.4, 1.0, 0.7,$  and  $0.4$ . The pressure versus the unburned gas temperature curves are shown in Fig. 4.17. The slopes of the isentropes are almost same because the difference of the specific heat ratio between the cases is small, though the specific heat ratio of the mixture increases slightly as the mixtures become lean.

In the figure 4.18, the laminar burning velocities were plotted with respect to the unburned gas temperature which may be considered as a progress variable because it is related to the pressure via the isentrope. The burning velocity was calculated from the time derivative of the integrated burned mass divided by the unburned gas density at the time of calculation. The interval of integration of the burned mass was from zero to the position of maximum chemical heat release, and the unburned gas density was assumed to be equal to the density of gas in the last zone of the domain.

Except for the short initial period where the flame speed is affected by the ignition source, the velocity is almost constant for stoichiometry and is not sensitive to the unburned gas temperature. Since the reaction rate is a strong function of temperature, the burning velocities are expected to increase with the unburned gas temperature, even after allowing for the pressure effects on the flame speed due to compression. This discrepancy may be caused by the underestimation of the dependency of the thermal and mass diffusivities on

temperature in the calculation. The temperature dependency of the diffusivities was set be proportional to  $T^{1.5}$  which is from the result of kinetic theory as in Eq. (3.10). For realistic intermolecular force potentials, however, the diffusivities are proportional to  $T^a$ , where  $1.5 \leq a \leq 2$  [2]. This scaling was not considered in the present study. The burning velocities at 300 K for various equivalence ratios are compared with the experimental results and literature data in Fig. 4.19. They are in good agreement around stoichiometry and slightly rich condition. The results of the present calculation show lower values in lean conditions and higher values in rich conditions than the data of Ref. 19. The burning velocity in rich conditions of the present experiment are higher than the data of Ref. 19 and decreases slowly as the mixture gets richer.

The propagation limit was calculated to be  $\phi = 0.35$ , below which the burned gas temperature does not sustain and the flame extinguishes quickly. Figure. 4.20 shows the temperature profiles of a non-ignitable mixture of  $\phi = 0.3$ , at various time. Soon after the ignition heat source is off, the flame extinguishes and the temperature profile diffuses due to heat transfer to the unburned gases.

## 2.2 Stratified charge burning.

### 2.2.1 Comparisons of the dynamic profiles of the stratified charge burning and the homogeneous charge burning.

Figure 4.21. shows the dynamic profiles of gas temperature for the burning of a stratified charge. The flame propagates from a stoichiometric mixture to a mixture of equivalence ratio  $\phi = 0.5$ . The flame front (reaction zone) is located approximately at the position of the steepest temperature. At the lapsed time of 5 ms, the flame is still in the rich mixture region, thus the temperature in the burned gas region is approximately the adiabatic flame temperature of stoichiometric methane-air mixture. Because there is insufficient time for the burned gases to get to spatial thermal equilibrium, the temperatures of the early burned gas are higher than that of the late burned gas due to the compression by the pressure rise in the enclosure. Because of the temperature gradient heat is transferred from the early burned gas to the late burned gas. At lapsed time of 7.62 ms, the burned mass

exceeds the mass of the rich mixture. The temperature gradient just behind the flame front is getting steeper than that of far behind of the flame, which means that the flame is propagating through the interfacial region into the lean mixture region.

Since the adiabatic flame temperature drops drastically as mixtures get lean from the stoichiometry, there are two different temperatures representing the burned gas region after the flame fully enters the lean region as shown in Fig. 4.21 (c)~(e). It is specially notable that the burned gas temperature just behind the flame front only relax to the lean value after a very long time (Fig. 4.21 (e)).

This effect can be clearly seen by comparing the temperature profiles of the stratified charge case with the homogeneous charge case as shown in Fig. 4.22. For the homogeneous burning case, the temperature gradients of the flame front at different time are almost constant and same as that of the case of lapsed time 100 ms in the stratified charge case.

The profiles of species mole fractions for the burning of a stratified charge and a homogeneous charge in Fig. 4.23 and 4.24, respectively. The flame transition from a stoichiometric to a lean region can be seen in the figure of stratified charge case through the evolution of  $[O_2]$  and  $[H_2O]$  concentrations. In Fig. 4.23 (c) and (d), the excessive oxygen of the lean mixture remains behind the flame front and diffuses to the burned gas of the rich mixture so that the mole fraction relax from the lean values to the values of the stoichiometric burned gas. In comparison, the mole fraction profile is almost constant at around 0.1 for both  $[O_2]$  and  $[H_2O]$  behind the flame front in the homogeneous lean charge at all times. At time 100 ms in the stratified charge case, the profile of  $[O_2]$  becomes almost flat behind the flame. Both the mole fraction and the temperature profiles at this time suggest that the back-support effect of the rich flame has vanished and the local flame behaves as if it is originally started in a homogeneous charge. In Fig. 4.24, the mole fraction of  $[CO]$  is negligible all the time of burning that it can not be distinguished easily in the figure.

Figures 4.25 and 4.26 show the dynamic profiles of the mole fraction of the radicals  $[H]$ ,  $[OH]$  and  $[HO_2]$  for the stratified charge burning and the homogeneous charge burning. The  $[HO_2]$  fraction is negligible during the whole combustion time. However the



[H] and [OH] radicals show a drastic transitional change of about an order of magnitude between the burning of the rich mixture and the lean mixture. During the relaxation period (8~20 ms of lapsed time) the mole fraction of [OH], which is important in the [CO] oxidation (reaction 47 in Table. 1), is about an order of magnitude higher than the [H] mole fraction. The effect of [H] diffusion into the lean unburned gas is thus not prominent.

In Fig. 4.27, the plots of vessel pressure versus time and unburned gas temperature are shown. For the combustion in the stratified charge case, the pressure rises rapidly at the beginning due to the burning of the rich mixture and follows a line of different slope in the region of lean mixture burning, while the pressure steadily increases from the initial value in the homogeneous charge case, as shown in Fig. 4.27 (a). This evolution of the pressure profiles is similar to the early part of the experimental results in Fig. 15. The correlation of pressure with unburned gas temperature, however, falls on a single isentrope in a wide range of the unburned gas temperature for the two cases, which makes it valid to compare burning velocities at the same unburned gas temperature between the stratified charge and the homogeneous charge.

### 2.2.2 Comparisons of burning velocity.

Figure 4.28 shows the comparison of the burning velocity between the burning of the stratified charge and that of the homogeneous charge at various times. In the figure, the left dotted line marks the point where the burned mass is equal to the mass of stoichiometric charge in stratified case. So, behind this time, the flame is propagating in the lean region. The right dotted line marks the point where the burning velocity of the stratified case becomes approximately equal to that of the homogeneous case. The relaxation of flame speed in the stratified charge burning can be clearly seen from the two velocity profiles since the time at the completion of combustion of the rich mixture. At long time, the two profiles do converge to the same flame velocities.

Figure 4.29 shows the comparison of the burning velocity between the burning of the stratified charge and the homogeneous charge at various unburned gas temperatures. The unburned gas temperature, which is related to the pressure through the isentrope, serves as a progress variable here so that the flame speeds of the stratified case and the homogeneous

case can be compared at the same pressure and unburned gas temperature. As shown in the Fig. 4.28, the two profiles converge to the same burning velocities eventually. The dotted line marks the point where the burned mass is equal to the mass of stoichiometric charge in the stratified case. For the stratified charge, the relaxation of the velocity to the right side of the dotted line is similar to our experimental results. Because there is some diffusion of species at the interfacial region until the flame gets there, the equivalence ratio of the gases in the diffusion layer becomes less than stoichiometry, thus the flame speed drops a little at that region. By the similar calculation to Eq. (4.1), the thickness of the diffusion layer is about  $0.45\text{ mm}$  which is about one tenth of the initial length of the stoichiometric mixture region

In Fig. 4.30, the burned gas temperature of the stratified charge is plotted versus unburned gas temperature, together with the homogeneous charge case. Since the flame propagation in an enclosure is an unsteady phenomenon, the burned gas temperature changes with time and position, thus there is no established way to indicate the point where the burned gas temperature is to be obtained. The temperature of the gas in the first zone of the calculational domain can be a good candidate. However, this zone can be substantially affected by the ignition like in this study and does not seem to properly represent the reaction intensity at the flame front, especially in a stratified charge burning. Therefore in the present study, the burned gas temperatures were obtained at the points where the second derivative of temperature with respect to distance became a minimum. These points are usually very close to the points of maximum chemical heat release which are located behind the flame [20], as shown in Fig. 4.31.

The trend of the profiles is very similar to the velocity versus unburned gas temperature plot in Fig. 4.29. This implies a probable correlation of the burning velocity with the burned gas temperature in the burning of a stratified charge, which will be discussed later. Because of the heating by the ignition source, the burned gas temperatures of the homogeneous charge are very high at the beginning of combustion and drop rapidly to around the adiabatic flame temperature of the lean mixture.

### 2.2.3 Characteristics of the stratified charge burning.

The thermodynamic effects of the stratified charge burning is as follows. When the stoichiometric flame just encounters the leaner charge, the burned gas temperature ( $T_b$ ) will be that of the stoichiometric mass. Dimensional argument leads to that  $S_L \sim \alpha / \delta_f$ , where  $\alpha$  is the thermal diffusivity in the preheat zone and  $\delta_f$  is the flame thickness. The burned gas temperature affects both  $\alpha$  ( $\alpha \propto T^{1.5}/P$ ) and  $\delta_f$ . If we assume that  $\alpha$  and  $\delta_f$  are only a function of  $T_b$  (the species concentration effects will be discussed later), then the flame speed will not be affected at first. In the subsequent flame development, however,  $T_b$  will decrease because of the smaller heat release from the leaner charge. This lower  $T_b$ , in turn, lowers  $S_L$ .

In addition to the thermodynamic effects, the previous burned gas of the rich mixture affects the burning of the subsequent lean mixture chemically as well. The concentration, the net rate of change, and the rate of change by diffusion, chemistry and hydrodynamic in the flame zone of a stratified charge for major species and radicals at the lapsed burning time of 10 ms and unburned gas temperature of 387 K, are shown in Fig. 4.32 and 4.33, respectively. The near flame zone can be divided into four regions according to the combustion characteristics, i.e.,

Region (I): the unburned zone, where the gas is in chemically frozen state and its temperature is increased by the adiabatic compression only because there can be assumed no heat transfer into the zone.

Region (II): the preheat zone, where heat transfer and species diffusion occurs, but there occur no noticeable reactions.

Region (III): the reaction zone, where the initiation, recombination, propagation and branching reactions occur. The front part of this region is dedicated to the initiation reactions and the radical recombination reactions such as the reactions 1-4, 52 and 53 in the Table 1. At the rear part (away from the unburned gas) of the region, the branching and propagating reactions occur vigorously, and most of the heat is released.

Region (IV): the burned zone, where the major combustion reactions are finished and the state of the gas is close to thermal equilibrium.

The concentration of [H] [OH] and [CH<sub>3</sub>] radicals varies substantially in the reaction

zone(III), while it is negligible in the preheat zone(II). By comparing the figures (c), (d) and (e) of Fig. 4.32 and 4.33, it can be figured out that the stable species such as  $\text{H}_2\text{O}$  and  $\text{CO}_2$  are diffused from the reaction zone(III) to the preheat zone(II), however, radicals such as  $[\text{H}]$  and  $[\text{OH}]$  are negligible in the preheat zone, because most of them are consumed by recombination reactions and initiation reactions in the front part of the reaction zone, which helps  $[\text{CH}_3]$  production there.

In the figure of net rate of change, all intermediate species such as  $[\text{H}]$ ,  $[\text{OH}]$ ,  $[\text{CH}_3]$  and  $[\text{CO}]$  show the behavior of production and then consumption, while the reactants and products are of negative and positive rates in the whole range of the reaction zone(III), respectively. The negative peak point of the rate of change of  $[\text{CO}]$  is located at the most retarded position among the species. This is consistent with previous studies that most of the  $[\text{CO}]$  consumption occurs at the rear part of the flame [20].

Because the preheat zone is chemically inert, the diffusion balances with the hydrodynamic change there. In the reaction zone, the chemistry balances with the diffusion. In the calculation, which was Lagrangian, the hydrodynamic change was defined as the sum of the advection term and the change due to the volume change by rezoning.

Figures 4.34 and 4.35 show some chemical characteristics of the burning of a homogeneous mixture to be compared with the stratified case at the same unburned gas temperature. In the stratified case of Fig. 4.32 and 4.33, the flame is in the transition period. Note that the radical concentrations and reaction rates are about an order of magnitude lower than those of the stratified case. Because of the lower reaction rate and diffusion flux, the thickness of the preheat zone and the reaction zone of the homogeneous case is also much bigger than that of the stratified case

Figure 4.36 shows the comparison of peak radical mole fraction at flame as a function of unburned gas temperature for the stratified charge case versus the homogeneous charge case. It is also seen that the mole fractions of the two cases converges to the same value eventually. The peak points are located at the rear of the flame because the maximum mole fraction of  $[\text{H}]$  radical occurs at the maximum reaction rate point where branching reactions are vigorously taking place, while the  $[\text{OH}]$  radical peak points are further behind the peak  $[\text{H}]$  radical points because the amount of  $[\text{OH}]$  radical is related to the  $[\text{CO}]$  oxidation.

Figure. 4.37 shows the comparison of the evolution of peak radical mole fraction with respect to time between two charge cases. Because of the flame speed enhancement, the profile of the stratified case changes more rapidly than the homogeneous case. In the figure, the left dotted line marks the point where the burned mass is equal to the mass of stoichiometric charge in stratified case and the right dotted line marks the point where the peak [OH] mole fraction of the stratified case is equal to that of the homogeneous case. It is notable that the time interval of approximately 40 ms between these two dotted line is about the same as that obtained from velocity plot in Fig. 4.28. This implies that the comparison of the peak [OH] mole fraction may be a good indication in determining the relaxation time in the numerical calculation of the stratified charge burning.

#### 2.2.4 Equivalence ratio difference effects.

Figure 4.38 shows the compared pressure profiles of the combustion of stratified charges at various equivalence ratio of the richer mixture. The lean mixture is fixed at  $\phi_2 = 0.4$ . The homogeneous case with  $\phi = 0.4$  is also included. The initial slope of curves varies depending on the equivalence ratio of the rich mixtures and the change of the slope at the interfacial region between the rich and the lean mixtures becomes slower as the rich mixture in a stratified charge becomes leaner. All the slopes of the curves in the region of lean mixture burning are steeper than that of the homogeneous case, implying that the burning in the stratified cases is faster than that in the homogeneous case.

The burning velocities versus unburned gas temperatures plots for various equivalence ratios of the rich mixtures with the lean mixture fixed at  $\phi = 0.4$  are shown in Fig. 4.39. The dotted line in Fig. 4.39 marks the point where the burned mass is equal to the mass of stoichiometric charge in the stratified case. The burning velocity behavior after the completion of burning of the rich mixture is similar to the experimental results in Fig. 4.8, 4.10 and 4.12. Due to the diffusion of species at the interface before flame arrival, the cases of richer mixtures than stoichiometry show higher burning velocity in the diffusion layer than the starting velocity and their burning velocity curves look as if the right side of the dotted line was shifted to the right away from the curve of stoichiometric mixture.

The enhancement of burning intensity in the stratified cases can be exhibited by

comparing the lapsed time of combustion of a certain amount of the mixture for various lean mixtures, as shown in Fig. 4.40. The lapsed time of stratified cases was calculated from the point where the burned mass is equal to the mass of the stoichiometric mixture, to the point where the burned mass fraction of the lean mixture becomes 0.2, while for the homogeneous cases, the starting point is where the unburned gas temperature is equal to that of the stratified case at the time of completion of the burning of stoichiometric mixture and the final point is where 20 % of initial mass of the mixture burns since the starting point. In all cases, the burning time of stratified case is much faster than that of the homogeneous case, though the difference of lapsed time between the two cases substantially decreases as the equivalence ratio of the lean mixture increases.

#### 2.2.5 Calculation of pocket burning.

Since the propagation limit of a charge with step stratification was calculated to be  $\phi_2=0.2$  (the average equivalence ratio of this case is equal to  $\bar{\phi}=0.2996$ , which is even below the ignition limit of  $\phi = 0.35$  in the homogeneous condition), the equivalence ratio of the pocket surrounded by a rich mixture was limited to  $\phi = 0.1$ . The equivalence ratio of the rich mixture was stoichiometry. Even though a flame does not fully propagate in a charge with step stratification of the stoichiometric mixture and the  $\phi = 0.1$  mixture, the flame can burn through a certain size of the lean region. Figure 4.41 shows the burning of a pocket of 1.2 cm in width which starts at 0.4 cm from the ignition point. The burning velocity drops rapidly as the flame enters the lean pocket region, stays at very low value for long time, and eventually is recovered to the same velocity as the initial velocity. This flame behavior can be also clearly seen in the pressure profile. Since, during the burning of the pocket region, the pressure rise is just small portion of the total pressure, the unburned gas temperature rise due to compression is small. After the burning of the stoichiometric mixture located at the first part of the domain is completed, the burned gas temperature steadily decreased until the other part of the stoichiometric mixture burns. This implies that the burned gas temperature will decrease further as the width of the pocket region increases and the flame will extinguish, when the burned gas temperature becomes too low to initiate the burning of the other part of the stoichiometric mixture.

### 3 Correlation of the burning velocity of stratified charge.

From the dimensional analysis for the flame zone, the flame speed  $S_L \sim \alpha/\delta_f$ , where  $\alpha$  is the thermal diffusivity in the preheat zone and  $\delta_f$  is the flame thickness. The values of  $\alpha$  and  $\delta_f$  are sensitive to temperature. Since the burned gas temperature  $T_b$  is essential to determine the temperature profile in flame zone (reaction zone + preheat zone),  $T_b$  will have a prominent effect on the values of  $\alpha$  and  $\delta_f$ , thus on  $S_L$ . Therefore it is reasonable to correlate  $S_L$  with  $T_b$  during the transition period. Such a correlation is shown in Fig. 4.42 for a flame traveling from  $\phi_1 = 1.0$  to  $\phi_2 = 0.5$ . The value of  $S_L$  may fit to be dependent on  $\exp(T_b)$ . The burning velocities in the log-scale is well related to burned gas temperature as a linear line between two points, which indicate the burning velocity and burned gas temperature of the rich and the lean mixtures in homogeneous condition. This implies that if the equivalence ratios of the two mixtures consisting a stratified charge are known for given initial temperature and pressure, the burning velocity during the transition period can be obtained from a simple equation of the burned gas temperature of the stratified charge. Similar correlations were explored at different values of  $\phi_1$ , with  $\phi_2$  fixed at 0.4 in Fig. 4.43. For the individual  $\phi_1$  values,  $S_L$  may be fit to  $\exp(T_b)$ . The equations of the fitted lines in Figs. 4.43 are listed in Table. 2. There is, however, a dependence of  $S_L$  on  $\phi_1$  through different slopes of the lines. Two simple equations to calculate the coefficients of the burning velocity equations given in Table. 2 in terms of the equivalence ratio of the rich mixture is shown in Table. 3.

## CHAPTER V Summary and conclusions.

In a spherical constant volume combustion vessel, the flame propagation from a rich methane-air mixture to a leaner methane-air mixture was experimented at the initial condition of 295 K and 1 atm. The mixtures at the two different equivalence ratios within the vessel were separated by a soap bubble. The rich mixture within the bubble was ignited by a pulsed laser beam focused at the center of the soap bubble. The flame propagation was monitored by high speed video combined with schlieren system and the pressure was recorded to be used for heat release analysis and burning velocity calculation. In order to help interpret the experimental results, one dimensional flame propagation in a charge with step stratification in an enclosure was calculated numerically using the computer code HCT developed at the Livermore National Laboratory for one-dimensional, time dependent calculation with hydrodynamics, transport and detailed chemical kinetics.

From the experimental and computational results, the behavior of an established flame propagating into a leaner region was determined. The conclusions of this study can be summarized as followings.

1. The flame behavior in a stratified charge shows that there is a memory of previous flame history so that a strong (with equivalence ratio close to stoichiometry) flame can sustain propagation into a much leaner region. There is a significant transition time through which the flame speed relaxes from the value in the richer region to that in the leaner region.
2. The local burned gas temperature plays a key role in the flame speed relaxation process. The hotter burned gas from the richer region "back-supports" the flame propagation into the leaner region.
3. Because of the back-support effect of the rich mixture, the usual concept of specifying the burning velocity as a function of the end gas state is inadequate. Instead, the burning velocity should be determined as a function of the conditions of the previous burned gas as well as the end gas state.
4. For a given lean mixture, the initial burning velocity enhancement in the transition increases as the richer mixture equivalence ratio  $\phi_1$  increases from lean to



stoichiometric. The curve, however, flattens out as  $\phi_1$  approaches stoichiometric and becomes slightly rich (up to  $\phi_1 = 1.3$ ).

5. For a flame propagating through a step change of equivalence ratio (from a richer to a leaner region), the burning velocity during the transition period can be correlated to the burned gas.

## REFERENCE

1. Heywood, J. B., *Internal Combustion Engine Fundamentals*, McGraw-Hill, New York, 1988.
2. Williams, F. A., *Combustion Theory*, 2<sup>nd</sup> Ed., Addison-Wesley Publishing Company, Redwood city, 1985.
3. Gomez, A. J., and Reinke, P. E., "Lean Burn: A Review of Incentives, Method, and Tradeoffs", SAE Paper 880291, 1988.
4. Takeda, K., Shiozawa, K., Oishi, K., and Inoue, T., "Toyota Central Injection System for Lean Combustion and High Transient Response", SAE Transaction 94, 6, Paper 851675, 1985.
5. Fujimoto, M., Nishida, K., and Hiroyasu, H., "Influence of Mixture Stratification Pattern on Combustion Characteristics in a Constant Volume Combustion Chamber", SAE Paper 952412, 1995.
6. Arcoumanis, C., Hull, D. R., and Whitelaw, J. H., "An Approach to Charge Stratification in Lean-Burn, Spark-Ignition Engines", SAE Paper 941878, 1994.
7. Date, T., and Yagi, S., "Research and Development of the Honda CVCC Engine", SAE Paper 740605, 1974.
8. "In-cylinder Direct Injection Gasoline Engine 4G23", Press release, Mitsubishi Motors Corporation, 1995.
9. Toyota Develops New D-4 Fuel Efficient, High Output Direct-Injection Gasoline Engine", Press release, Toyota Motor Co., 1996.
10. Gill, A., Gutheil, E., and Warnatz, J., "Numerical Investigation of the Combustion Process in a Direct Injection Stratified Charge Engine", *Combust. Sci. Tech.*, 1996, Vol. 115, pp. 317-333.
11. Williams, T. H., "A New Class of Stratified-Charge Internal Combustion Engine", SAE Paper 950088, 1995.
12. Goto, S., Itoh, Y., Higuchi, Y., and Nagai, T., "NIGATA Ultra Lean Burn SI Gas Engines-Achieving High Efficiency and Low Nox Emission", SAE Paper 901605, 1990.
13. Kiyota, Y., Akishimo, K., and Ando, H., "Concept of Lean Combustion by Barrel-Stratification", SAE Paper 920678, 1992.
14. Kuwahara, K., Watanabe, T., Takemura, J., Omori, S., Kume, T., and Ando, H., "Optimization of In-Cylinder Flow and Mixing for a Center-Spark Four-Valve Engine Employing the Concept of Barrel-Stratification", SAE Paper 940986, 1994.
15. Masuya, G., "Influence of Laminar Flame Speed on Turbulent Premixed Combustion", *Combustion and Flame*, 1986, Vol. 64, pp. 353-367.
16. Gaydon, A. G., and Wolfhard, H. G., *Flames*, 4<sup>th</sup> Ed., John Wiley and Sons, New York, 1979.
17. Andrews, G. E., and Bradley, D., "Determination of Burning Velocities: A Critical Review", *Combustion and Flame*, 1972, Vol. 18, pp. 133-153.
18. Metghalchi, M., and Keck, J. C., "Laminar Burning Velocity of Propane-Air Mixtures at High Temperature and Pressure", *Combustion and Flame*, 1980, Vol. 38, pp. 143-154.
19. Egolfopoulos, F. N., Cho, P., and Law, C. K., "Laminar Flame Speed of Methane-Air

- Mixtures Under Reduced and Elevated Pressure”, *Combustion and Flame*, 1989, Vol. 76, pp. 375-391.
20. Westerbrook, C. K., and Dryer, F. L., “Chemical Kinetic Modeling of Hydrocarbon Combustion”, *Prog. Energy Combust. Sci.* 1984, Vol. 10, pp. 1-57.
  21. Rafael, S., and Sher, E., “Reaction Kinetics of Hydrogen-Enriched Methane-Air and Propane-Air Flame”, *Combustion and Flame*, 1989, Vol. 78, pp. 326-338.
  22. Götting, J., Mauss, F., and Peters, N., “Analytic Approximations of Burning Velocities and Flame Thicknesses of Lean Hydrogen, Methane, Ethylene, Ethane, Acetylene, and Propane Flames”, *Twenty-Fourth Symposium (International) on Combustion*, Combustion Institute, Pittsburgh, 1992, pp. 129-135.
  23. Müller, U. C., Bollig, M., and Peters, N., “Analytic Approximations of Burning Velocities and Markstein Numbers for Lean Hydrocarbon and Methanol Flames”, *Combustion and Flame*, 1997, Vol. 108, pp. 349-356.
  24. Sung, C. J., Law, C. K., and Chen, J. Y., “An Augmented Reduced Mechanism for Methane Oxidation with Comprehensive Global Parametric Validation”, *Twenty-Seventh Symposium (International) on Combustion*, Combustion Institute, Pittsburgh, 1998, pp. 295-304.
  25. Andrews, G. E., and Bradley, D., “Burning Velocity of Methane-Air Mixtures”, *Combustion and Flame*, 1972, Vol. 19, pp. 275-288.
  26. Metghalchi, M., and Keck, J.C., “Burning Velocity of Mixtures of Air with Methanol, Isooctane, and Indolene at High Temperature and Pressure”, *Combustion and Flame*, 1982, Vol. 48, pp. 191-210.
  27. Bradley, D., El-Din Habik, S., and El-Sherif, A., “A generalization of Laminar Burning Velocities and Volumetric Heat Release Rates”, *Combustion and Flame*, 1991, Vol. 87, pp. 336-336.
  28. Yu, G., Law, C. K., and Wu, C. K., “Laminar Flame Speeds of Hydrocarbon + Air Mixtures with Hydrogen Addition”, *Combustion and Flame*, 1986. Vol. 63, pp. 339-347.
  29. Bell, S. R., and Gupta, M., “Extension of the Lean Operating Limit for Natural Gas Fueling of a Spark Ignited Engine Using Hydrogen Blending”, *Combust. Sci. Tech.*, 1997, Vol. 123, pp. 23-48.
  30. Murase, E., Ono, S., Hanada, K., and Oppenheim, A. K., “Initiation of Combustion in Lean Mixtures by Flame Jets”, *Combust. Sci. Tech.*, 1996, Vols. 113-114, pp. 167-177.
  31. Kesler, M., and Rynchter, T., “A Jet Dispersed Combustion (JDC) Method to Stimulate Lean Burning in SI Piston Engines”, SAE Paper 951006, 1995.
  32. Moriyoshi, Y., Morikawa, H., Kamimoto, T., and Hayashi, T., “Combustion Enhancement of Lean Premixture Part in Stratified Charge Conditions”, SAE Paper 962087, 1996.
  33. Furuno, S., Iguchi, S., and Inoue, T., “Lean Combustion Characteristics of Locally Stratified Charge Mixture, Basic Studies of In-vessel Combustion Ignited by Laser”, Toyota Motor Co. Report.
  34. Hecht, E., *Optics*, 2<sup>nd</sup> Ed., Addison-Wesley Publishing Company, 1987, p576.
  35. Strehlow, R. A., *Combustion Fundamentals*, McGraw-Hill, New York, 1988.
  36. Lund, C. M., HCT Manual, revised version, Lawrence Livermore National Laboratory, 1995.

37. Kanury, A. M., *Introduction to Combustion Phenomena*, Gordon and Breach, New York, 1977, pp. 130-131.
38. Coward, H. F., and Jones, G. W., *Limits of Flammability of Gases and Vapors*, U.S. Government Printing Office, Washington, 1952.
39. Law, C. K., and Egolfopoulos, F. N., 'A United Chain-Thermal Theory of Fundamental Flammability Limits', *Twenty-Fourth Symposium(international) on Combustion*, Combustion Institute, Pittsburgh, 1992, pp. 137-144.
40. JANAF Thermodynamic Tables, Dow Chemical Company, Midland, Michigan, 1974.
41. Hamamoto, Y., Tomita, E., Yamanaka, M., and Kataoka, M., 'Heat Transfer to the Wall of End Gas Side During Propagation of Premixed Flame in a Closed Vessel', *JSME International Journal*, 1996, Series B, Vol. 39, pp. 836-843.
42. Marzouk, Y. M., 'The Effect of Flow and Mixture Inhomogeneity on the Dynamics of Strained Flames', Master Thesis, MIT, 1999.

TABLE 1.

Mechanism of the oxidation of methane. The reaction rate equation used in the calculation is

$$K = aT^b \exp(-c/RT)$$

and

frc, frp and frx are a, b and c in the above reaction rate equation for forward reaction.  
 rrc, rrp and rrx are a, b and c in the above reaction rate equation for backward reaction.

reaction	frc	frp	frx	rrc	rrp	rrx
<b>CH<sub>4</sub> Formation and Consumption</b>						
1 CH <sub>4</sub> +H = CH <sub>3</sub> +H <sub>2</sub>	2.240E+04	3.00	8.750E+03	2.890E+02	3.12	8.711E+03
2 CH <sub>4</sub> +O = CH <sub>3</sub> +OH	1.170E+07	2.08	7.630E+03	2.000E+05	2.08	5.055E+03
3 CH <sub>4</sub> +OH = CH <sub>3</sub> +H <sub>2</sub> O	1.600E+06	2.10	2.460E+03	4.820E+02	2.90	1.486E+04
4 CH <sub>4</sub> = CH <sub>3</sub> +H	6.300E+14	0.00	1.040E+05	6.000E+16	-1.00	0.000E+00
<b>CH<sub>3</sub> Formation and Consumption</b>						
5 CH <sub>3</sub> +O = CH <sub>2</sub> O+H	7.800E+13	0.00	0.000E+00	1.020E+15	0.00	6.963E+04
6 CH <sub>3</sub> +O <sub>2</sub> = CH <sub>3</sub> O+O	2.400E+13	0.00	2.900E+04	1.520E+14	0.00	7.330E+02
7 CH <sub>3</sub> +HO <sub>2</sub> = CH <sub>4</sub> +O <sub>2</sub>	1.000E+12	0.00	4.000E+02	7.630E+13	0.00	5.859E+04
<b>CH<sub>2</sub> Formation and Consumption</b>						
8 CH <sub>2</sub> +O <sub>2</sub> = CO <sub>2</sub> +H+H	1.300E+13	0.00	1.505E+03	0.000E+00	0.00	0.000E+00
9 CH <sub>2</sub> +O = CO+H+H	7.800E+13	0.00	0.000E+00	0.000E+00	0.00	0.000E+00
<b>CH<sub>3</sub>O Formation and Consumption</b>						
10 CH <sub>3</sub> O = CH <sub>2</sub> O+H	3.888E+37	-6.65	3.326E+04	7.708E+32	-5.65	9.696E+03
11 CH <sub>3</sub> O+H = CH <sub>2</sub> O+H <sub>2</sub>	2.000E+13	0.00	0.000E+00	7.480E+12	0.00	8.388E+04
12 CH <sub>3</sub> O+OH = CH <sub>2</sub> O+H <sub>2</sub> O	1.000E+13	0.00	0.000E+00	1.620E+13	0.00	9.903E+04
13 CH <sub>3</sub> O+O = CH <sub>2</sub> O+OH	1.000E+13	0.00	0.000E+00	1.640E+12	0.00	8.178E+04
14 CH <sub>3</sub> O+O <sub>2</sub> = CH <sub>2</sub> O+HO <sub>2</sub>	7.600E+10	0.00	2.700E+03	7.614E+09	0.00	3.083E+04
<b>CH<sub>2</sub>O Formation and Consumption</b>						
15 CH <sub>2</sub> O+H = HCO+H <sub>2</sub>	2.500E+13	0.00	3.989E+03	2.640E+13	0.00	2.517E+04
16 CH <sub>2</sub> O+O = HCO+OH	5.000E+13	0.00	4.600E+03	1.750E+12	0.00	1.717E+04
17 CH <sub>2</sub> O+OH = HCO+H <sub>2</sub> O	3.000E+13	0.00	1.194E+03	2.590E+12	0.00	2.999E+04
<b>HCO Formation and Consumption</b>						
18 HCO = H+CO	2.500E+14	0.00	1.680E+04	6.900E+14	0.00	1.670E+03
19 HCO+H = CO+H <sub>2</sub>	2.000E+14	0.00	0.000E+00	1.310E+15	0.00	9.000E+04
20 HCO+O = CO+OH	3.020E+13	0.00	0.000E+00	8.697E+13	0.00	8.790E+04

TABLE 1.(continued)

21	HCO+O	= CO <sub>2</sub> +H	3.000E+13	0.00	0.000E+00	3.230E+15	0.00	1.102E+05
22	HCO+OH	= CO+H <sub>2</sub> O	5.000E+13	0.00	0.000E+00	8.574E+14	0.00	1.052E+05
23	HCO+O <sub>2</sub>	= CO+HO <sub>2</sub>	3.000E+12	0.00	0.000E+00	6.730E+12	0.00	3.229E+04
HC Formation and Consumption								
24	CH+O	= CO+H	4.000E+13	0.00	0.000E+00	2.774E+15	0.00	1.760E+05
25	CH+O <sub>2</sub>	= CO+OH	1.350E+11	0.67	2.570E+04	5.187E+11	0.67	1.856E+05
C <sub>2</sub> H <sub>6</sub> Formation and Consumption								
26	C <sub>2</sub> H <sub>6</sub>	= CH <sub>3</sub> +CH <sub>3</sub>	2.500E+19	-1.00	8.831E+04	2.400E+14	-0.40	0.000E+00
27	C <sub>2</sub> H <sub>6</sub> +H	= C <sub>2</sub> H <sub>5</sub> +H <sub>2</sub>	5.370E+02	3.50	5.200E+03	9.720E+02	3.50	2.732E+04
28	C <sub>2</sub> H <sub>6</sub> +OH	= C <sub>2</sub> H <sub>5</sub> +H <sub>2</sub> O	6.300E+06	2.00	6.450E+02	1.010E+07	2.06	2.298E+04
29	C <sub>2</sub> H <sub>6</sub> +O	= C <sub>2</sub> H <sub>5</sub> +OH	1.400E+07	2.00	4.000E+03	2.570E+06	2.00	8.873E+03
C <sub>2</sub> H <sub>5</sub> Formation and Consumption								
30	C <sub>2</sub> H <sub>5</sub> +H	= CH <sub>3</sub> +CH <sub>3</sub>	3.160E+13	0.00	0.000E+00	8.000E+14	0.00	2.651E+04
31	C <sub>2</sub> H <sub>5</sub>	= C <sub>2</sub> H <sub>4</sub> +H	2.000E+13	0.00	3.965E+04	7.800E+08	1.00	-3.000E+03
32	C <sub>2</sub> H <sub>5</sub> +O <sub>2</sub>	= C <sub>2</sub> H <sub>4</sub> +HO <sub>2</sub>	2.000E+12	0.00	5.000E+03	2.000E+11	0.00	1.750E+04
C <sub>2</sub> H <sub>4</sub> Formation and Consumption								
33	C <sub>2</sub> H <sub>4</sub> +H <sub>2</sub>	= CH <sub>3</sub> +CH <sub>3</sub>	5.630E+19	-0.54	8.971E+04	1.000E+16	0.00	3.203E+04
34	C <sub>2</sub> H <sub>4</sub> +OH	= C <sub>2</sub> H <sub>3</sub> +H <sub>2</sub> O	3.000E+13	0.00	2.986E+03	1.015E+13	0.00	2.022E+04
35	C <sub>2</sub> H <sub>4</sub> +O	= CH <sub>3</sub> +HCO	6.400E+10	0.63	1.370E+03	1.574E+11	0.00	3.118E+04
C <sub>2</sub> H <sub>3</sub> Formation and Consumption								
36	C <sub>2</sub> H <sub>3</sub> +H	= C <sub>2</sub> H <sub>2</sub> +H <sub>2</sub>	2.000E+13	0.00	0.000E+00	1.331E+13	0.00	6.808E+04
37	C <sub>2</sub> H <sub>3</sub> +O <sub>2</sub>	= C <sub>2</sub> H <sub>2</sub> +HO <sub>2</sub>	1.000E+12	0.00	0.000E+00	7.751E+11	0.00	1.983E+04
38	C <sub>2</sub> H <sub>3</sub>	= C <sub>2</sub> H <sub>2</sub> +H	1.600E+14	0.00	3.798E+04	5.500E+12	0.00	2.410E+03
C <sub>2</sub> H <sub>2</sub> Formation and Consumption								
39	C <sub>2</sub> H <sub>2</sub> +O	= CH <sub>2</sub> +CO	4.100E+08	1.50	1.696E+03	1.260E+13	0.00	5.467E+04
40	C <sub>2</sub> H <sub>2</sub> +O	= HCCO+H	4.300E+14	0.00	1.211E+04	5.030E+02	2.70	1.279E+04
41	C <sub>2</sub> H <sub>2</sub> +OH	= CH <sub>2</sub> CO+H	3.200E+11	0.00	2.000E+02	3.158E+12	0.00	2.086E+04
CH <sub>2</sub> CO Formation and Consumption								
42	CH <sub>2</sub> CO+O	=HCO+HCO	1.000E+13	0.00	2.400E+03	3.500E+11	0.00	3.350E+04
43	CH <sub>2</sub> CO+OH	=CH <sub>2</sub> O+HCO	2.800E+13	0.00	0.000E+00	2.800E+13	0.00	1.850E+04
HCCO Formation and Consumption								
44	HCCO+H	= CH <sub>2</sub> +CO	3.000E+13	0.00	0.000E+00	6.660E+13	0.00	3.926E+04
45	HCCO+O	= HCO+CO	3.400E+13	0.00	2.000E+03	8.330E+13	0.00	1.283E+05
CO Formation and Consumption								

TABLE 1.(continued)

46	CO <sub>2</sub>	= CO+O	2.328E+19	-1.00	1.231E+05	7.100E+13	0.00	-4.538E+03
47	CO+OH	= CO <sub>2</sub> +H	4.400E+06	1.50	-7.404E+02	1.680E+09	1.30	2.157E+04
Chain Propagation and Branching								
48	H+O <sub>2</sub>	= OH+O	1.200E+17	-0.90	1.650E+04	1.305E+13	0.00	6.770E+02
49	O+H <sub>2</sub>	= H+OH	1.500E+07	2.00	7.548E+03	2.231E+04	2.67	4.197E+03
50	OH+H <sub>2</sub>	= H+H <sub>2</sub> O	1.000E+08	1.60	3.296E+03	9.352E+08	1.51	1.858E+04
51	H <sub>2</sub> O+O	= OH+OH	1.213E+05	2.62	1.537E+04	1.230E+04	2.62	-1.878E+03
Recombination and Dissociation Reactions								
52	H <sub>2</sub>	= H+H	1.735E+21	-1.60	1.074E+05	9.200E+16	-0.60	0.000E+00
53	H <sub>2</sub> O	= H+OH	1.837E+27	-3.00	1.226E+05	2.250E+22	-2.00	0.000E+00
Formation and Consumption of HO <sub>2</sub>								
54	HO <sub>2</sub>	= H+O <sub>2</sub>	3.574E+24	-2.74	5.162E+04	2.000E+18	-0.80	0.000E+00
55	HO <sub>2</sub> +H	= OH+OH	1.500E+14	0.00	1.000E+03	2.863E+14	-0.33	4.027E+04
56	HO <sub>2</sub> +H	= H <sub>2</sub> +O <sub>2</sub>	2.500E+13	0.00	7.000E+02	5.500E+13	0.00	5.780E+04
57	HO <sub>2</sub> +OH	= H <sub>2</sub> O+O <sub>2</sub>	2.000E+13	0.00	0.000E+00	2.220E+16	-0.68	7.097E+04

TABLE 2.

---


$$\phi_1 = 1.0 \rightarrow \phi_2 = 0.5: \quad \log S_L = 2.4149T^* - 3.5161$$

$$\phi_1 = 1.0 \rightarrow \phi_2 = 0.4: \quad \log S_L = 3.0937T^* - 4.9902$$

$$\phi_1 = 0.8 \rightarrow \phi_2 = 0.4: \quad \log S_L = 3.4144T^* - 5.4859$$

$$\phi_1 = 0.7 \rightarrow \phi_2 = 0.4: \quad \log S_L = 4.0700T^* - 6.4650$$

$$\phi_1 = 0.6 \rightarrow \phi_2 = 0.4: \quad \log S_L = 5.4096T^* - 8.4695$$

,where  $T^* = T_b/1000$

---

TABLE 3.

---


$$\phi_1 \rightarrow \phi_2 = 0.4: \quad \log S_L = aT^* - b$$

,where  $T^* = T_b/1000$

$$a = -44.229\phi_1^3 + 127.08\phi_1^2 - 122.43\phi_1 + 42.672$$

$$b = 67.238\phi_1^3 - 192.47\phi_1^2 + 184.86\phi_1 - 64.622$$


---



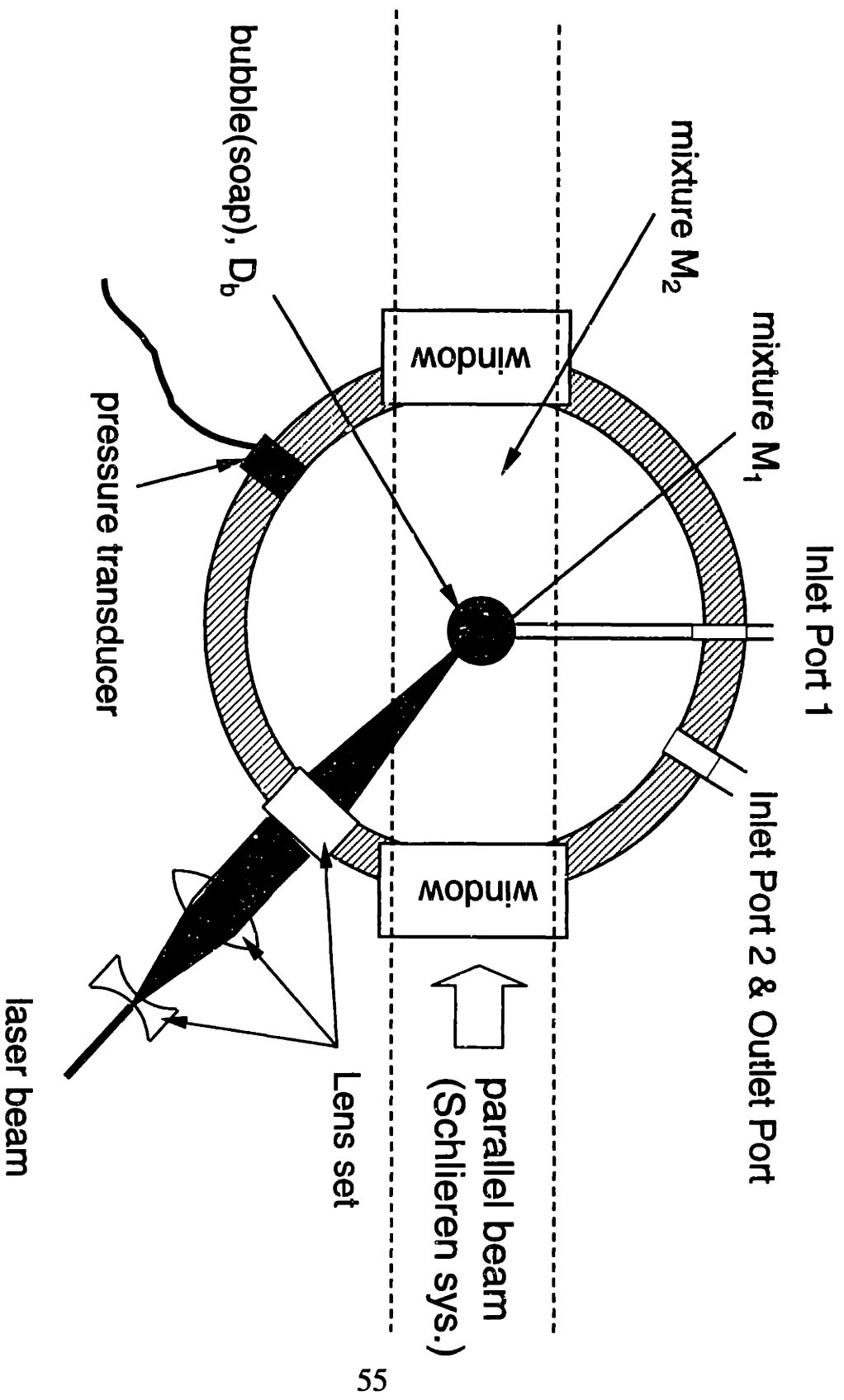


Fig. 2.1 Schematic diagram of the constant volume combustion vessel.

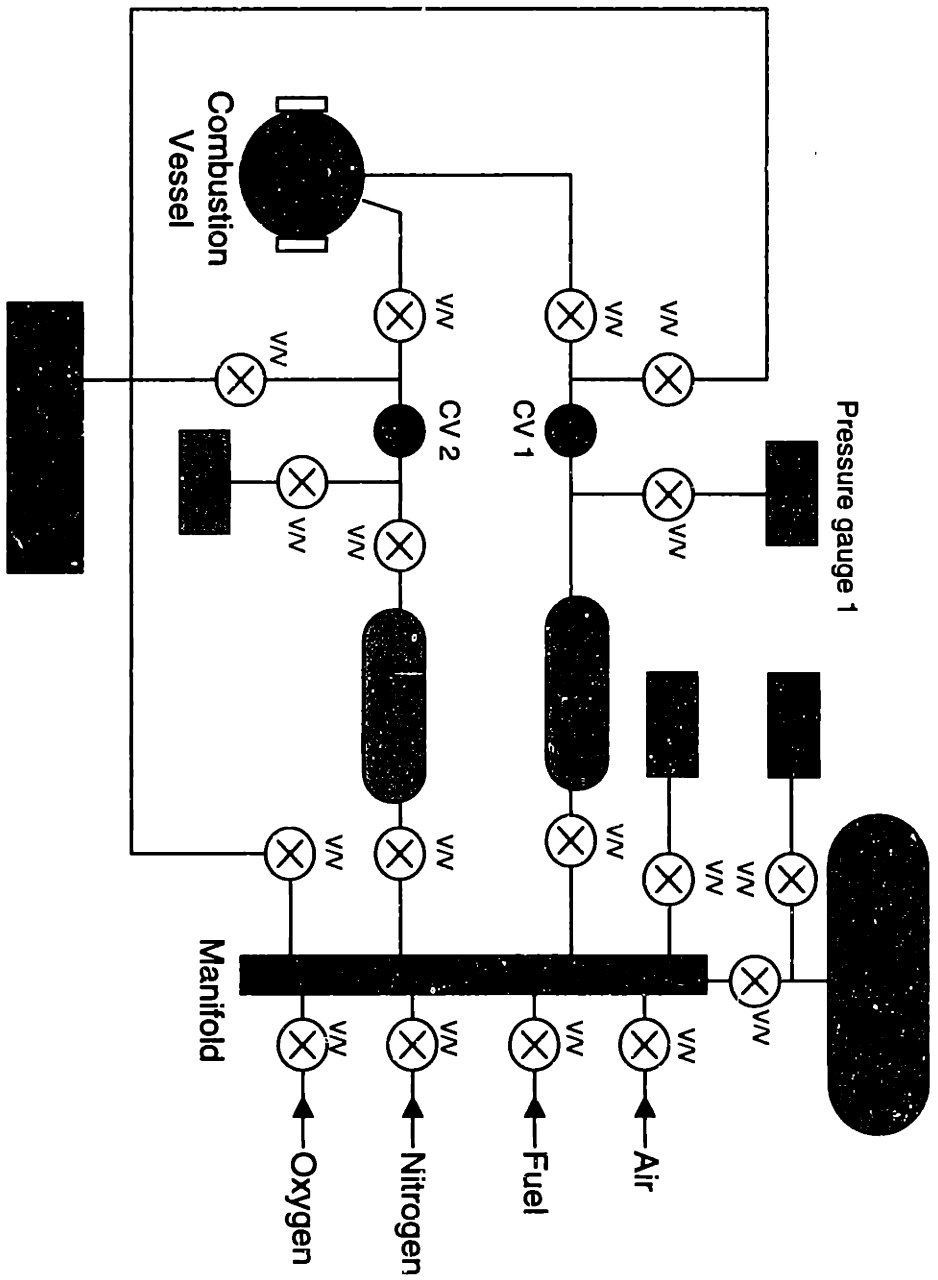


Fig. 2.2 Schematic diagram of the mixture preparation setup.



Fig. 2.3 Photo of a bubble at the center of the combustion vessel.

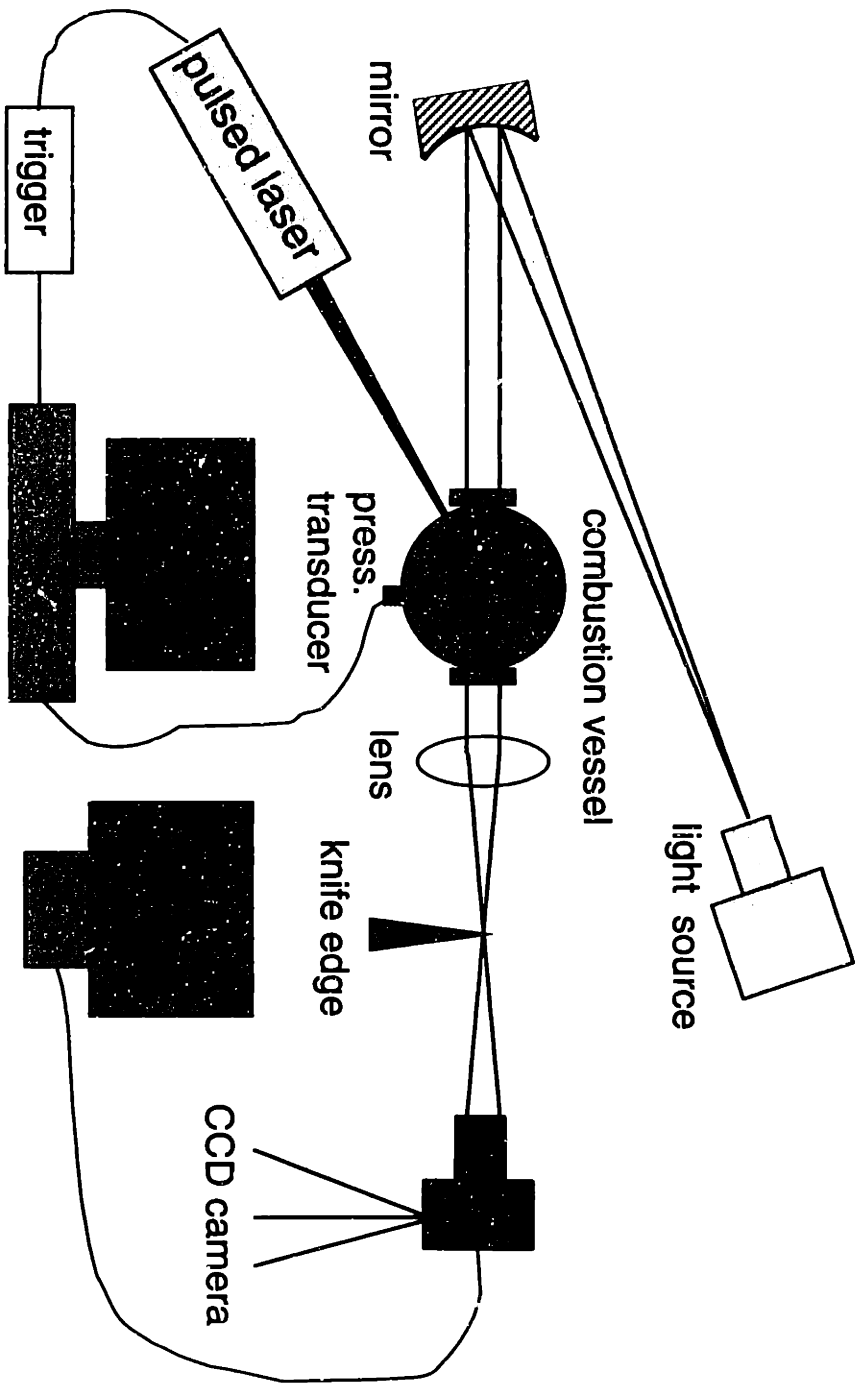


Figure 2.4 Schematic diagram of the experimental setup.

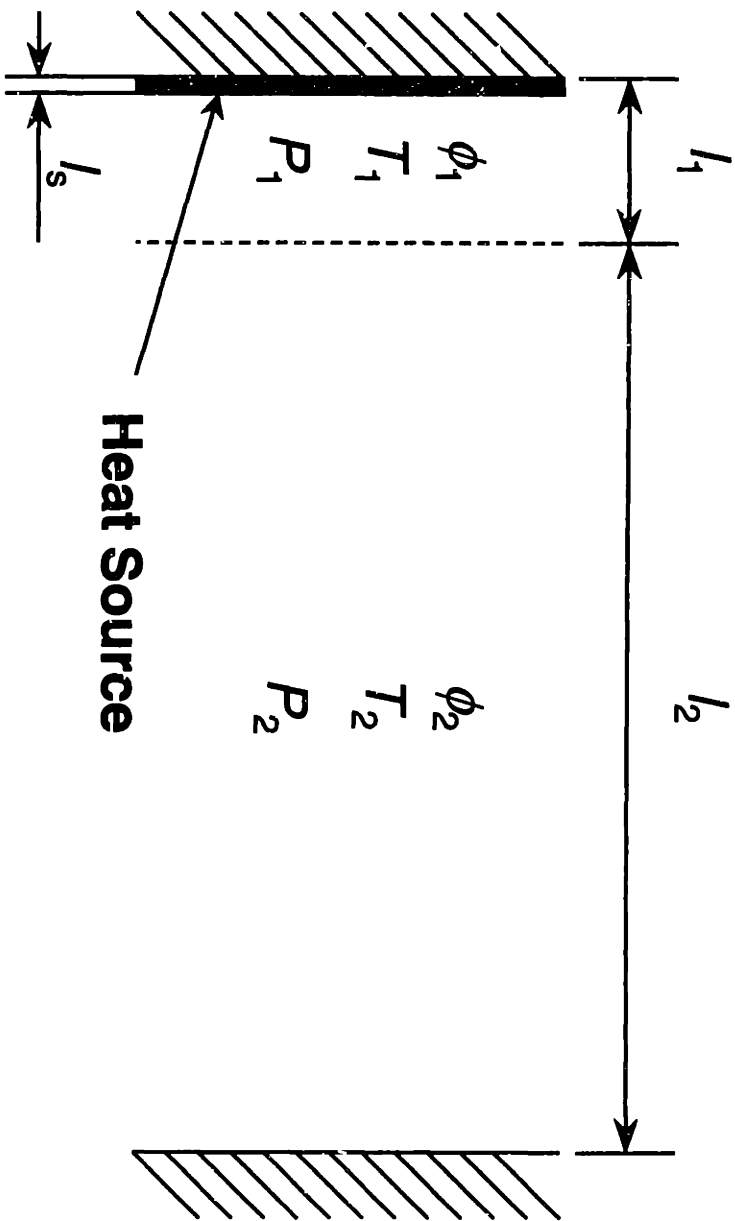


Fig. 3.1 Domain of numerical calculation.

$l_1 = 0.4$  cm,  $l_2 = 2.6$  cm,  $l_s = 0.012$  cm

$\phi_1 = 1.0$ ,  $\phi_2 = 0.5$

$T_1 = T_2 = T_i = 300$  K,  $P_1 = P_2 = P_i = 1$  bar

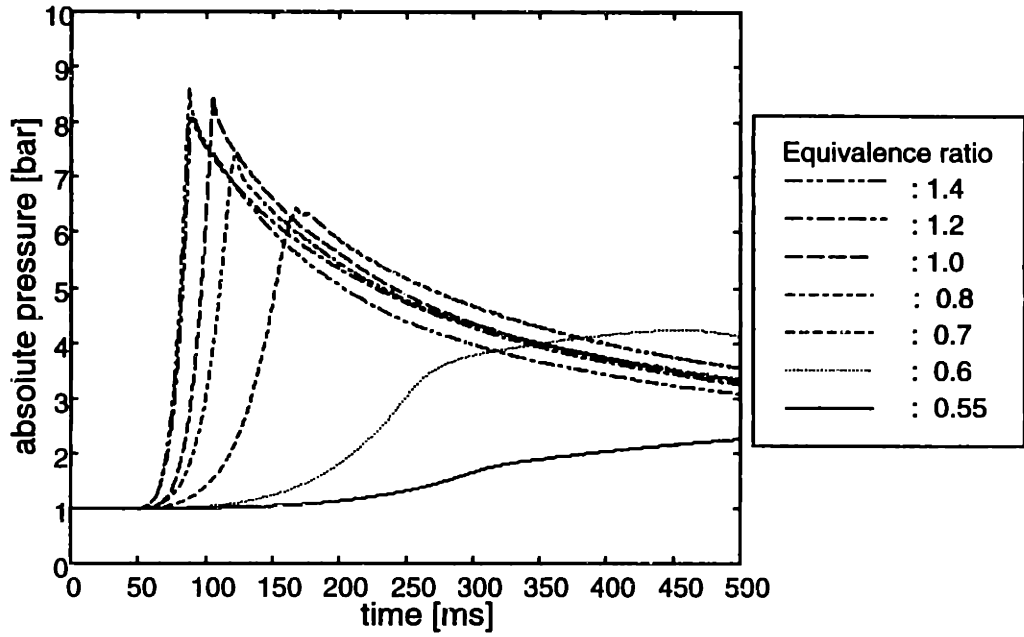


Fig. 4.1 Pressure trajectories of homogeneous charge burning (experiment).

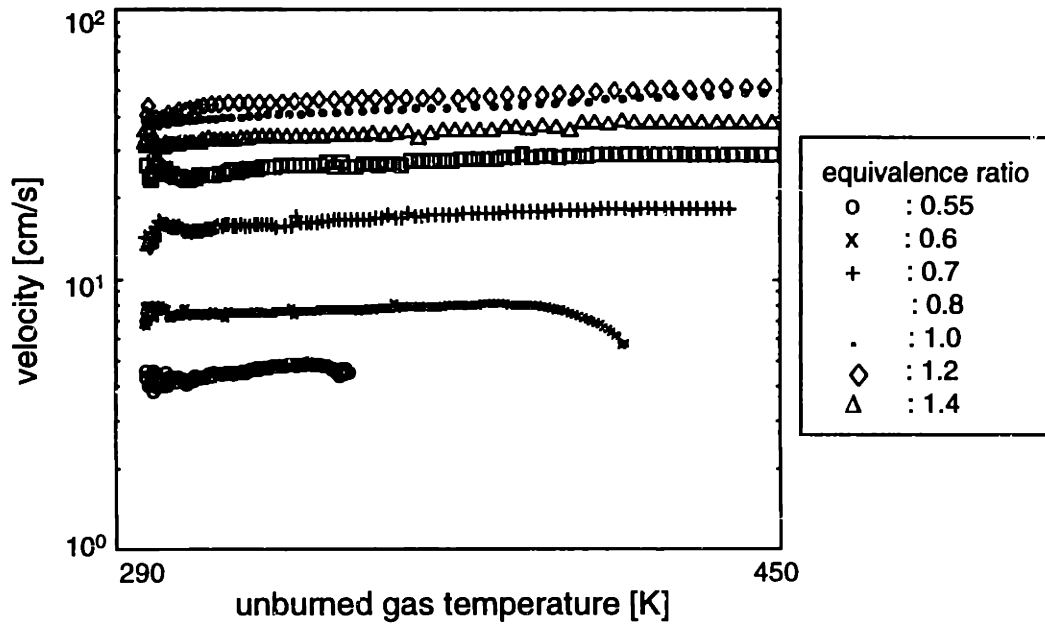


Fig. 4.2 Burning velocity profiles of homogeneous charge burning (experiment).

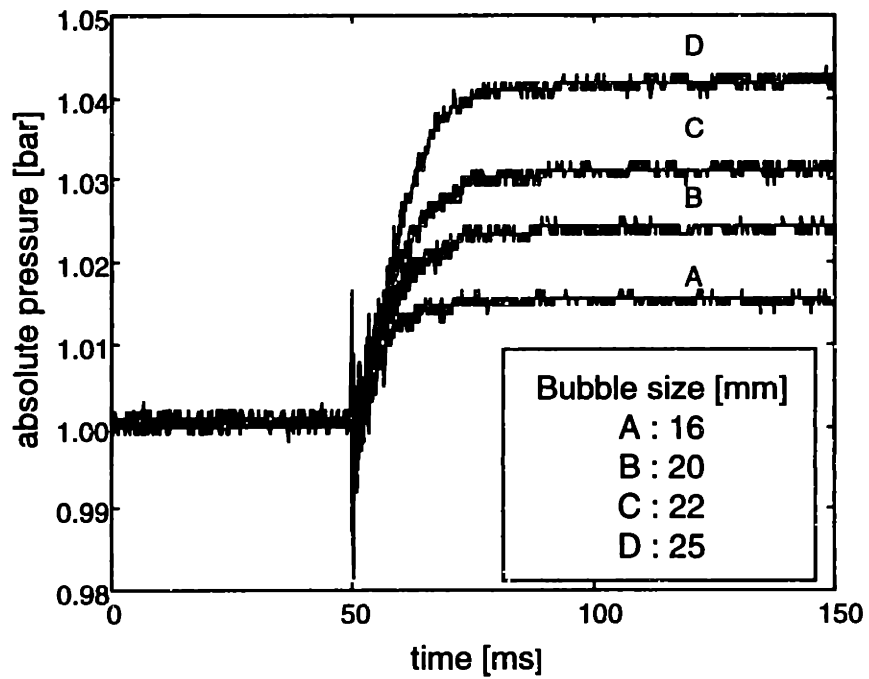


Fig. 4.3 Pressure trajectories of the burning of the mixture in bubble. Mixture = propane + air. Equivalence ratio:  $\phi_1=1.0$ ,  $\phi_2=0$  (air only).

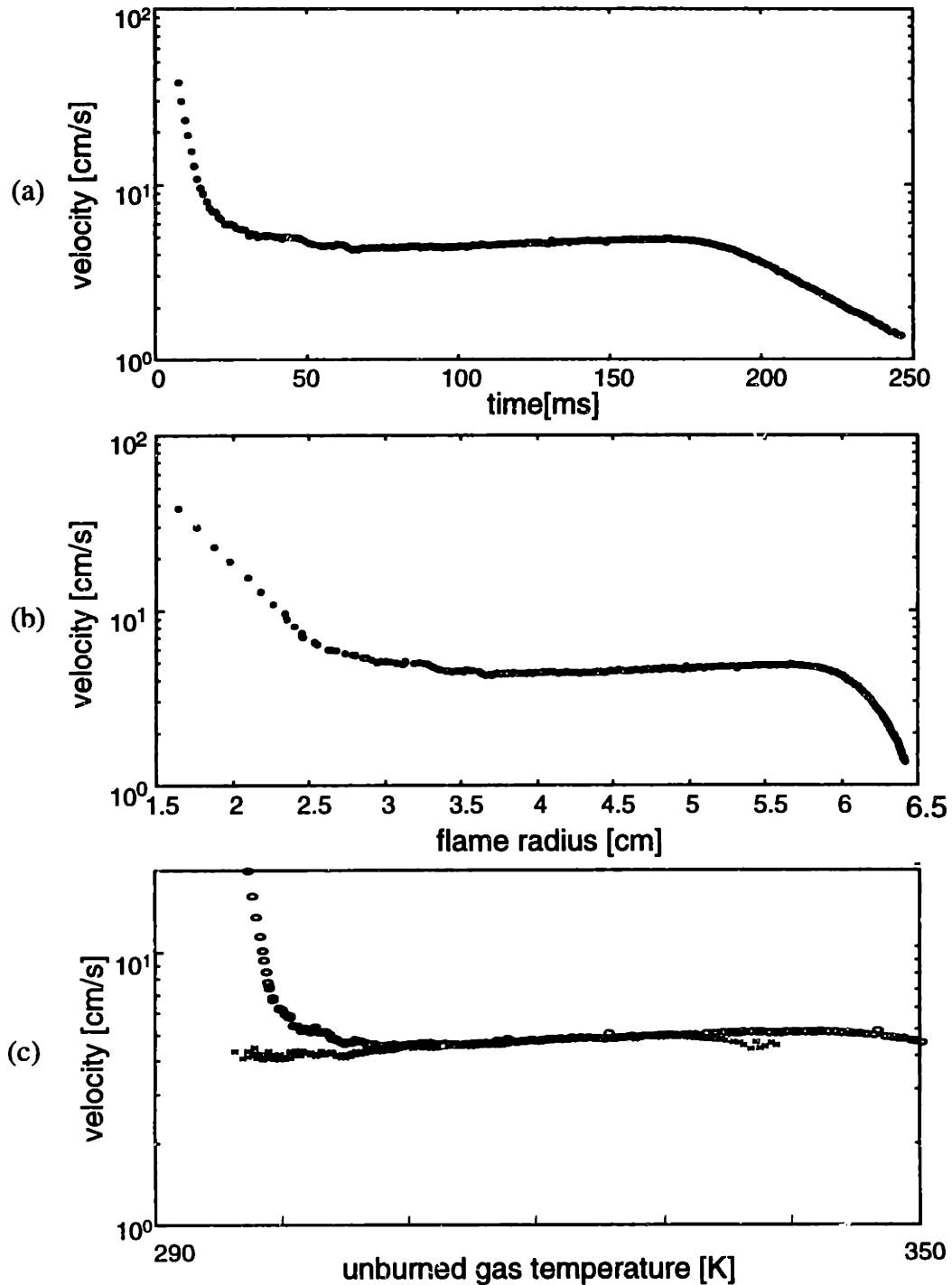


Fig. 4.4 Laminar flame behavior of stratified charge burning.  
 Equivalence ratio:  $\phi_1=1.0$ ,  $\phi_2=0.55$ , bubble size~15 mm.  
 (a) velocity w.r.t. time, (b) velocity w.r.t. flame radius, (c) velocity w.r.t. unburned gas; values for the homogeneous charge also plotted(as crosses)



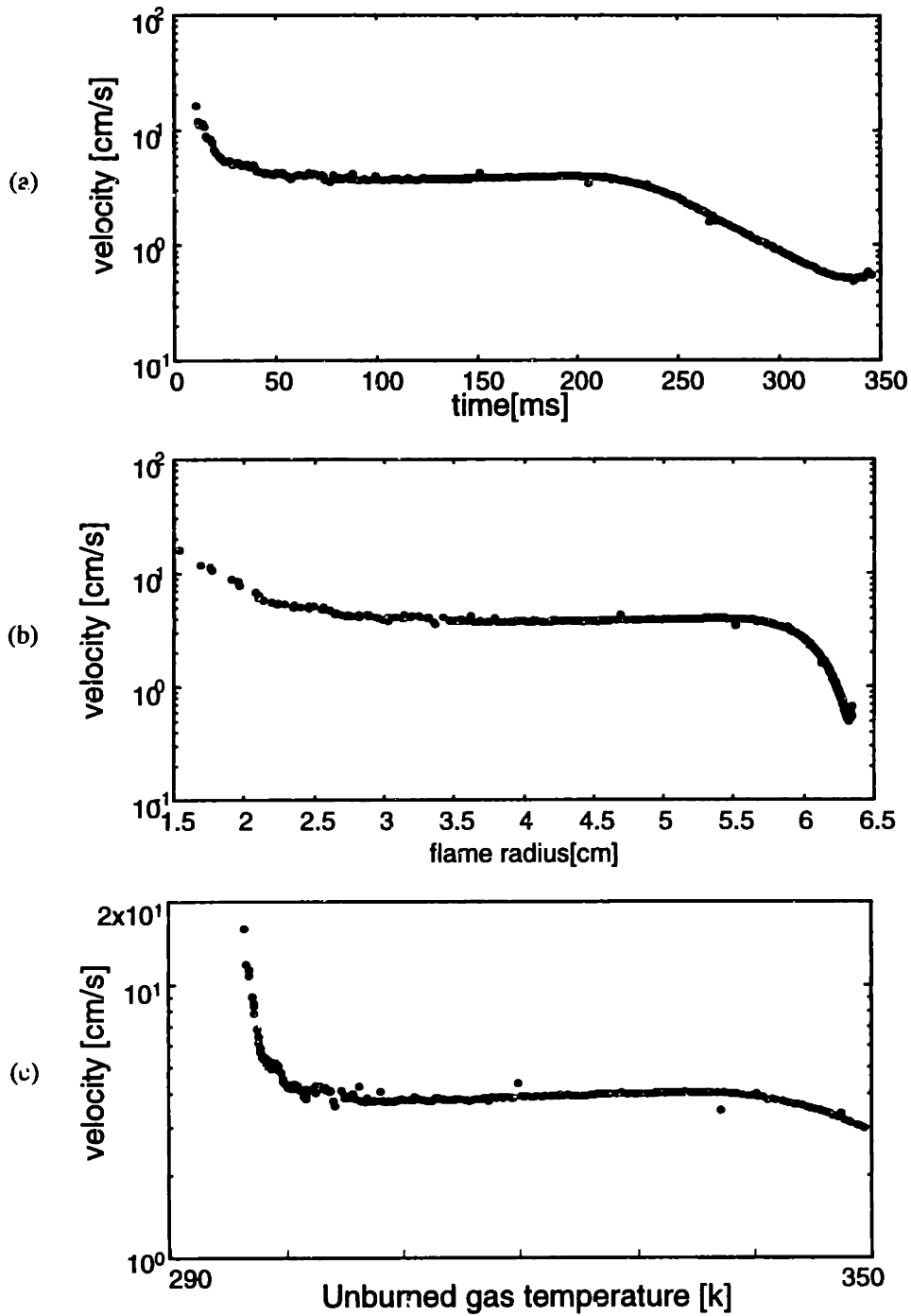


Fig. 4.5 Laminar flame behavior of stratified charge burning. Equivalence ratio  $\phi_1=1.0$ ,  $\phi_2=0.52$ . (a) velocity w.r.t. time, (b) velocity w.r.t. flame radius, (c) velocity w.r.t. unburned gas.

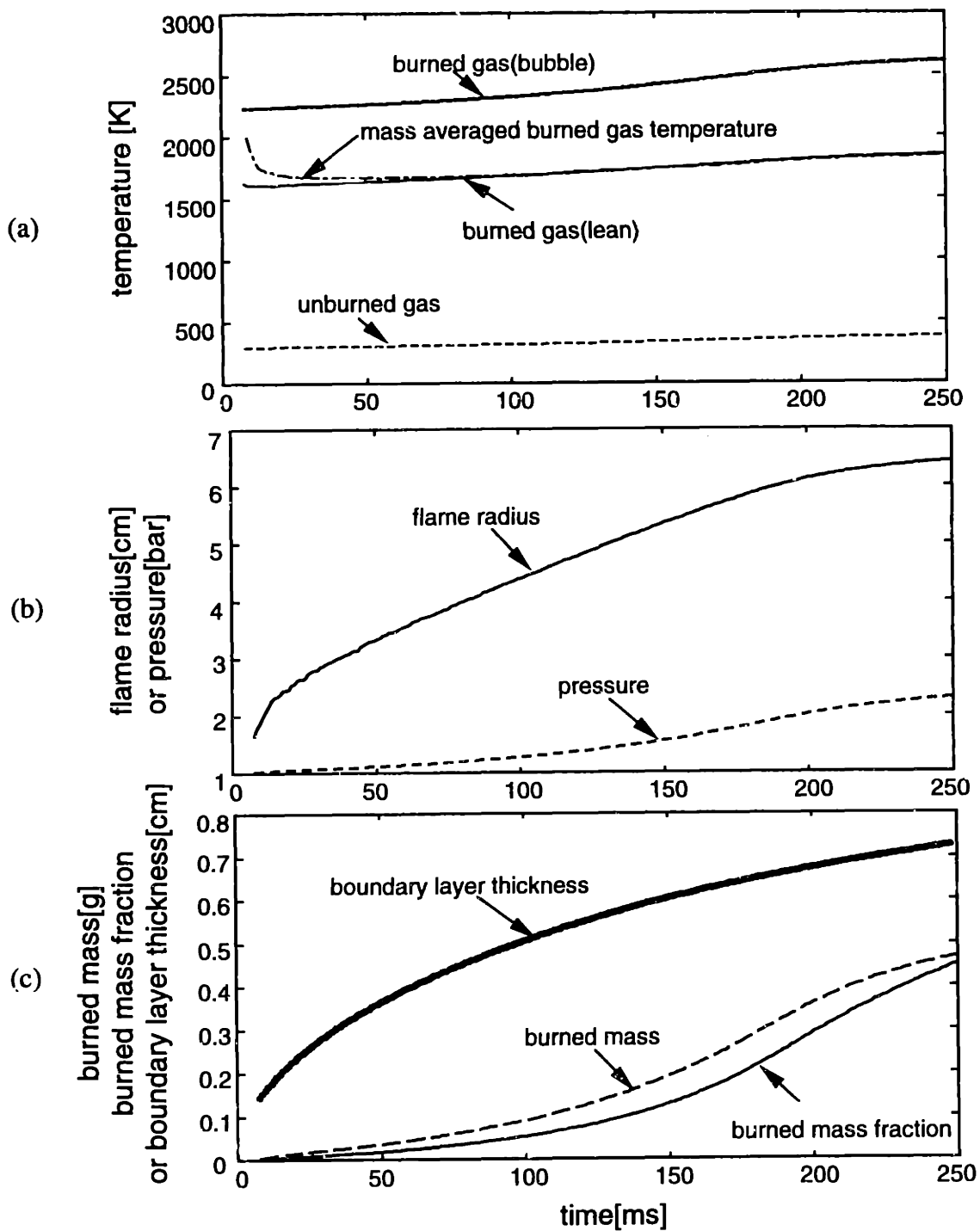


Fig. 4.6 Time history of the burning of stratified charge. Equivalence ratio:  $\phi_1=1.0$ ,  $\phi_2=0.55$ . (a) Temperature profiles of the unburned and burned gas of the lean mixture and the burned gas of the rich mixture, (b) Profiles of pressure and flame radius, (c) Profiles of burned mass, burned mass fraction and boundary layer thickness.

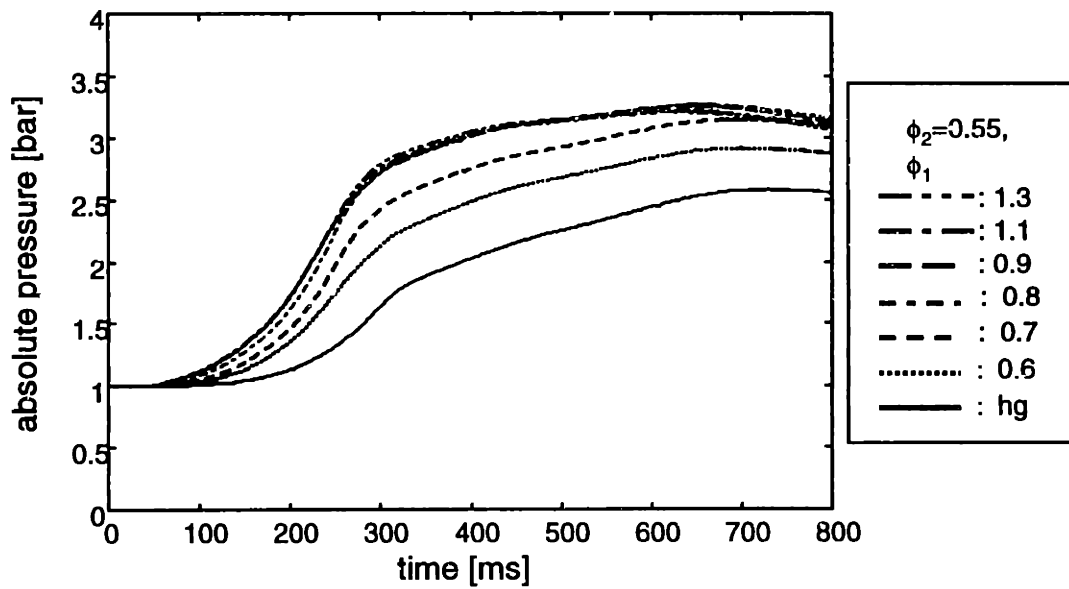


Fig. 4.7 Pressure trajectories of the stratified charge with various rich mixtures (experiment). Equivalence ratio:  $\phi_1=0.6 \sim 1.3$ ,  $\phi_2=0.55$ ;  $\phi_{hg}=0.55$ .

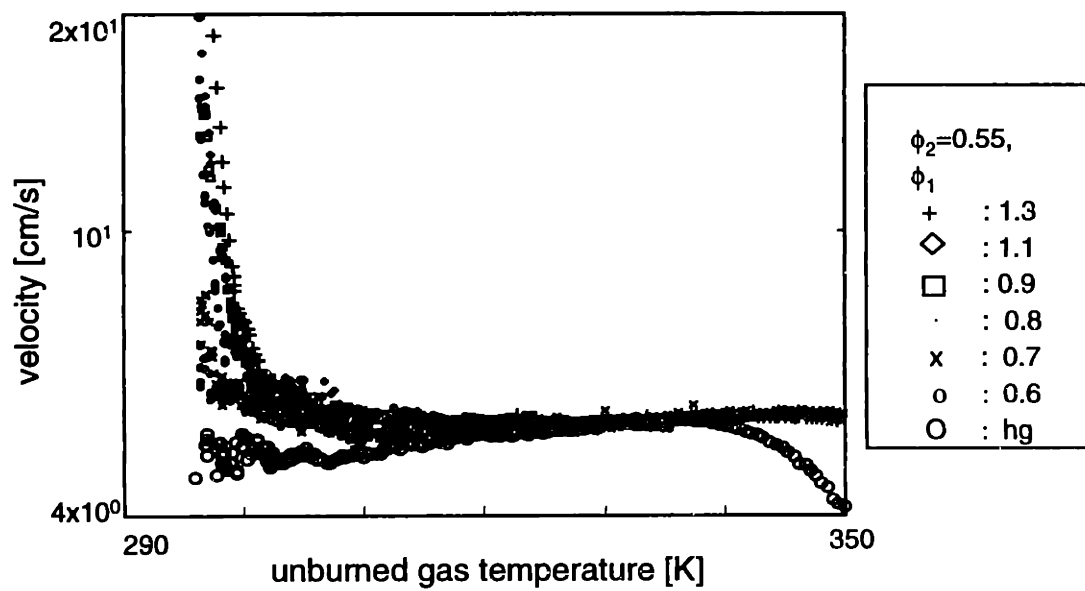


Fig. 4.8 Burning velocity profiles of the stratified charge with various rich mixtures (experiment). Equivalence ratio:  $\phi_1=0.6 \sim 1.3$ ,  $\phi_2=0.55$ ;  $\phi_{hg}=0.55$ .

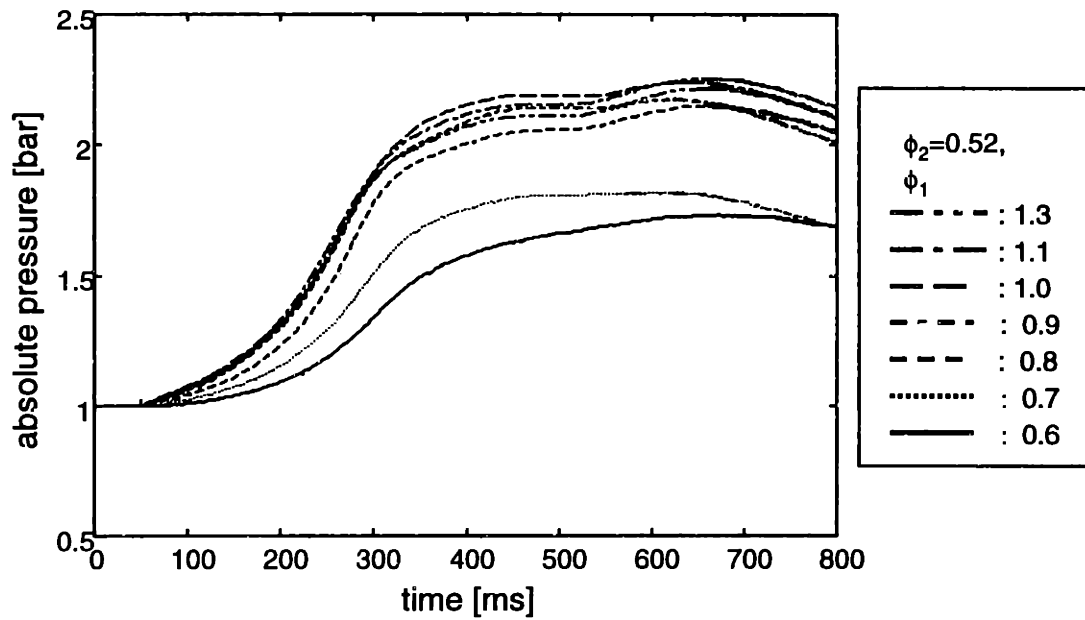


Fig. 4.9. Pressure trajectories of the stratified charge with various rich mixtures (experiment). Equivalence ratio:  $\phi_1=0.6 \sim 1.3$ ,  $\phi_2=0.52$ .

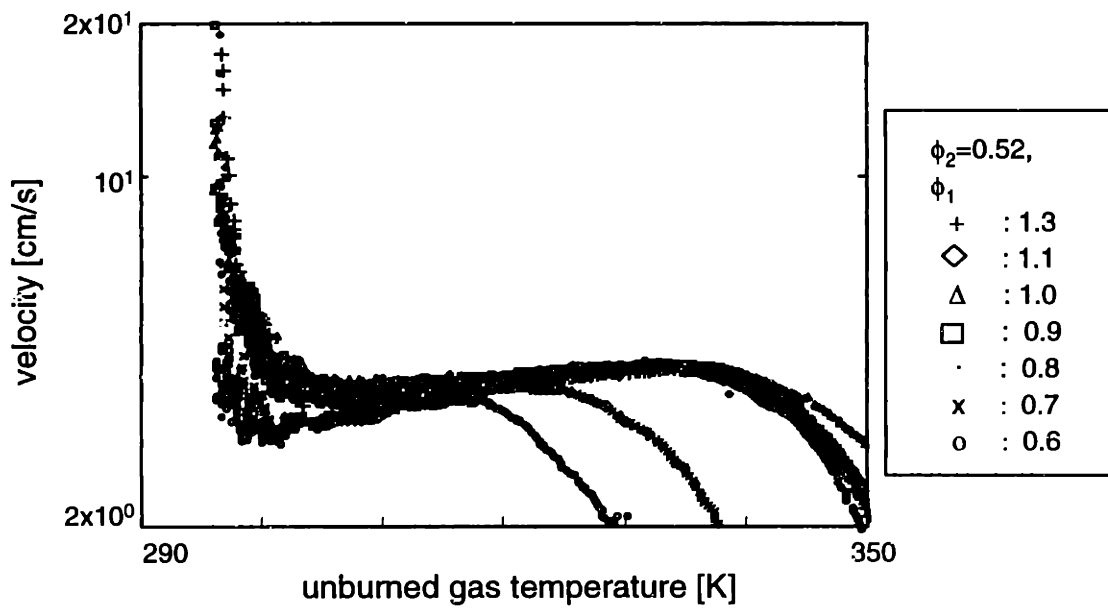


Fig. 4.10. Burning velocities profiles of the stratified charge with various rich mixtures (experiment). Equivalence ratio:  $\phi_1=0.6 \sim 1.3$ ,  $\phi_2=0.52$ .

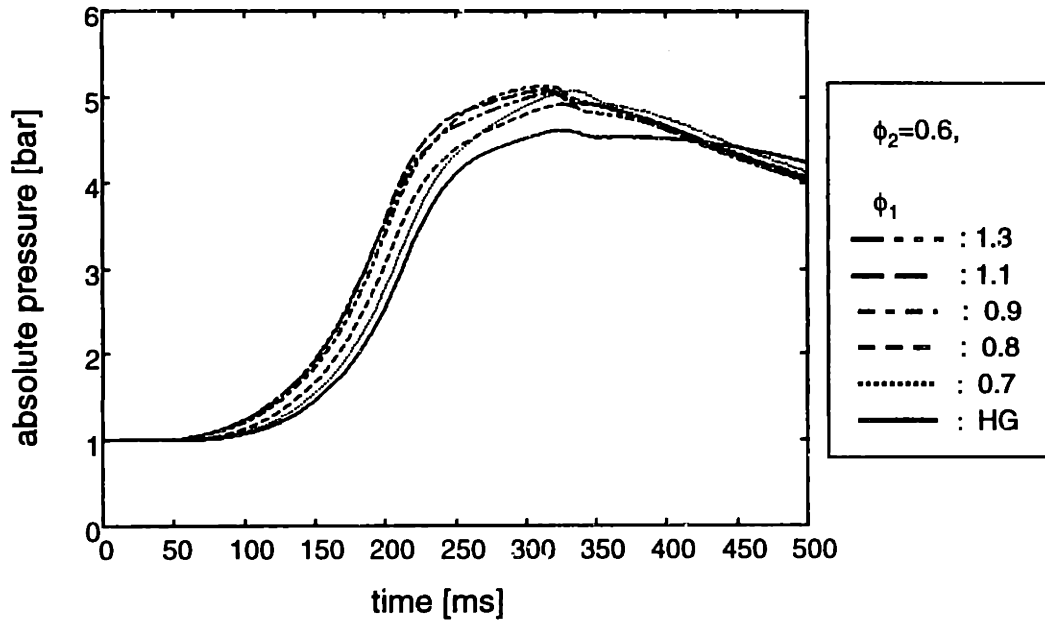


Fig. 4.11. Pressure trajectories of stratified charge burning with various rich mixtures (experiment). Equivalence ratio:  $\phi_1=0.7 \sim 1.3$ ,  $\phi_2=0.6$ ;  $\phi_{hg}=0.6$ .

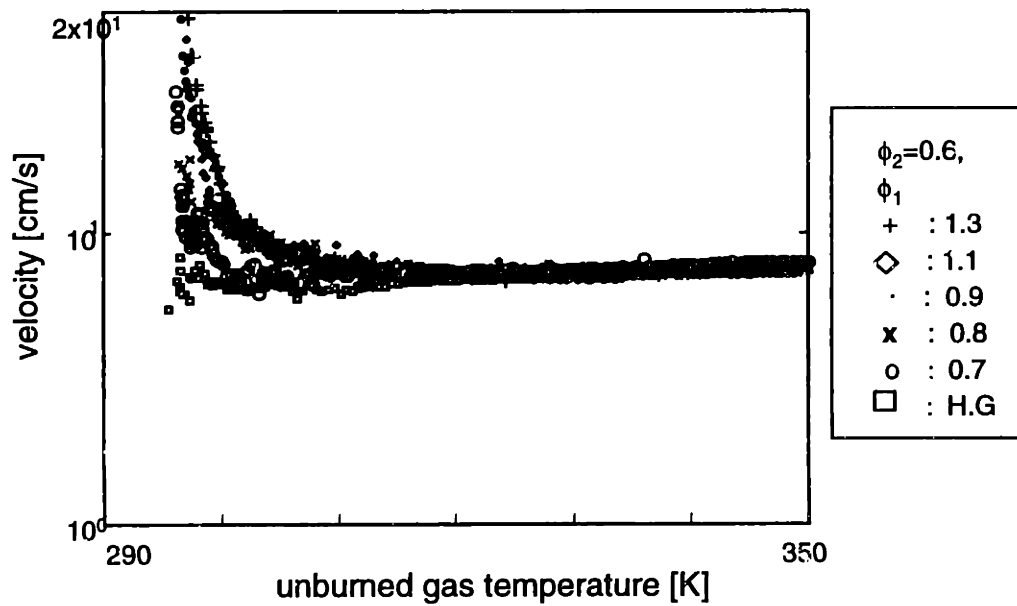


Fig. 4.12. Burning velocities profiles of stratified charge burning with various rich mixtures (experiment). Equivalence ratio:  $\phi_1=0.7 \sim 1.3$ ,  $\phi_2=0.6$ ;  $\phi_{hg}=0.6$ .

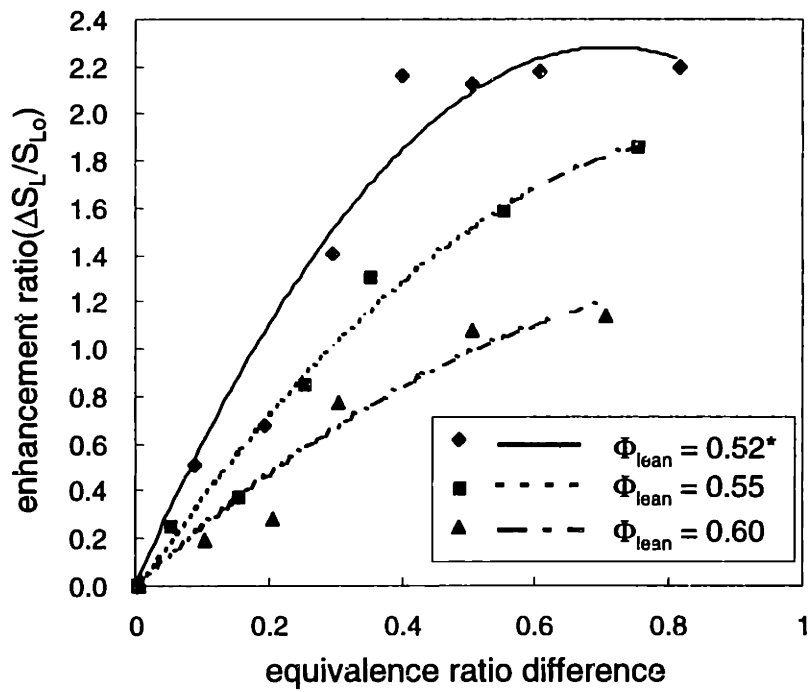


Fig. 4.13 The effect of equivalence ratio difference on the burning velocity enhancement. The second order curves are fitted to the experimental data.  
 \* the reference homogeneous velocity was extrapolated from the burning velocities of the  $\phi=0.55$  and  $\phi=0.6$  cases

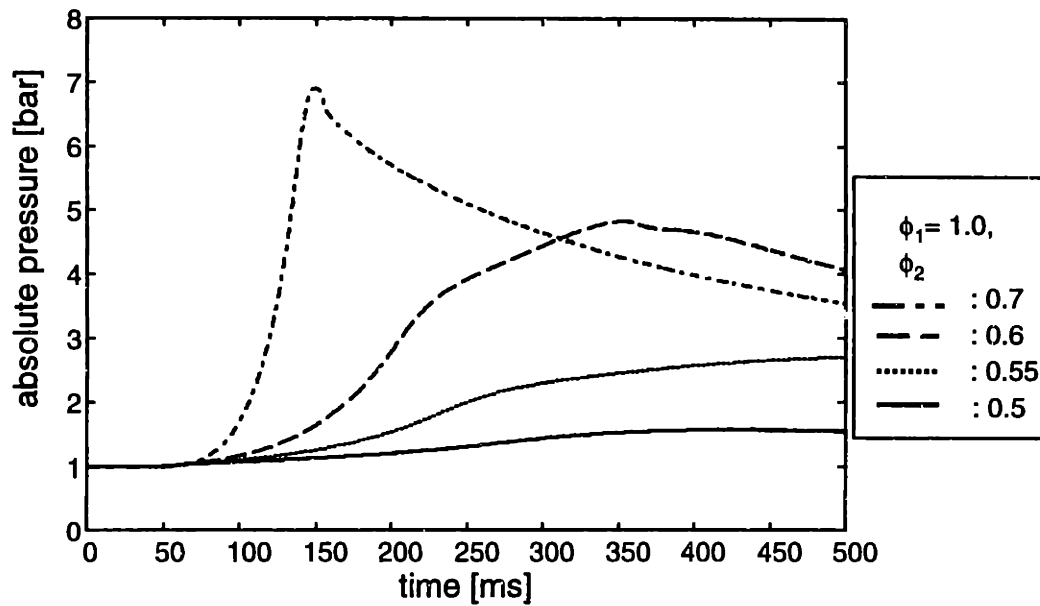


Fig. 4.14 Pressure trajectories of the stratified charge with various lean mixtures. Equivalence ratio:  $\phi_1=1.0$ ,  $\phi_2=0.5 \sim 0.7$ .

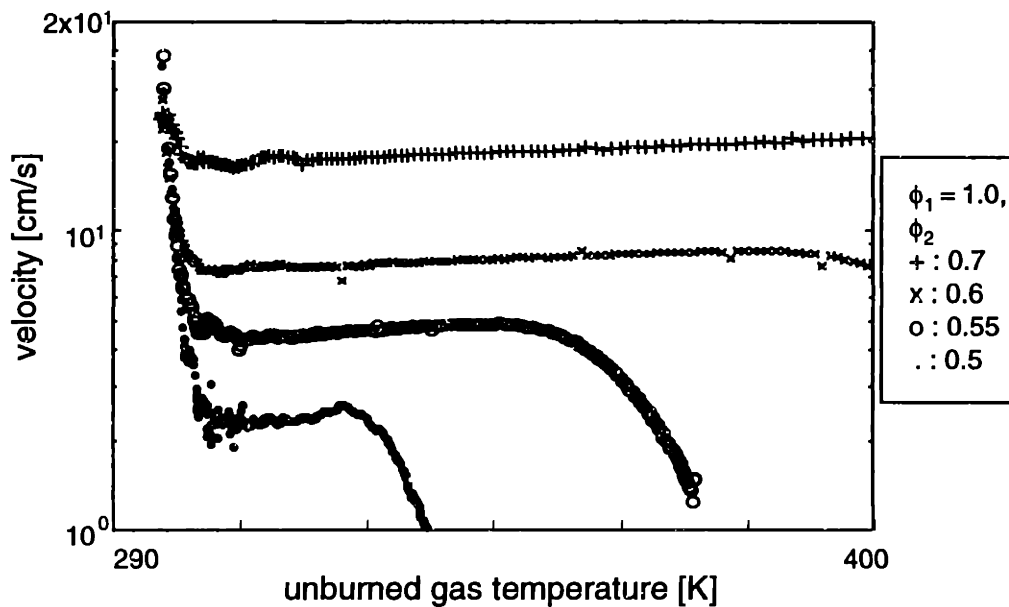


Fig. 4.15 Burning velocity profiles of the stratified charge with various lean mixtures. Equivalence ratio:  $\phi_1=1.0$ ,  $\phi_2=0.5 \sim 0.7$ .

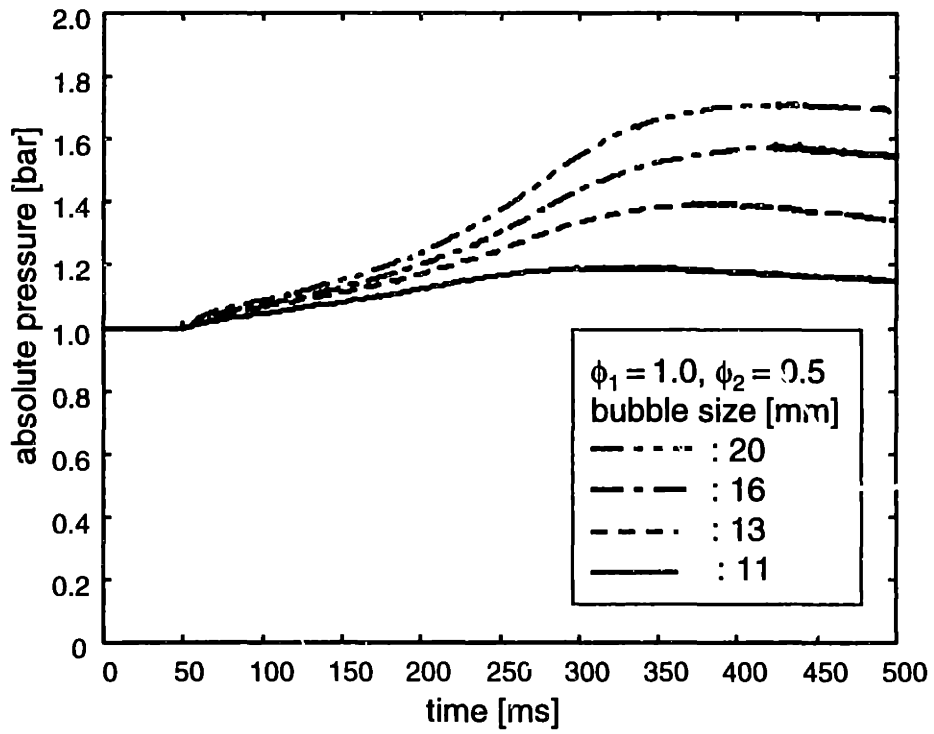


Fig. 4.16 Pressure trajectories of stratified charge burning for various size of region 1.



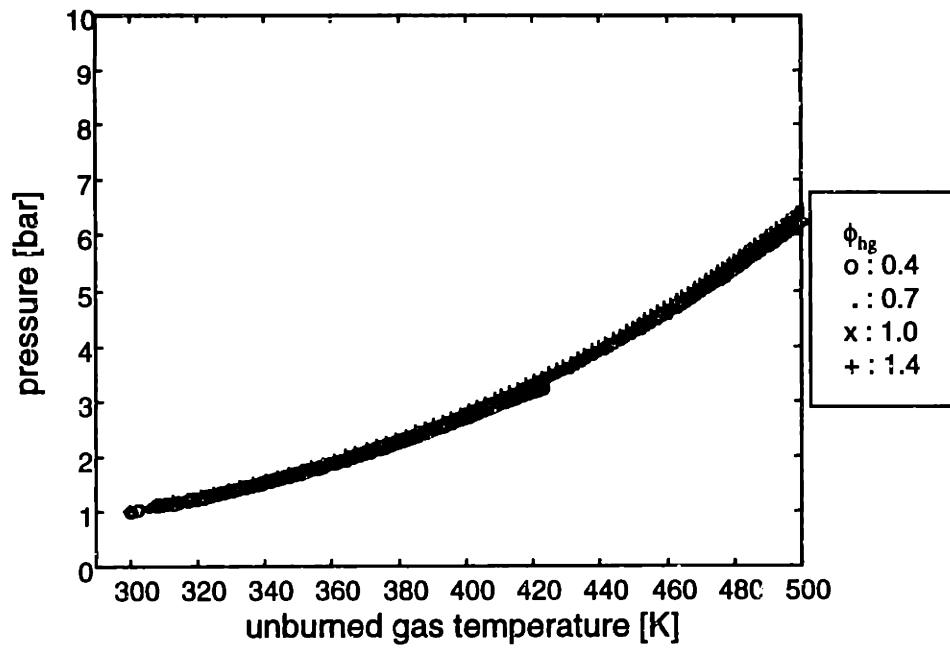


Fig. 4.17 Pressure trajectories of homogeneous charge burning (numerical simulation).

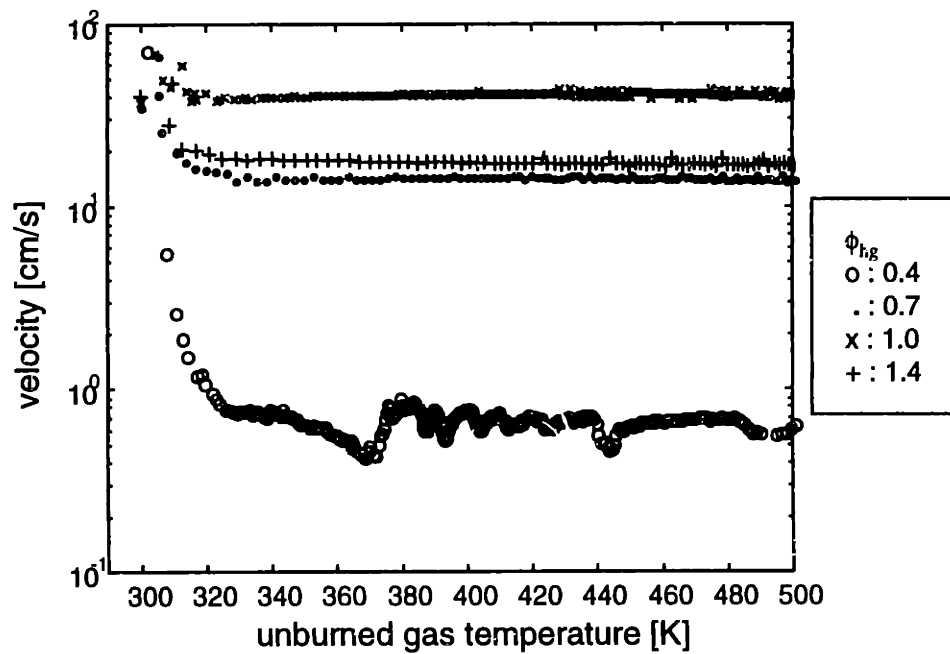


Fig. 4.18 Burning velocity profiles of homogeneous charge burning (numerical simulation).

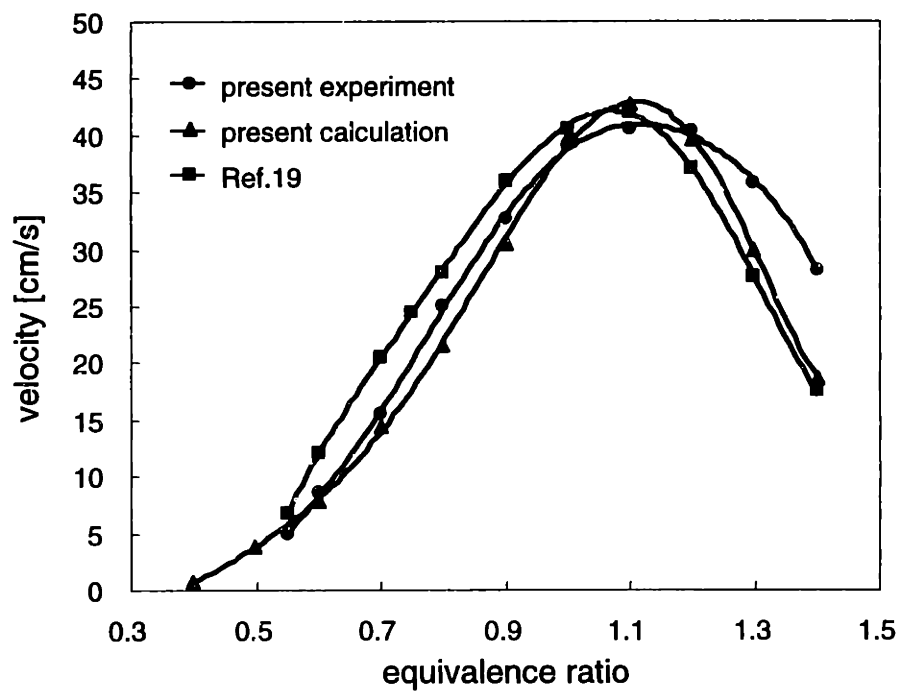


Fig. 4.19 Comparison of calculated burning velocity with experimental result and literature data. The present experimental results are at 300 K, 1.08 bar, the present calculational results are extrapolated to the condition of 300 K, 1 bar, and literature data are at 300 K and 1 atm.

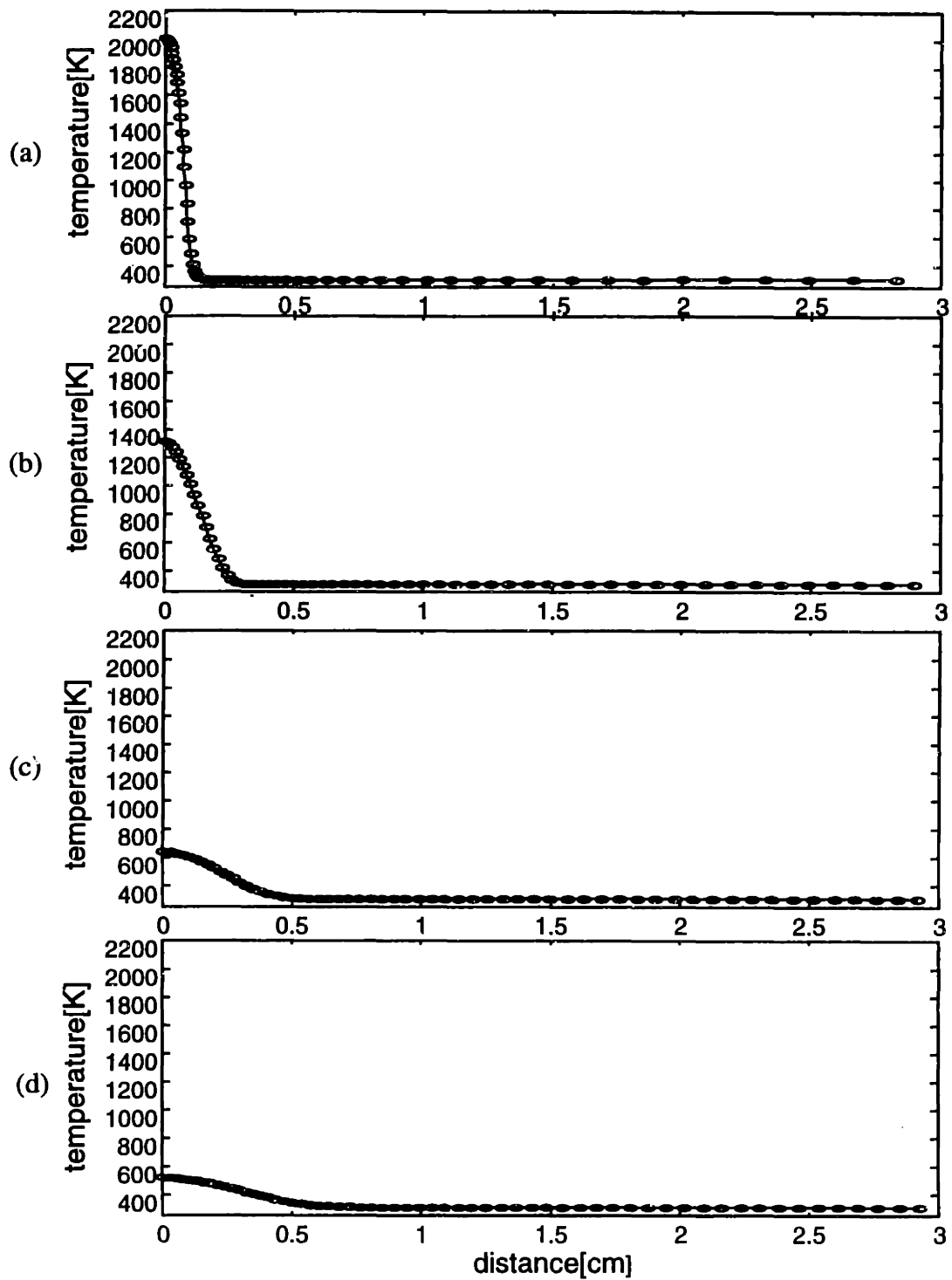


Fig. 4.20 Dynamic profiles of gas temperature in homogeneous charge burning. Equivalence ratio:  $\phi_{hg}=0.3$ . At lapsed time (a) 0.3 ms, (b) 6.6 ms, (c) 45 ms, (d) 105 ms.

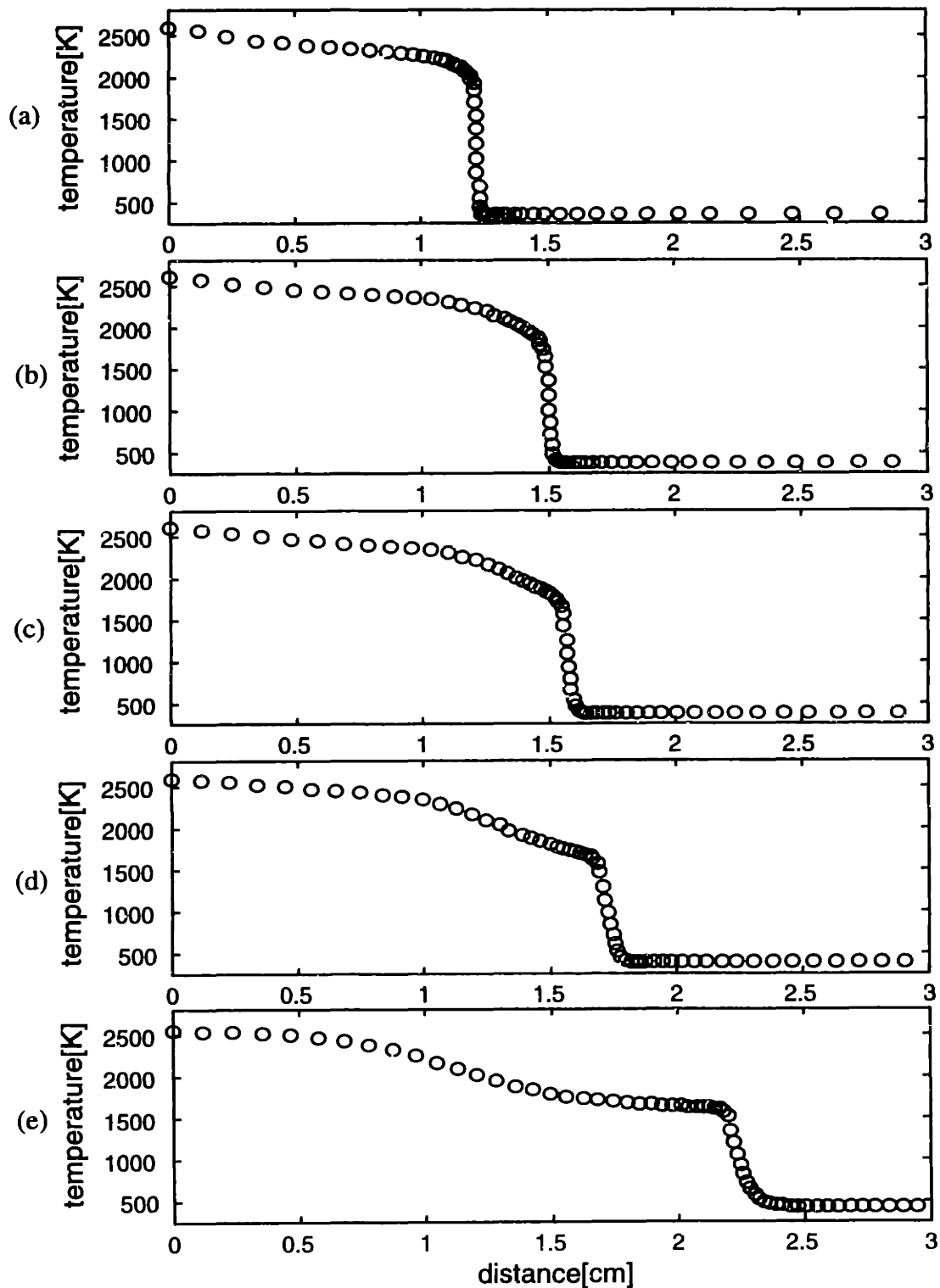


Fig. 4.21 Dynamic profiles of gas temperature in stratified charge burning. Equivalence ratio:  $\phi_1=1.0$ ,  $\phi_2=0.5$ . At lapsed time (a) 5 ms, (b) 8 ms, (c) 10 ms, (d) 20 ms, (e) 100 ms. The starting time at which flame begins to burn the lean mixture is 7.62 ms.

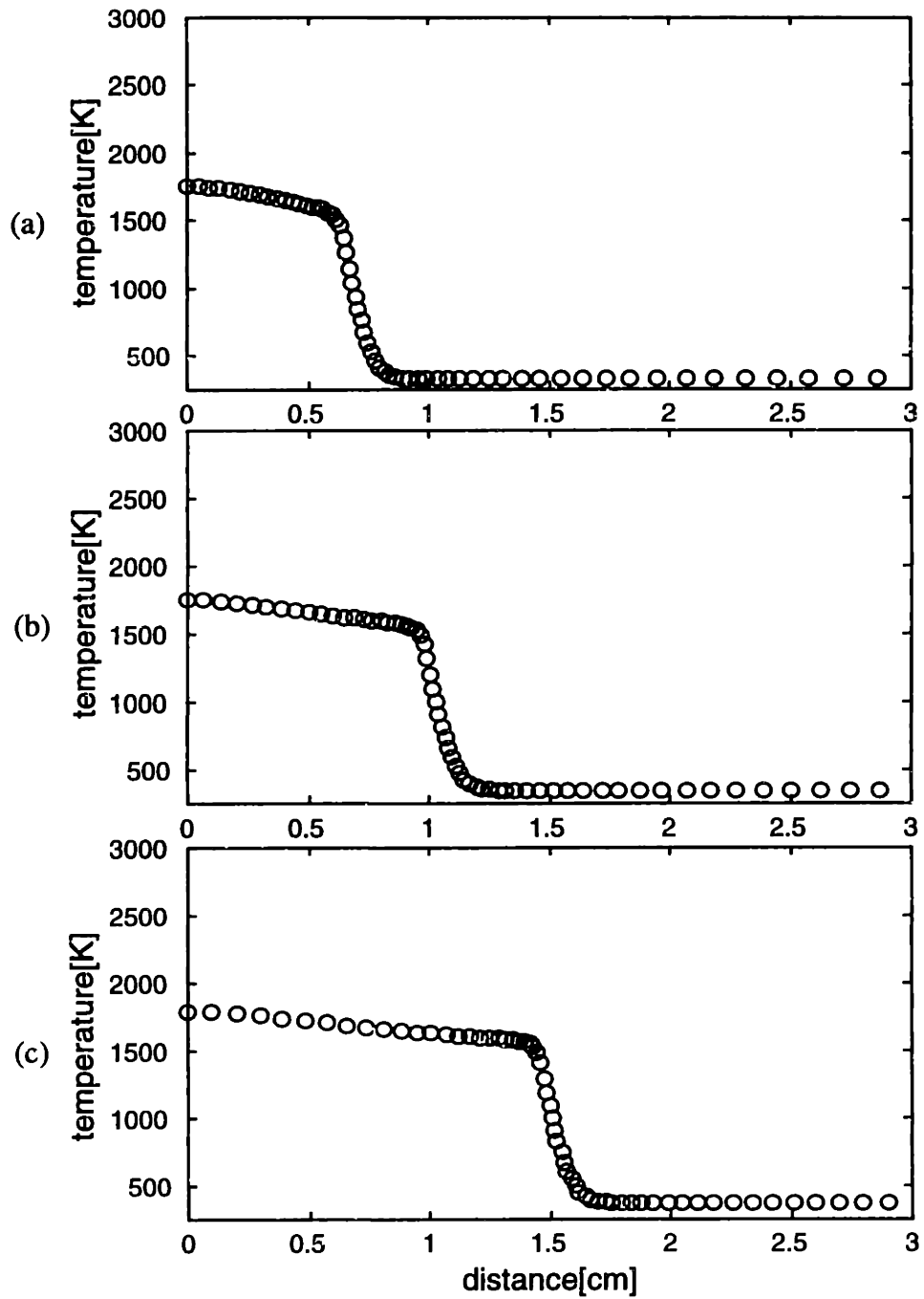


Fig. 4.22 Dynamic profiles of gas temperature in homogeneous charge burning. Equivalence ratio:  $\phi_{hg}=0.5$ . At lapsed time (a) 25 ms, (b) 50 ms, (c) 100ms.

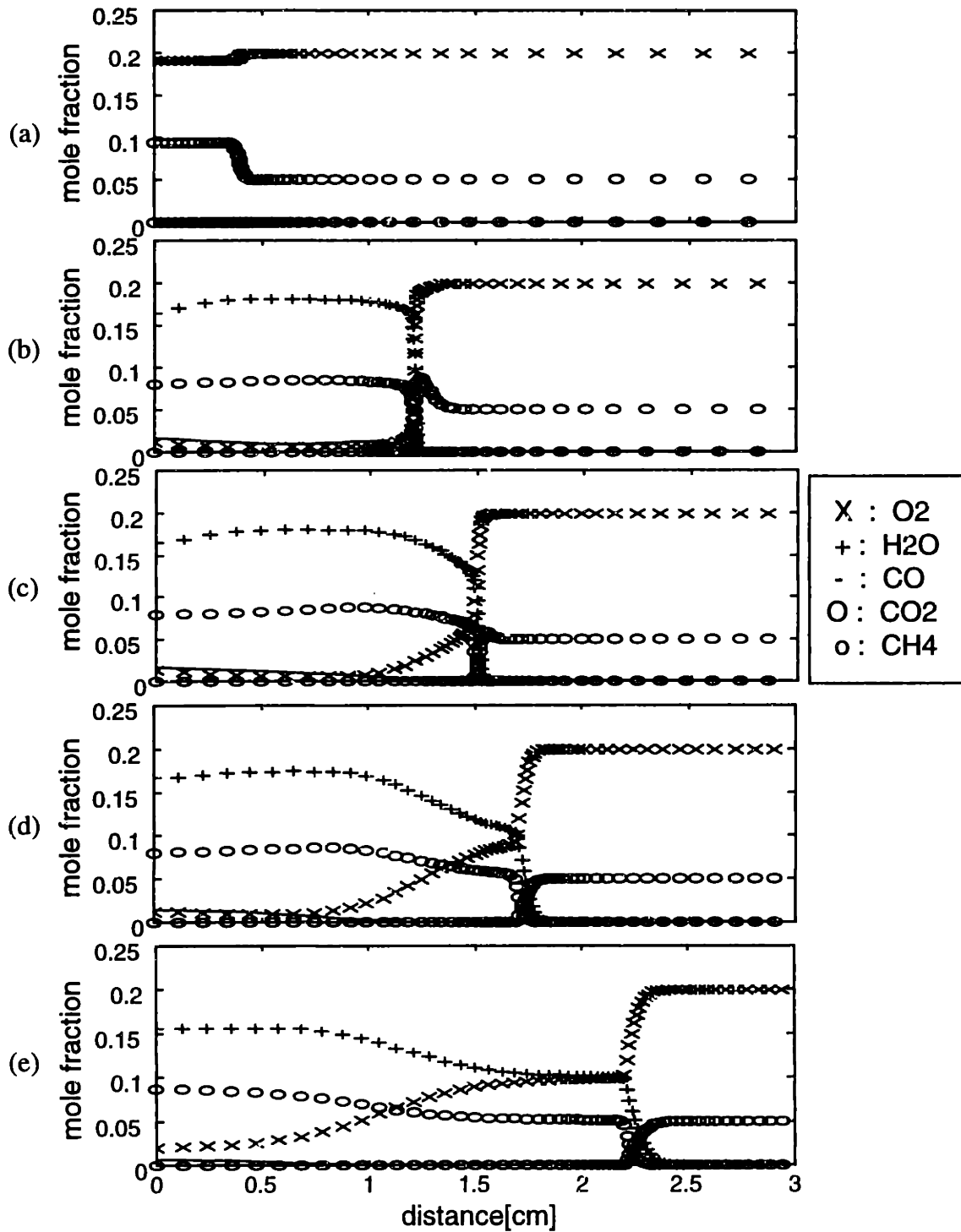


Fig. 4.23 Dynamic profiles of the mole fraction of major species in stratified charge burning. Equivalence ratio:  $\phi_1=1.0$ ,  $\phi_2=0.5$ . At lapsed time (a) 0 ms, (b) 5 ms, (c) 8 ms, (d) 20 ms, (e) 100 ms.

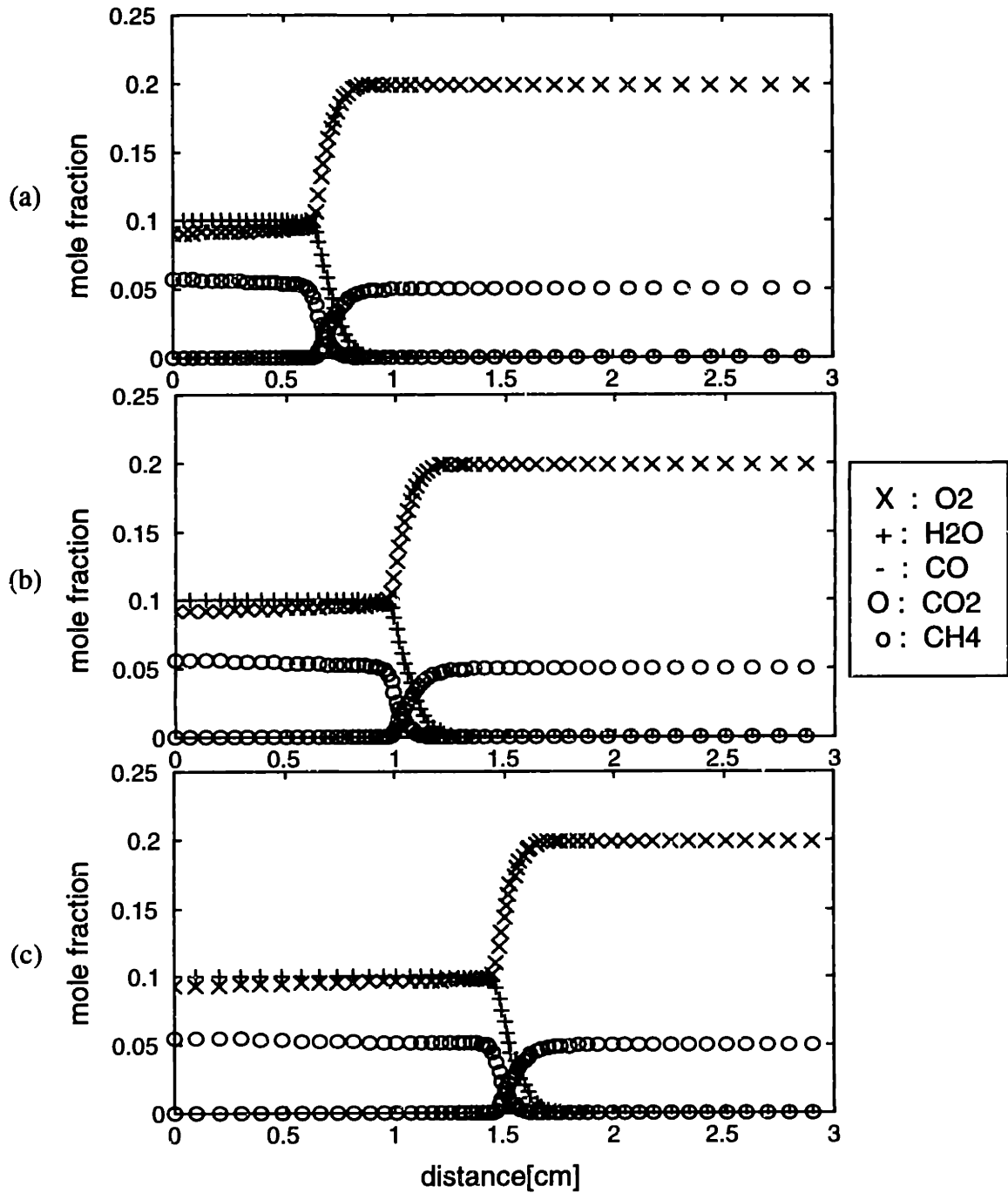


Fig. 4.24 Dynamic profiles of the mole fraction of major species in homogeneous charge burning. Equivalence ratio:  $\phi_{hg}=0.5$ . At lapsed time (a) 25 ms, (b) 50 ms, (c) 100 ms.

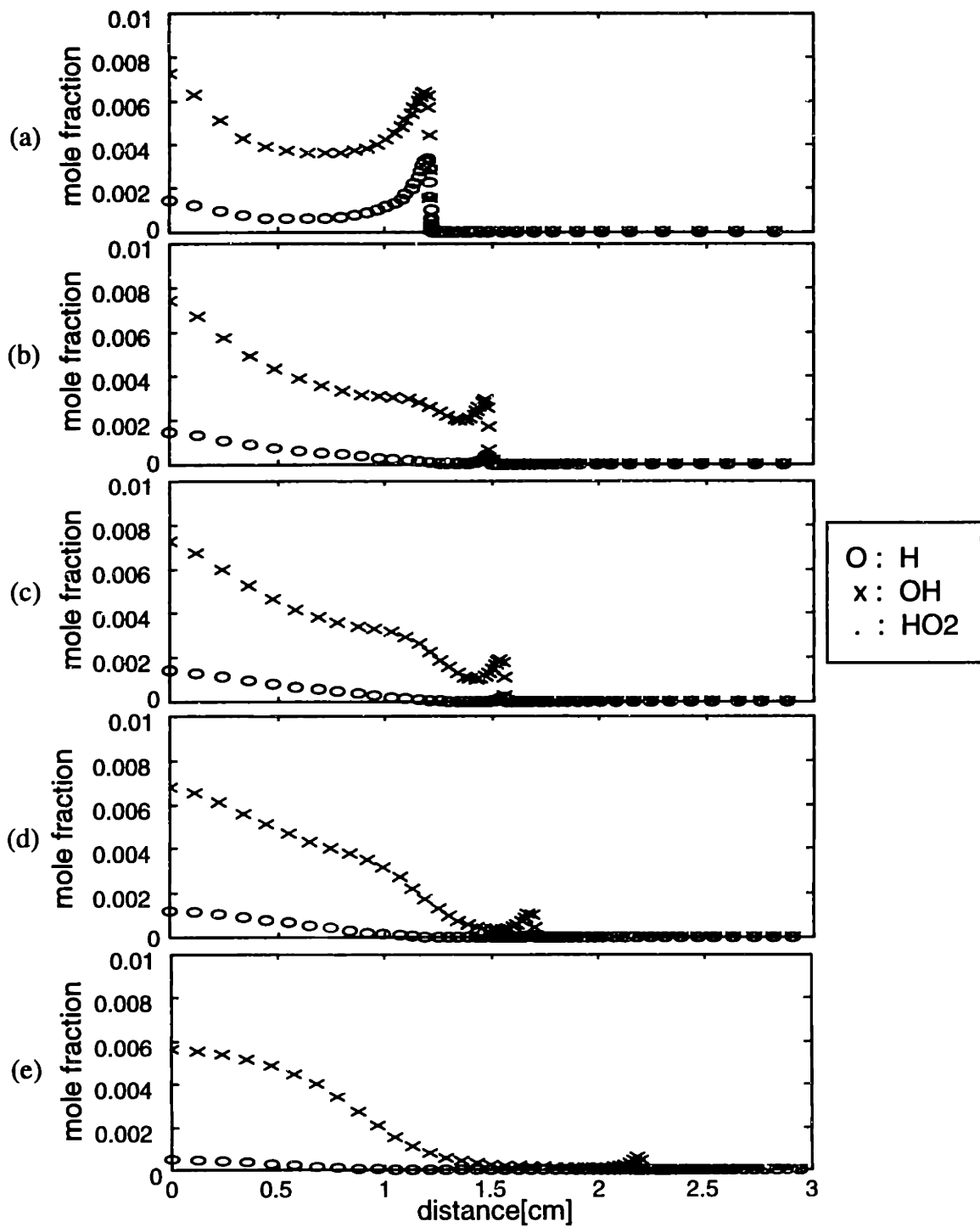


Fig. 4.25 Dynamic profiles of radical mole fraction in stratified charge burning. Equivalence ratio:  $\phi_1=1.0$ ,  $\phi_2=0.5$ . At lapsed time (a) 5 ms, (b) 8 ms, (c) 10 ms, (d) 20 ms, (e) 100 ms.



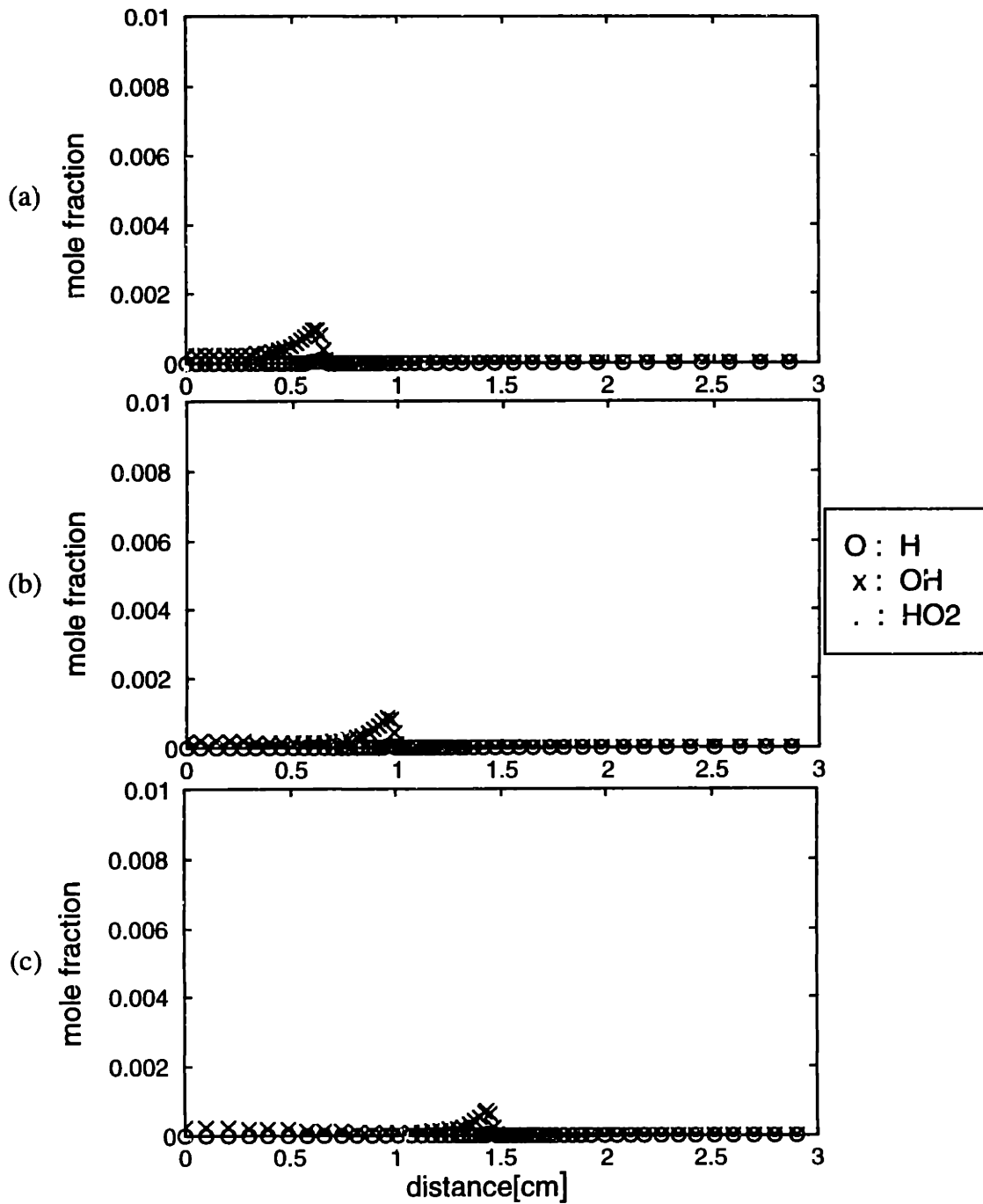
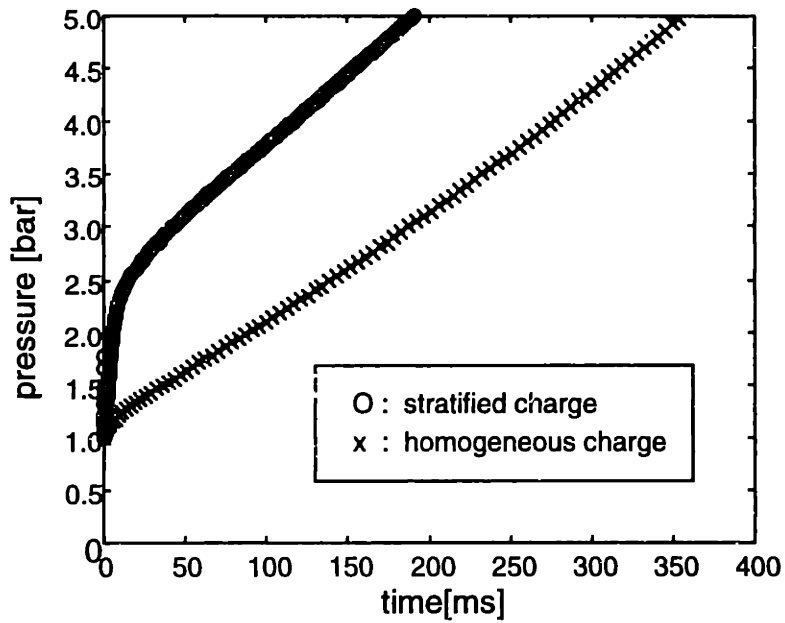
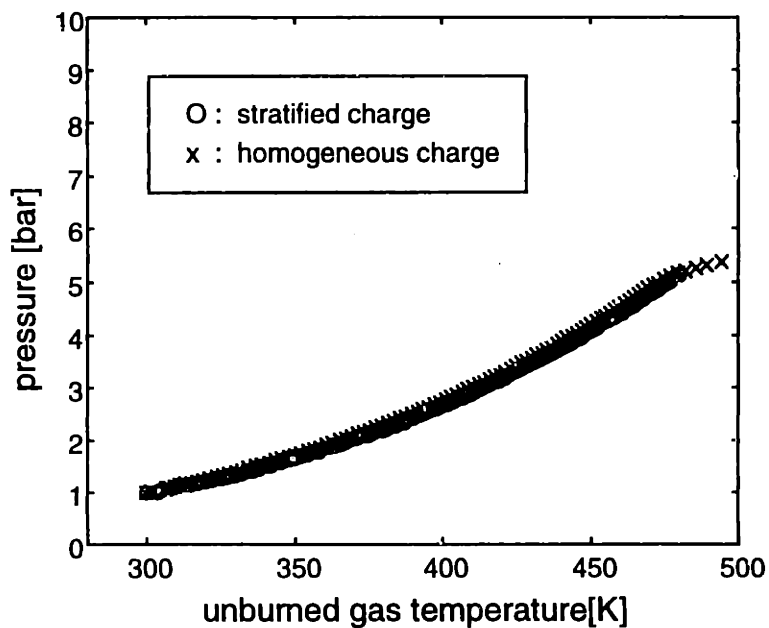


Fig. 4.26 Dynamic profiles of radical mole fraction in homogeneous charge burning. Equivalence ratio:  $\phi_{hg}=0.5$ . At lapsed time (a) 25 ms, (b) 50 ms, (c) 100 ms.



(a)



(b)

Fig. 4.27 Comparison of pressure profiles between stratified case and homogeneous case. Equivalence ratio: stratified charge;  $\phi_1=1.0$ ,  $\phi_2=0.5$ , homogeneous charge;  $\phi_{hg}=0.5$ . (a) pressure w.r.t. time (b) pressure w.r.t. unburned gas temperature.

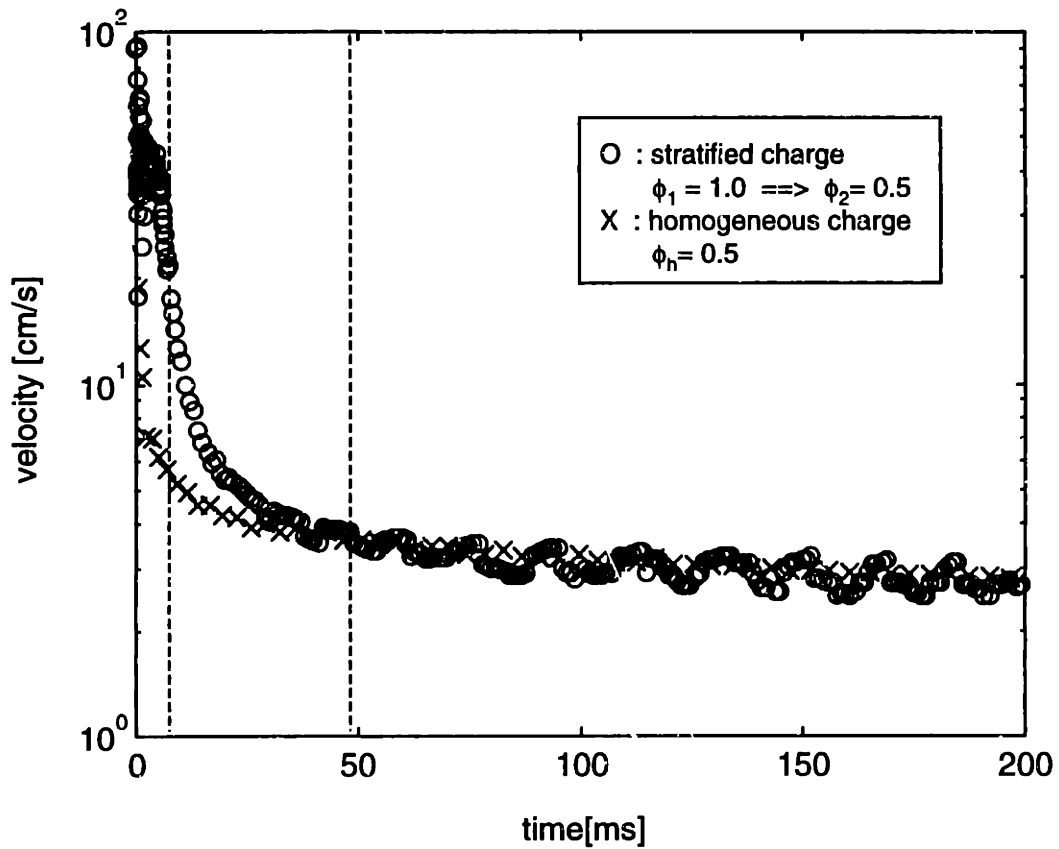


Fig. 4.28 Comparison of burning velocity between stratified and homogeneous charge cases. Plot of evolution with respect to time. Equivalence ratio: stratified charge:  $\phi_1=1.0$ ,  $\phi_2=0.5$ , homogeneous charge:  $\phi_{hg}=0.5$ . The left dotted line marks the point where the burned mass in the stratified case is equal to the mass of the stoichiometric mixture and the right dotted line marks the point where the burning velocities of the two profiles are approximately equal.

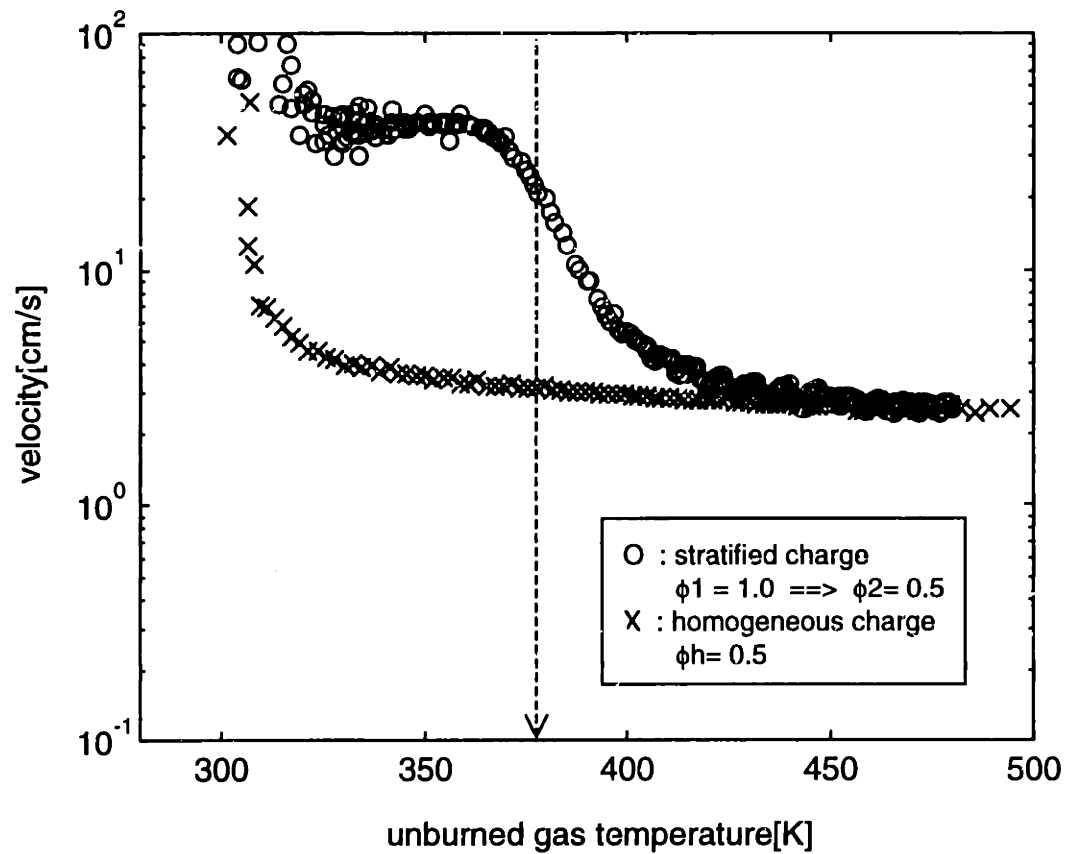


Fig. 4.29 Comparison of burning velocity between stratified and homogeneous charge cases. Plot of evolution with respect to unburned gas temperature. Equivalence ratio: stratified charge:  $\phi_1=1.0, \phi_2=0.5$ , homogeneous charge:  $\phi_{hg}=0.5$ . The dotted line marks the point at which the burned mass in the stratified case is equal to the mass of the stoichiometric mixture.

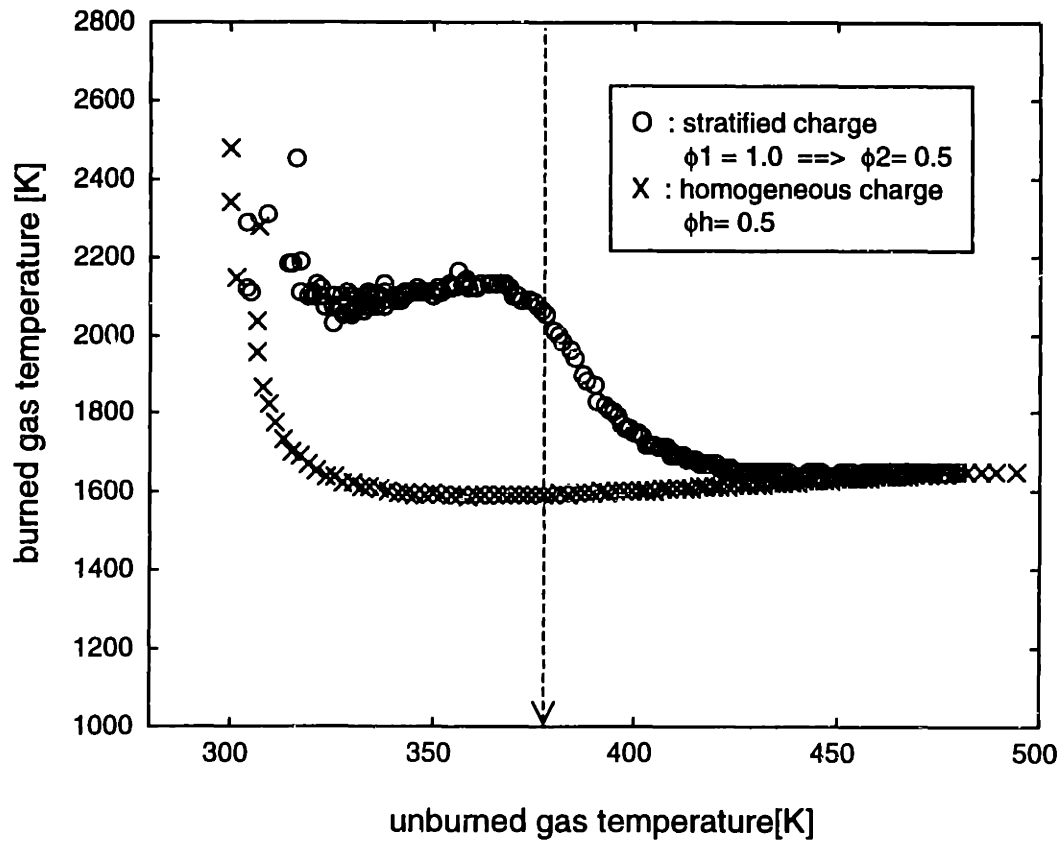


Fig. 4.30 Comparison of burned gas temperature between stratified and homogeneous charge cases. Plot of evolution with respect to unburned gas temperature. Equivalence ratio: stratified charge:  $\phi_1=1.0$ ,  $\phi_2=0.5$ , homogeneous charge:  $\phi_{hg}=0.5$ . The dotted line marks the point at which the burned mass in the stratified case is equal to the mass of the stoichiometric mixture.

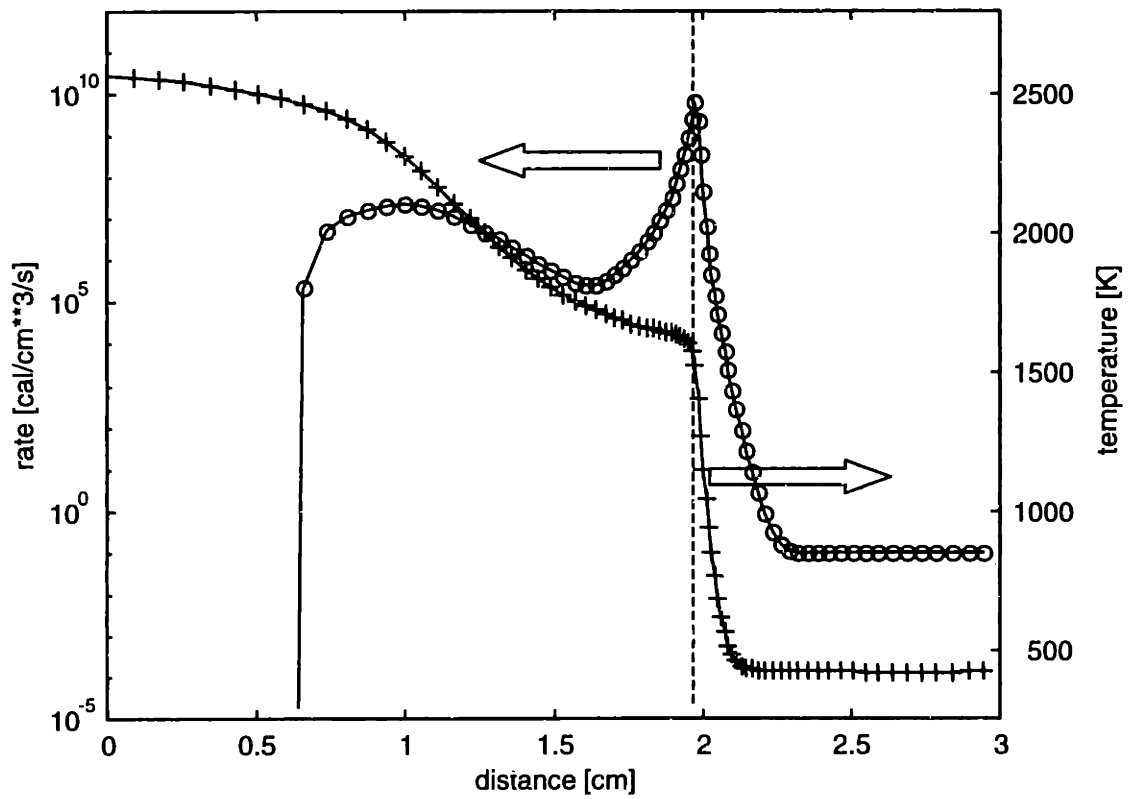
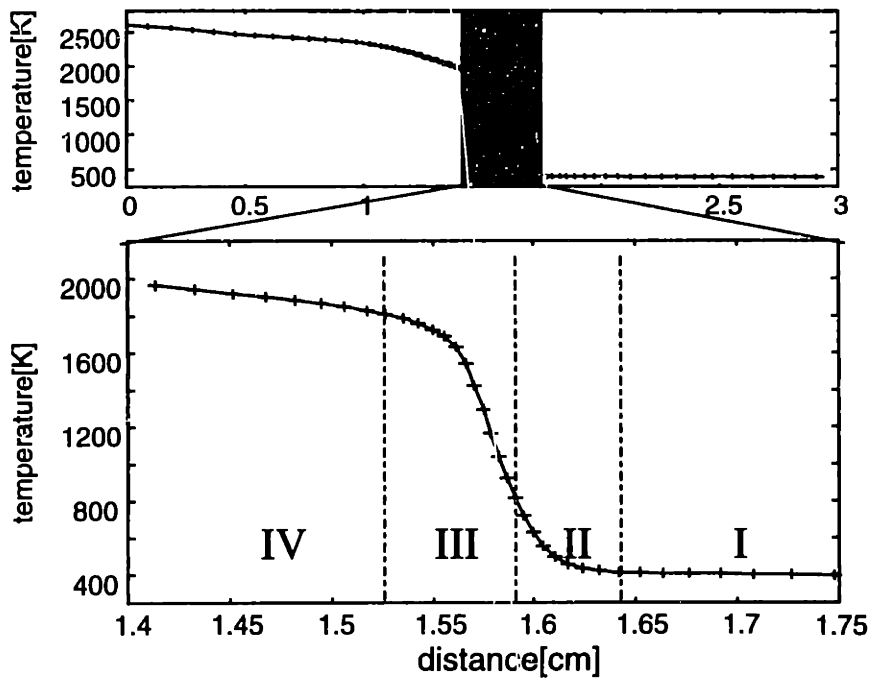
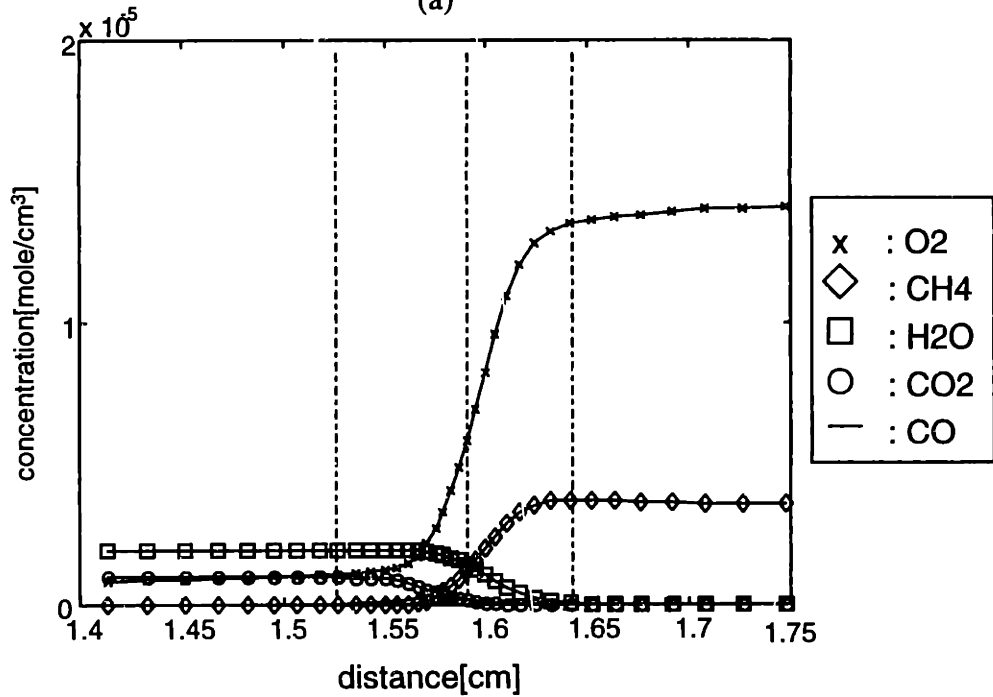


Fig. 4.31 Profile of the rate of chemical energy production in stratified charge burning. Gas temperature profile is plotted for comparison. Equivalence ratio:  $\phi_1=1.0$ ,  $\phi_2=0.5$ , at time 50 ms.



(a)



(b)

Fig. 4.32 Reaction characteristics of major species in stratified charge burning. At time = 10 ms, unburned gas temperature = 387 K, equivalence ratio:  $\phi_1=1.0$ ,  $\phi_2=0.5$ . (a) distinction of flame zone, (b) concentration of species.

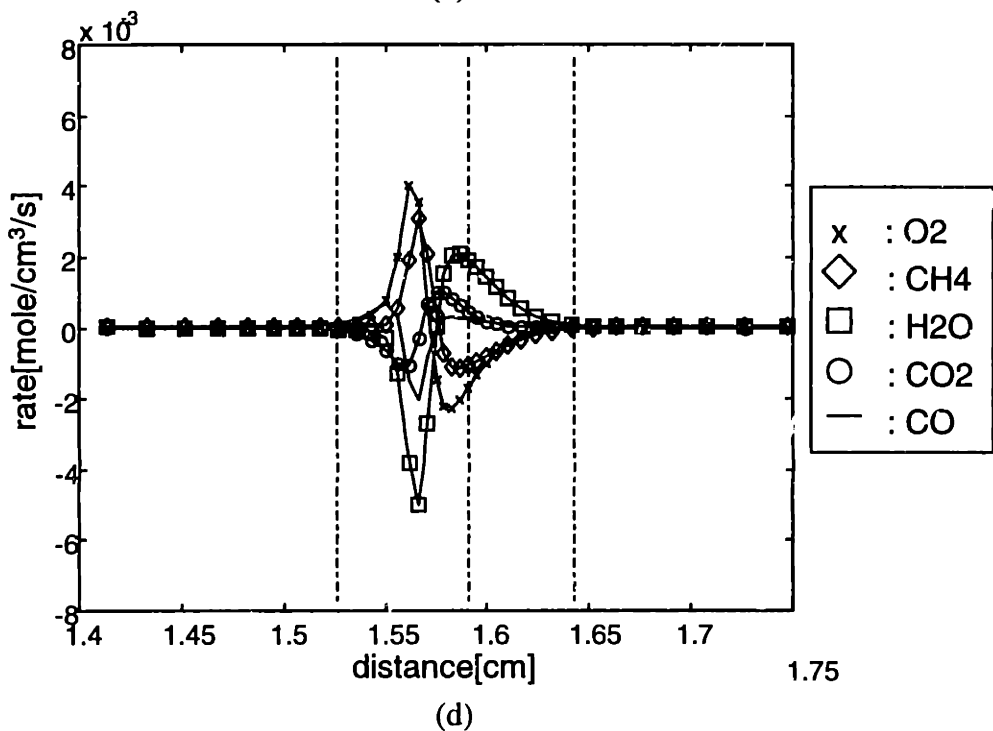
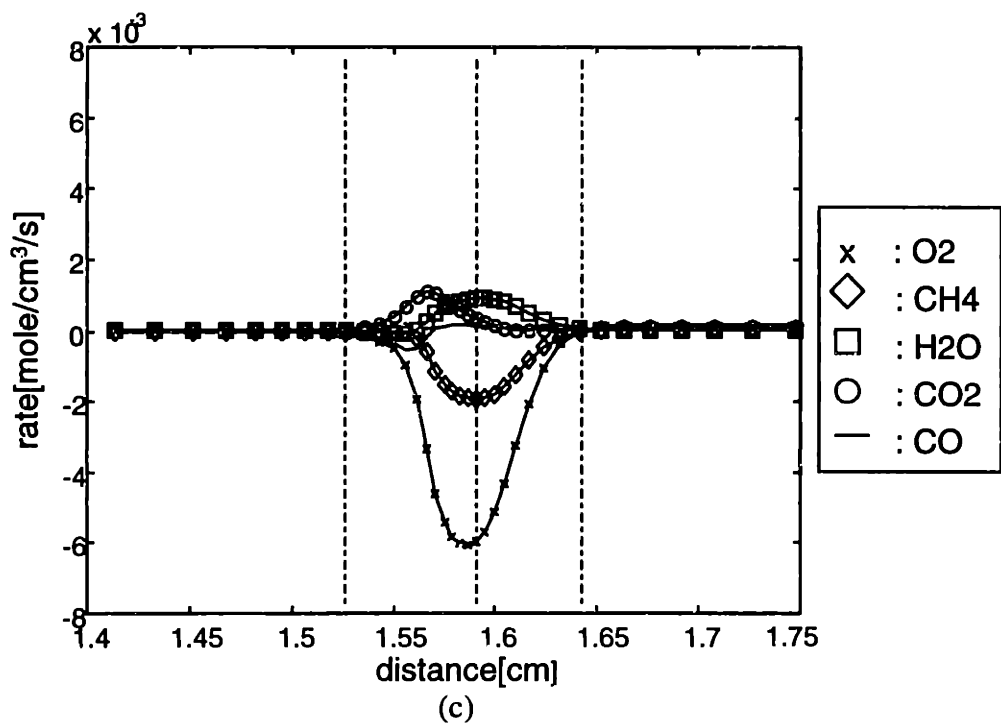
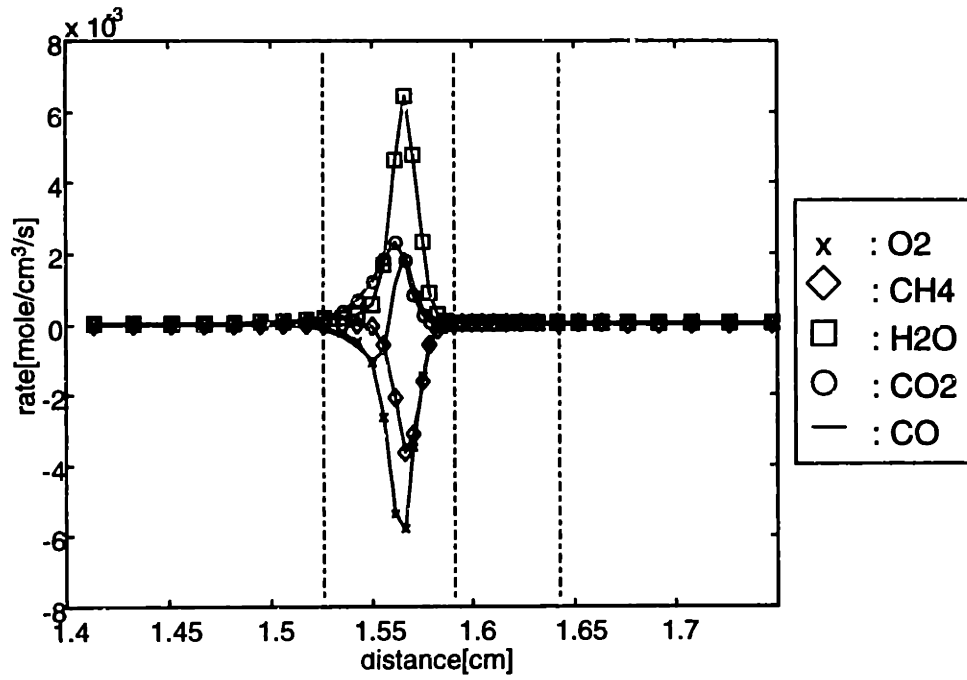
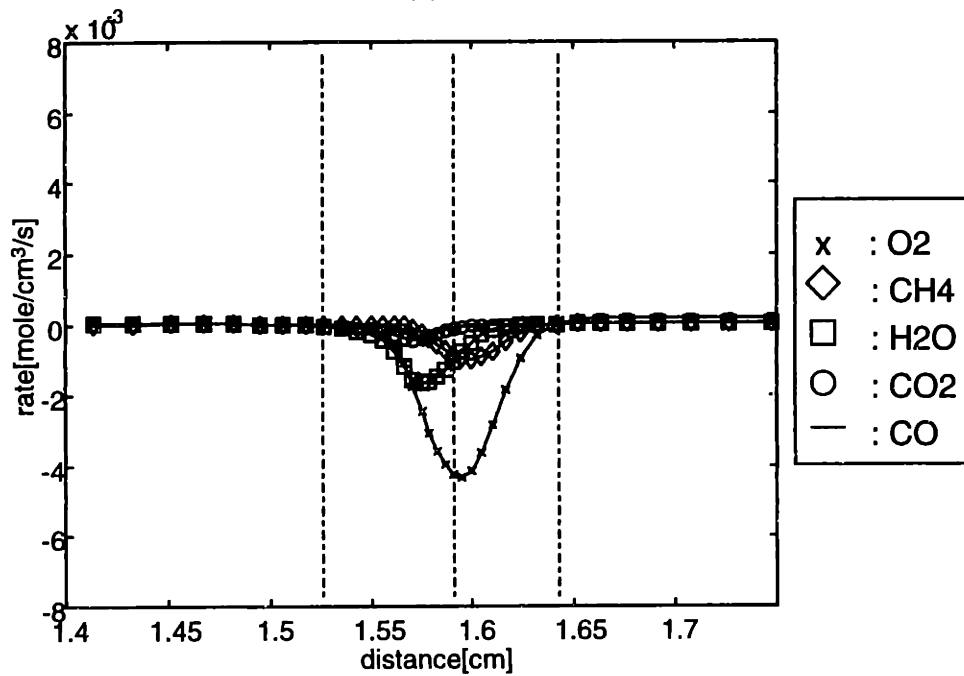


Fig. 4.32 Reaction characteristics of major species in stratified charge burning(continued). At time =10 ms, unburned gas temperature = 387 K, equivalence ratio:  $\phi_1=1.0$ ,  $\phi_2=0.5$ . (c) net rate of change, (d) rate of change by diffusion.



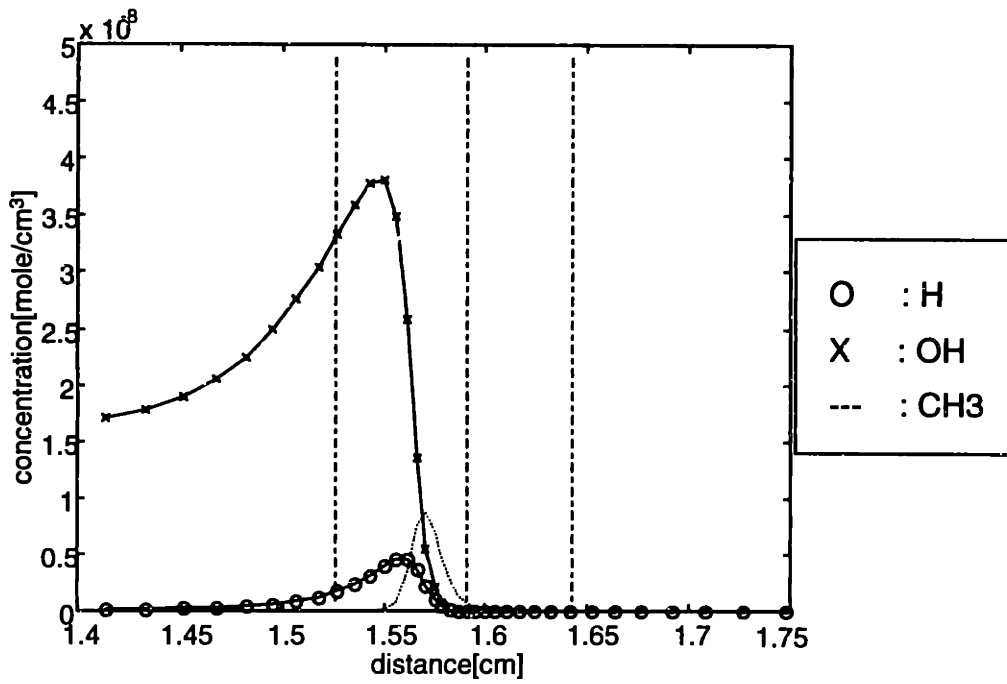


(e)

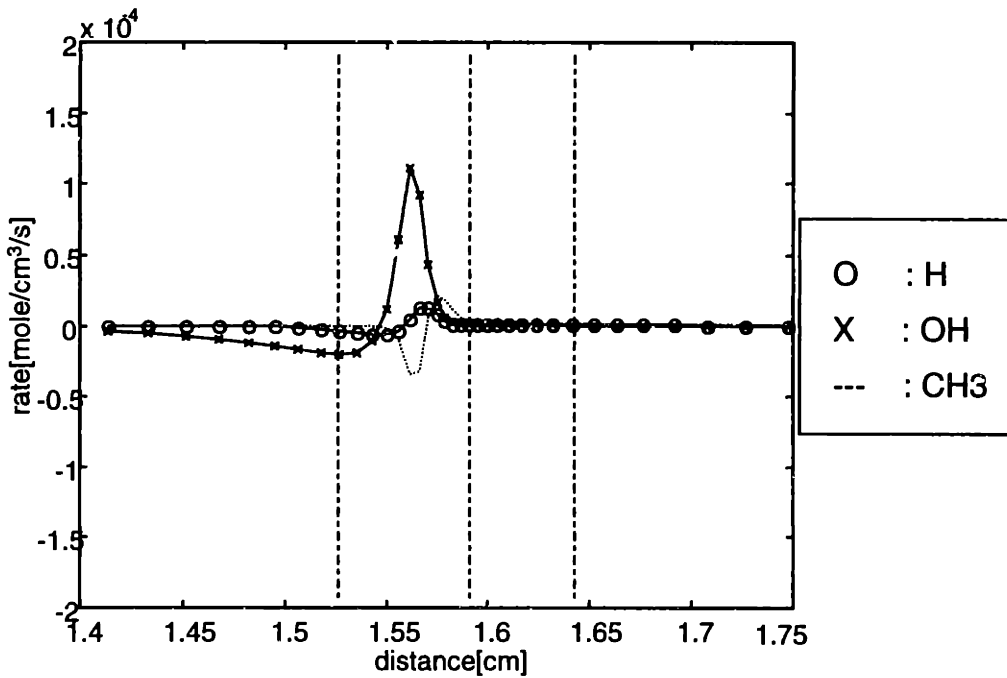


(f)

Fig. 4.32 Reaction characteristics of major species in stratified charge burning(continued). At time =10 ms, unburned gas temperature = 387 K, equivalence ratio:  $\phi_1=1.0$ ,  $\phi_2=0.5$ . (e) rate of change by chemical reaction, (f) rate of change by hydrodynamics.



(a)



(b)

Fig. 4.33 Reaction characteristics of radicals in stratified charge burning. At time = 10 ms, unburned gas temperature = 387 K, equivalence ratio:  $\phi_1=1.0$ ,  $\phi_2=0.5$ . (a) concentration of species, (b) net rate of change.

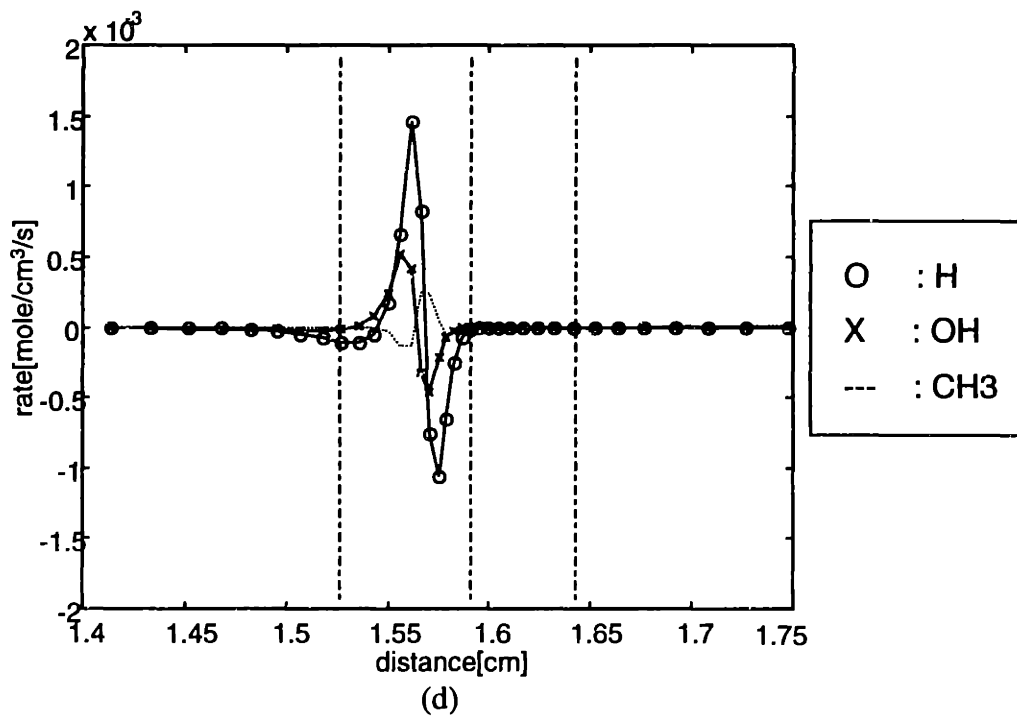
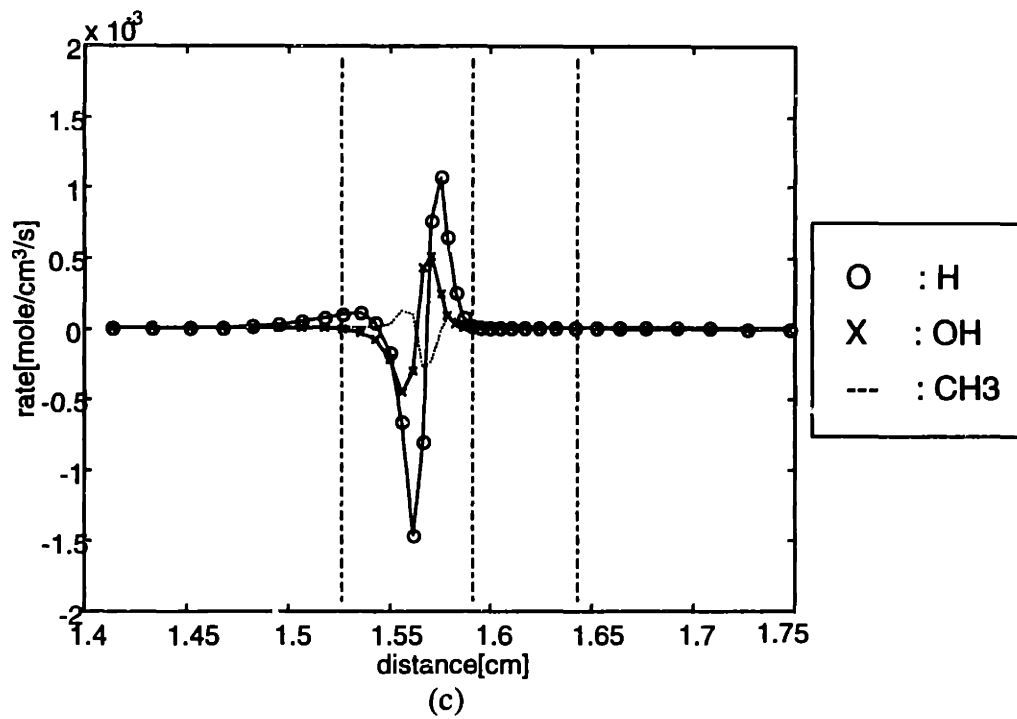


Fig. 4.33 Reaction characteristics of radicals in stratified charge burning (continued). At time=10 ms, unburned gas temperature = 387 K, equivalence ratio:  $\phi_1=1.0$ ,  $\phi_2=0.5$ . (c) rate of change by diffusion, (d) rate of change by chemical reaction.

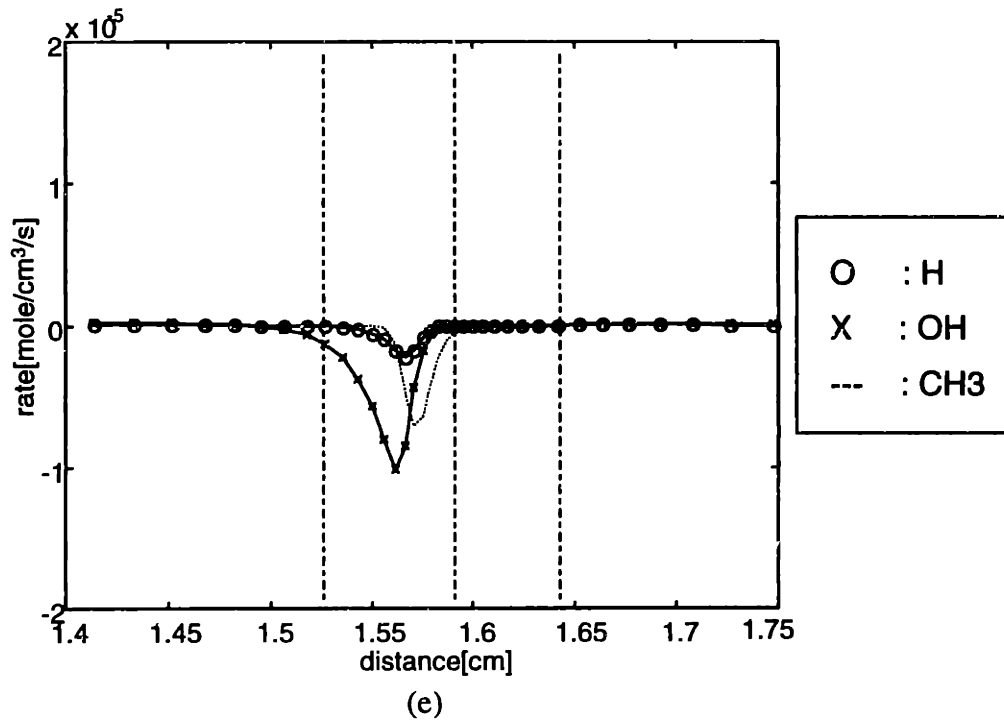
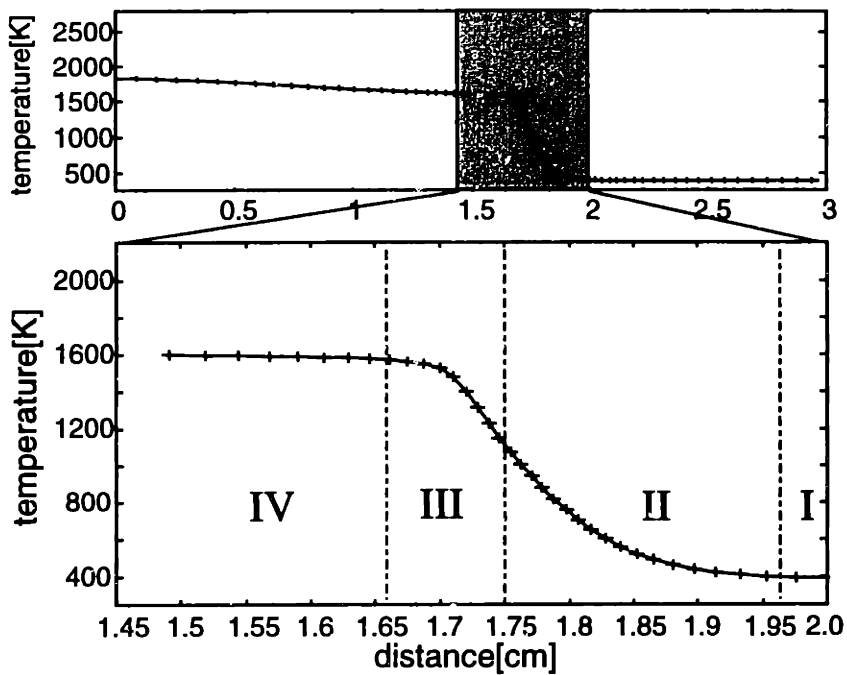
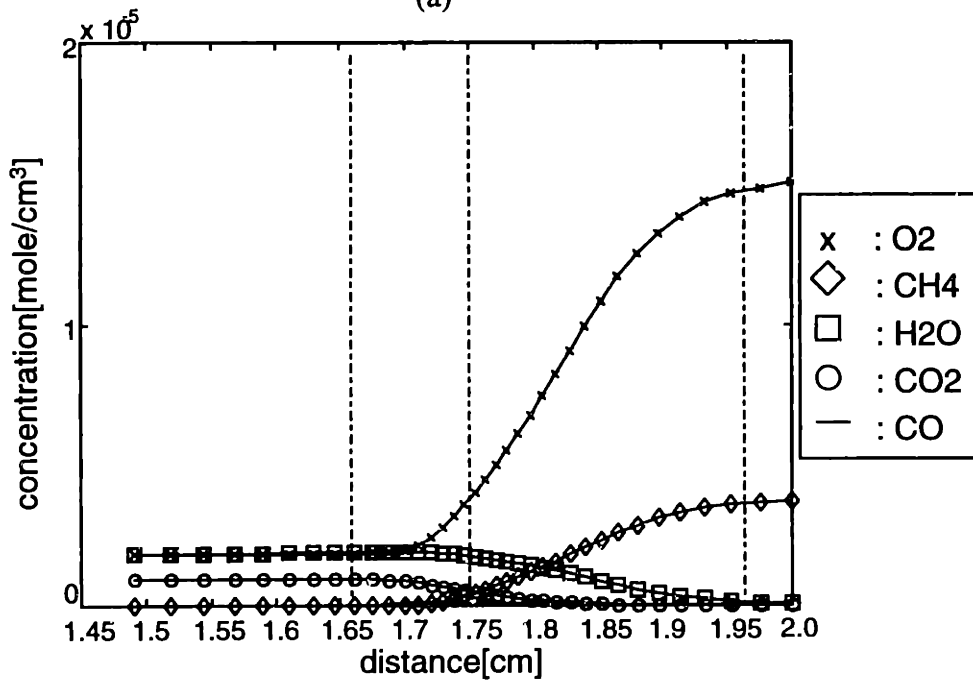


Fig. 4.33 Reaction characteristics of radicals in stratified charge burning (continued). At time=10 ms, unburned gas temperature = 387 K, equivalence ratio:  $\phi_1=1.0$ ,  $\phi_2=0.5$ . (e) rate of change by hydrodynamics.

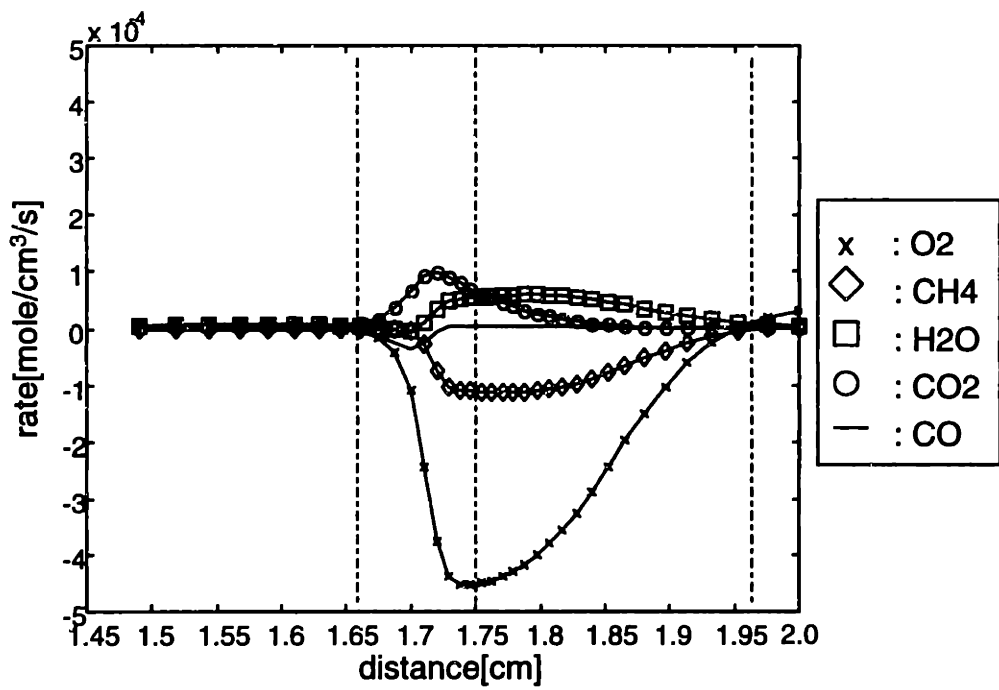


(a)

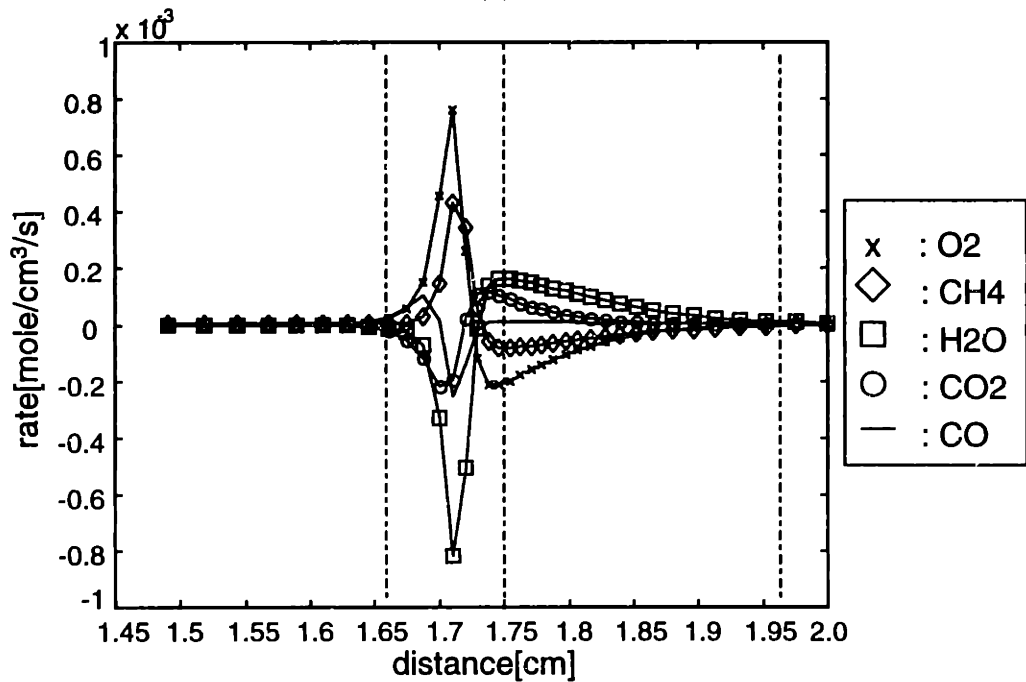


(b)

Fig. 4.34 Reaction characteristics of major species in homogeneous charge burning. At time=134 ms, unburned gas temperature = 387 K, equivalence ratio:  $\phi=0.5$ . (a) distinction of flame zone, (b) concentration of species.

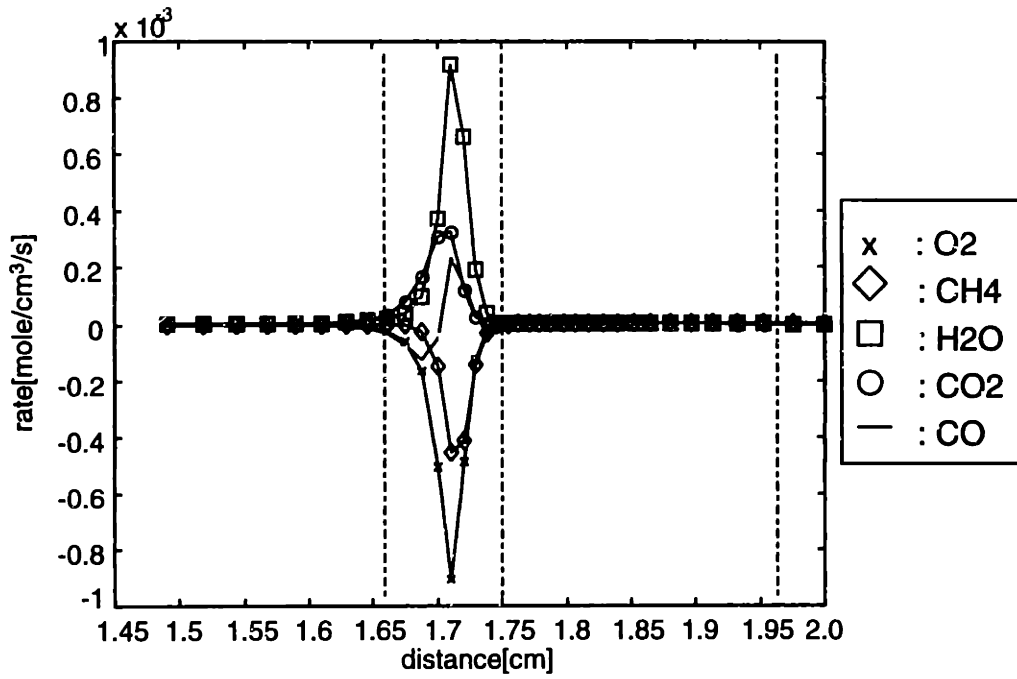


(c)

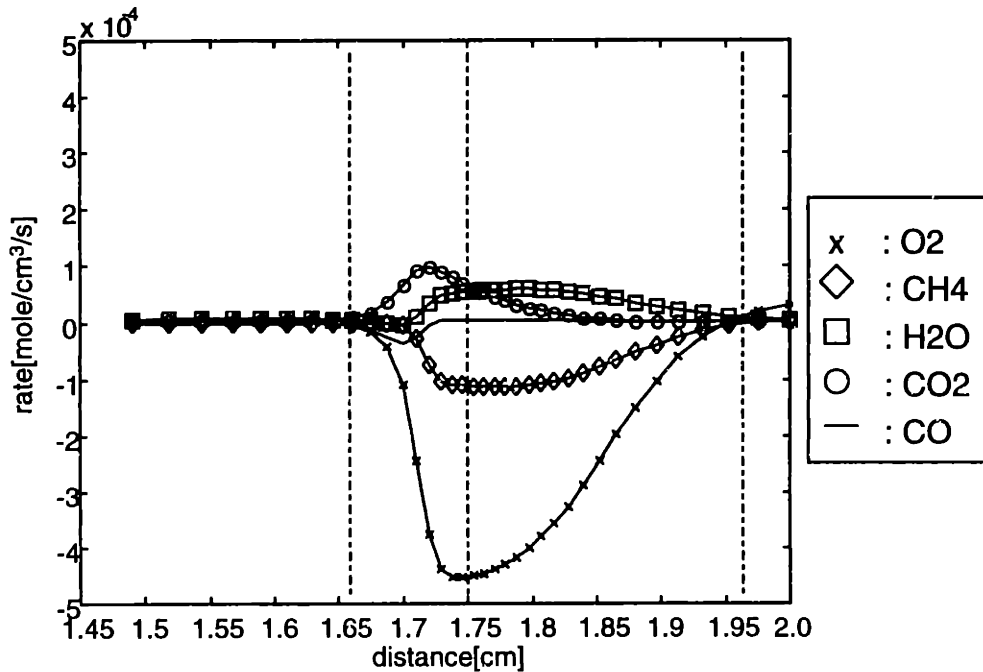


(d)

Fig. 4.34 Reaction characteristics of major species in homogeneous charge burning(continued). At time=134 ms, unburned gas temperature = 387 K, equivalence ratio:  $\phi=0.5$ . (c) net rate of change, (d) rate of change by diffusion.

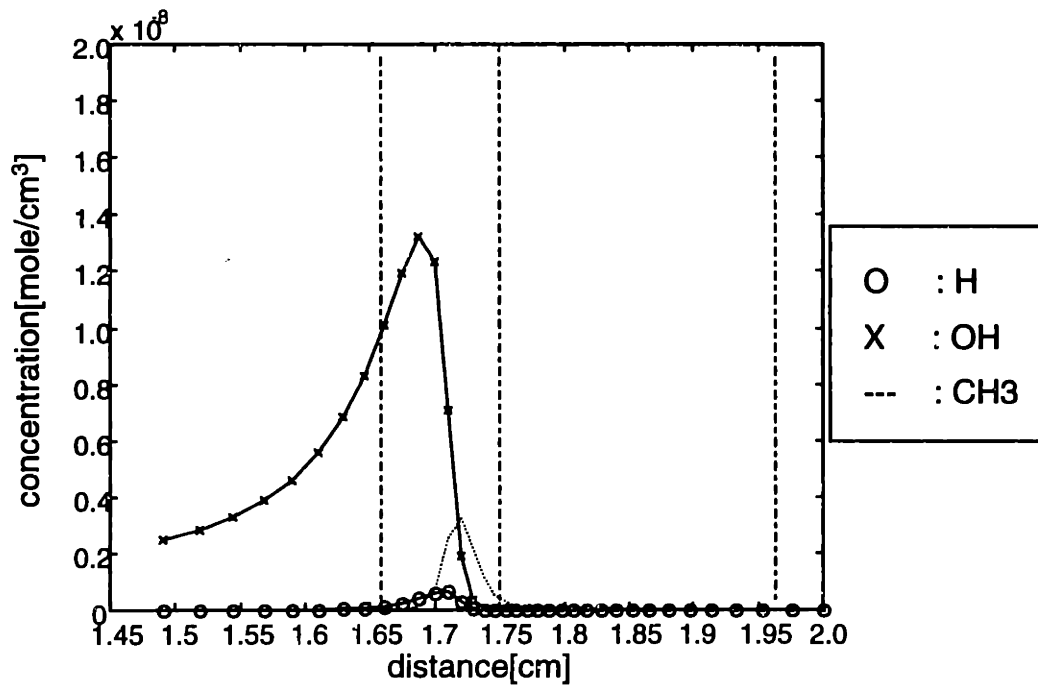


(e)

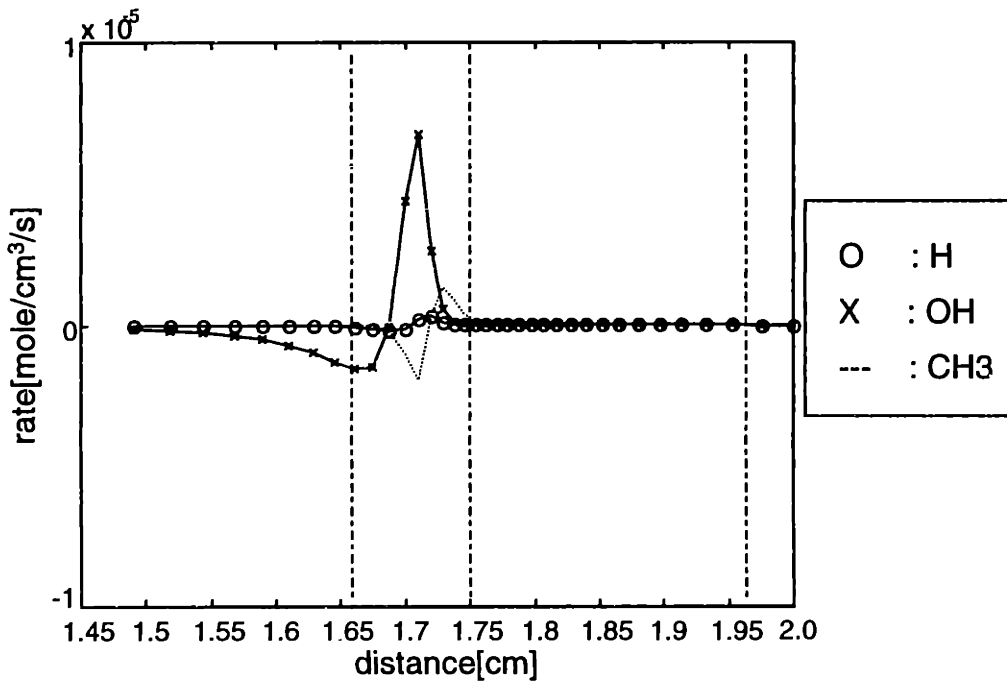


(f)

Fig. 4.34 Reaction characteristics of major species in homogeneous charge burning(continued). At time=134 ms, unburned gas temperature = 387 K, equivalence ratio:  $\phi=0.5$ . (e) rate of change by chemical reaction, (f) rate of change by hydrodynamics.



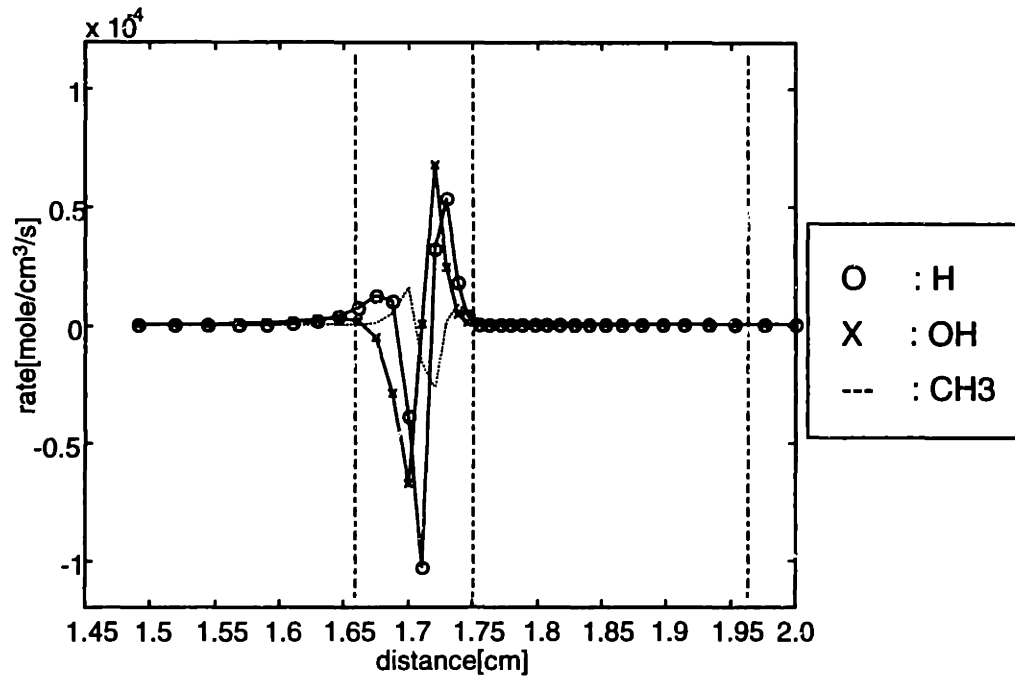
(a)



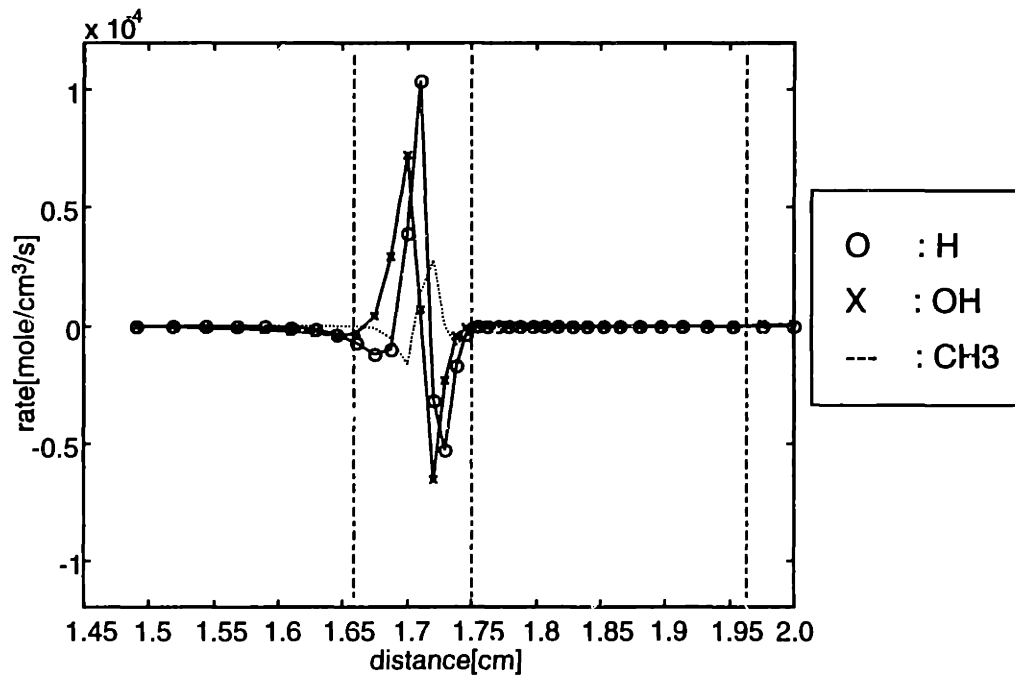
(b)

Fig. 4.35 Reaction characteristics of radicals in homogeneous charge burning. At time=134 ms, unburned gas temperature = 387 K, equivalence ratio:  $\phi=0.5$ . (a) concentration of species, (b) net rate of change.



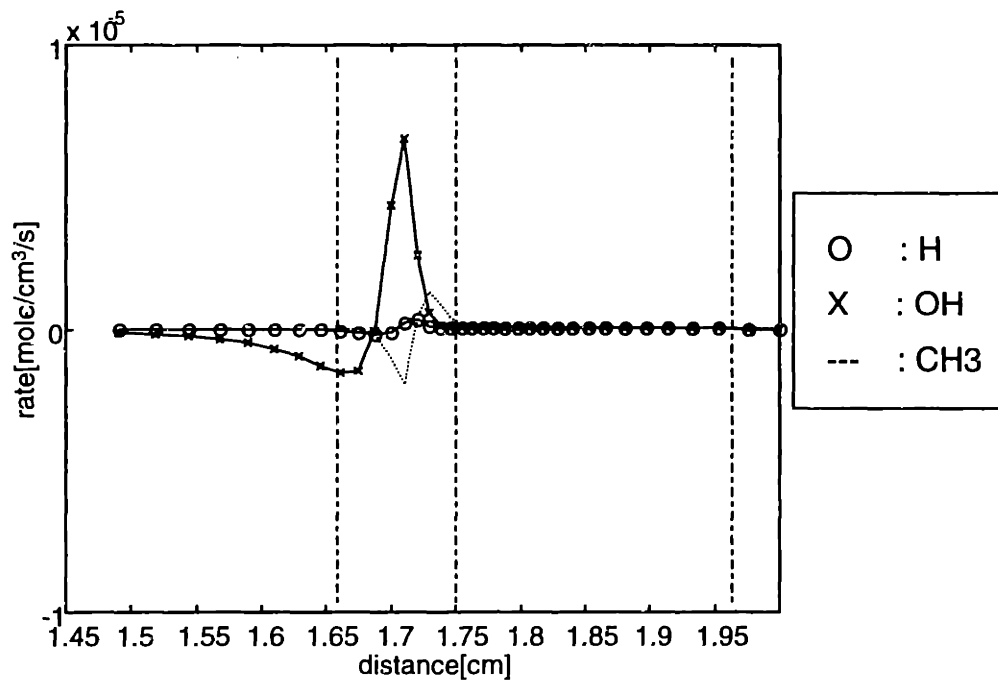


(c)



(d)

Fig. 4.35. Reaction characteristics of radicals in homogeneous charge burning (continued). At time=134 ms, unburned gas temperature = 387 K, equivalence ratio:  $\phi=0.5$ . (c) rate of change by diffusion, (d) rate of change by chemical reaction.



(e)

Fig. 4.35. Reaction characteristics of radicals in homogeneous charge burning (continued). At time=134 ms, unburned gas temperature = 387 K, equivalence ratio:  $\phi=0.5$ . (e) rate of change by hydrodynamics.

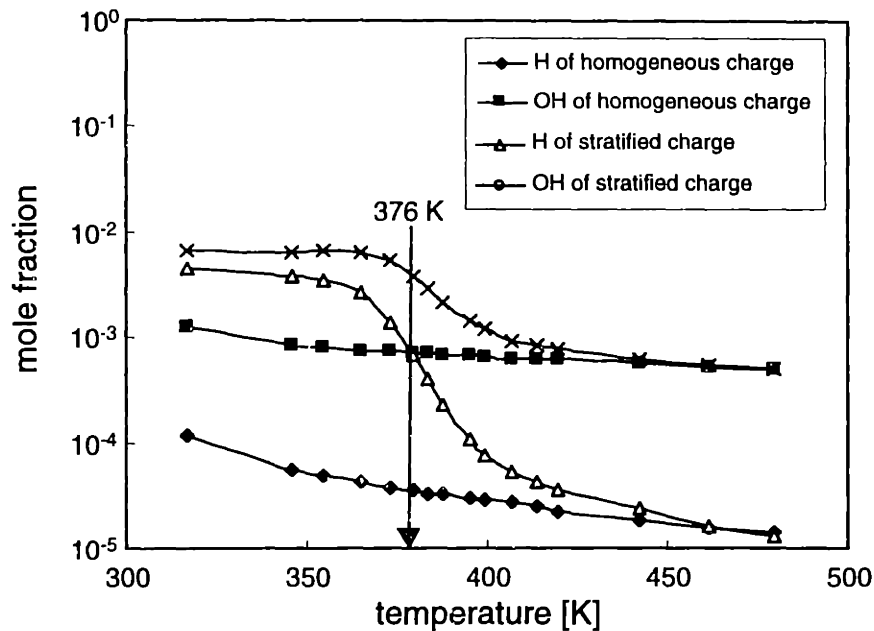


Fig. 4.36 Comparison of peak radical mole fraction at flame zone w.r.t unburned gas temperature between stratified case and homogeneous case. Equivalence ratio: stratified charge:  $\phi_1=1.0$ ,  $\phi_2=0.5$ , homogeneous charge:  $\phi_{hg}=0.5$ . The arrow marks the point at which the burned mass is equal to the mass of stoichiometric mixture.

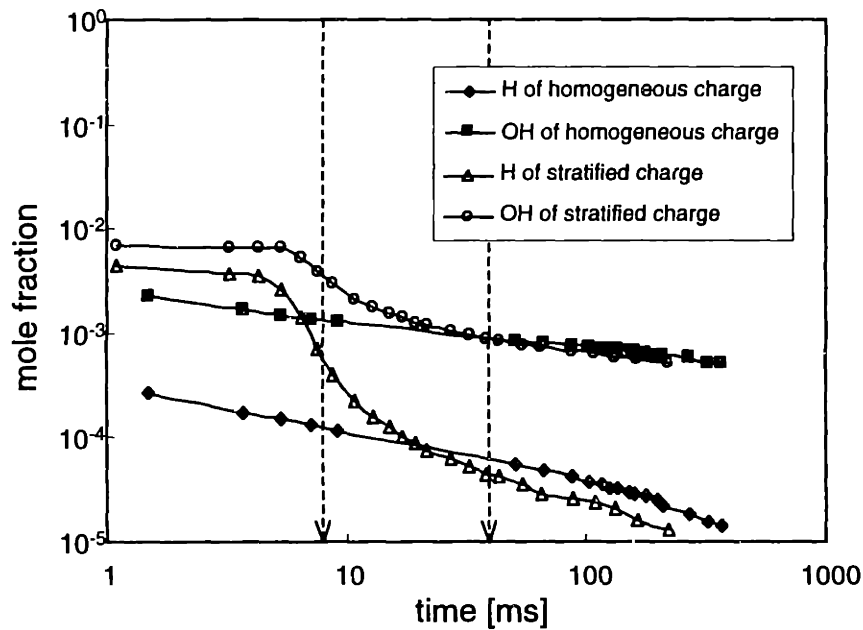


Fig. 4.37 Comparison of the evolution of peak mole fraction at flame zone between stratified case and homogeneous case. Equivalence ratio: stratified charge:  $\phi_1=1.0$ ,  $\phi_2=0.5$ , homogeneous charge:  $\phi_{hg}=0.5$ . The dotted arrows mark the points at which the burned mass is equal to the mass of stoichiometric mixture and the [OH] mole fractions of the two cases become equal, respectively.

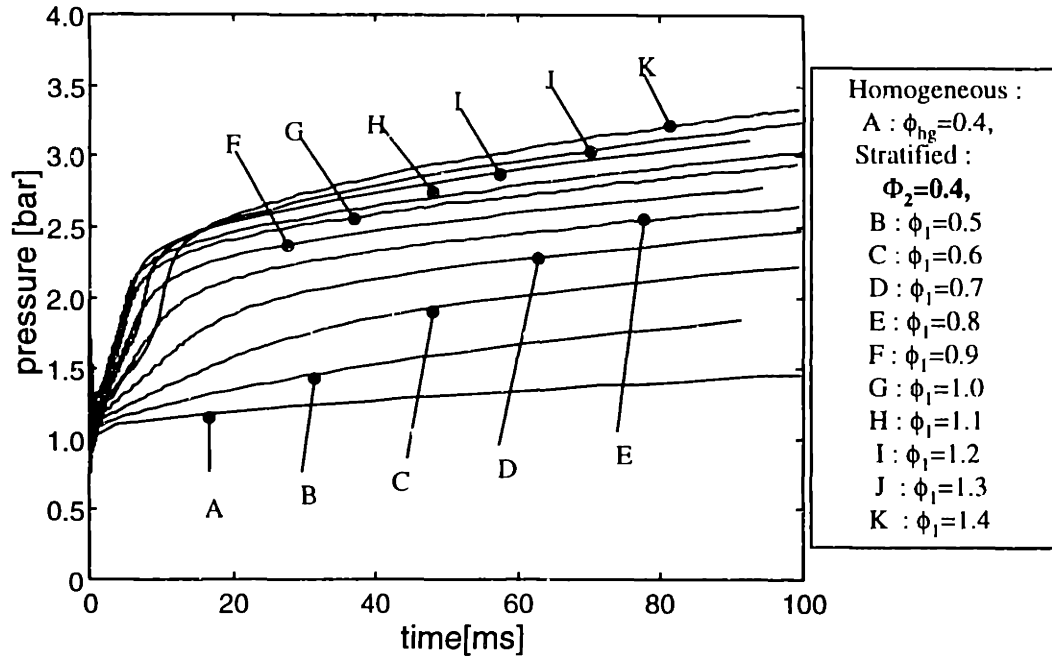


Fig. 4.38 Pressure trajectories of stratified charge burning with various rich mixtures (numerical simulation). Equivalence ratio:  $\phi_1=0.5\sim 1.4$ ,  $\phi_2=0.4$ ;  $\phi_{hg}=0.4$ .

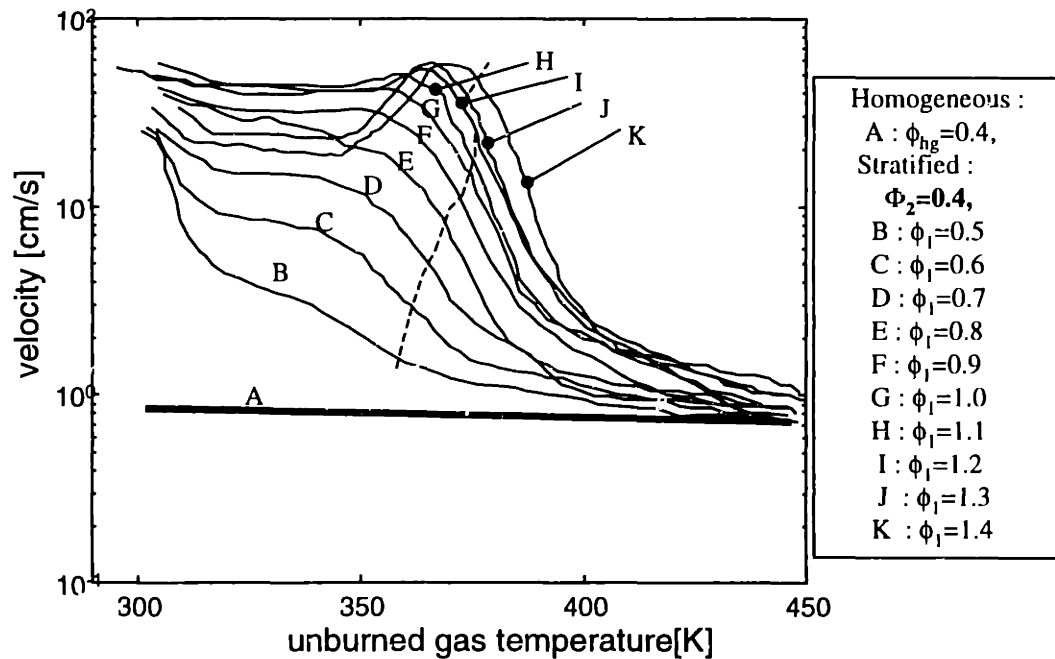


Fig. 4.39 Burning velocity profiles of stratified charge burning with various rich mixtures (numerical simulation). Equivalence ratio:  $\phi_1=0.5 \sim 1.4$ ,  $\phi_2=0.4$ ;  $\phi_{hg}=0.4$ . The dotted line marks the point at which the burned mass is equal to the mass of the rich mixture.

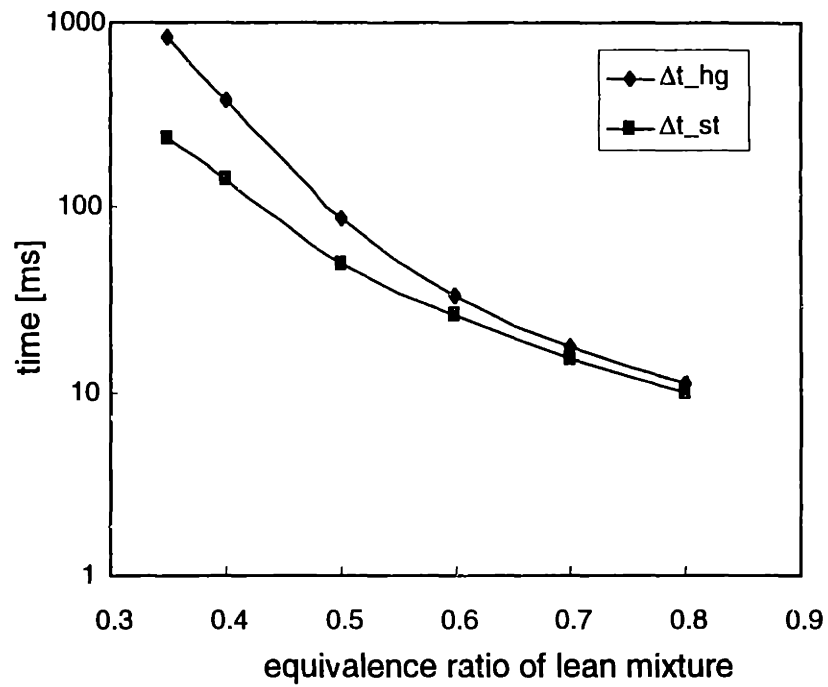


Fig. 4.40 Comparison of lapsed time of burning between stratified and homogeneous cases. Burned mass = 20 % of the initial mass of lean mixture. Equivalence ratio: stratified charge:  $\phi_1=1.0$ ,  $\phi_2=0.35 \sim 0.8$ , homogeneous charge:  $\phi_h=0.35 \sim 0.8$ .

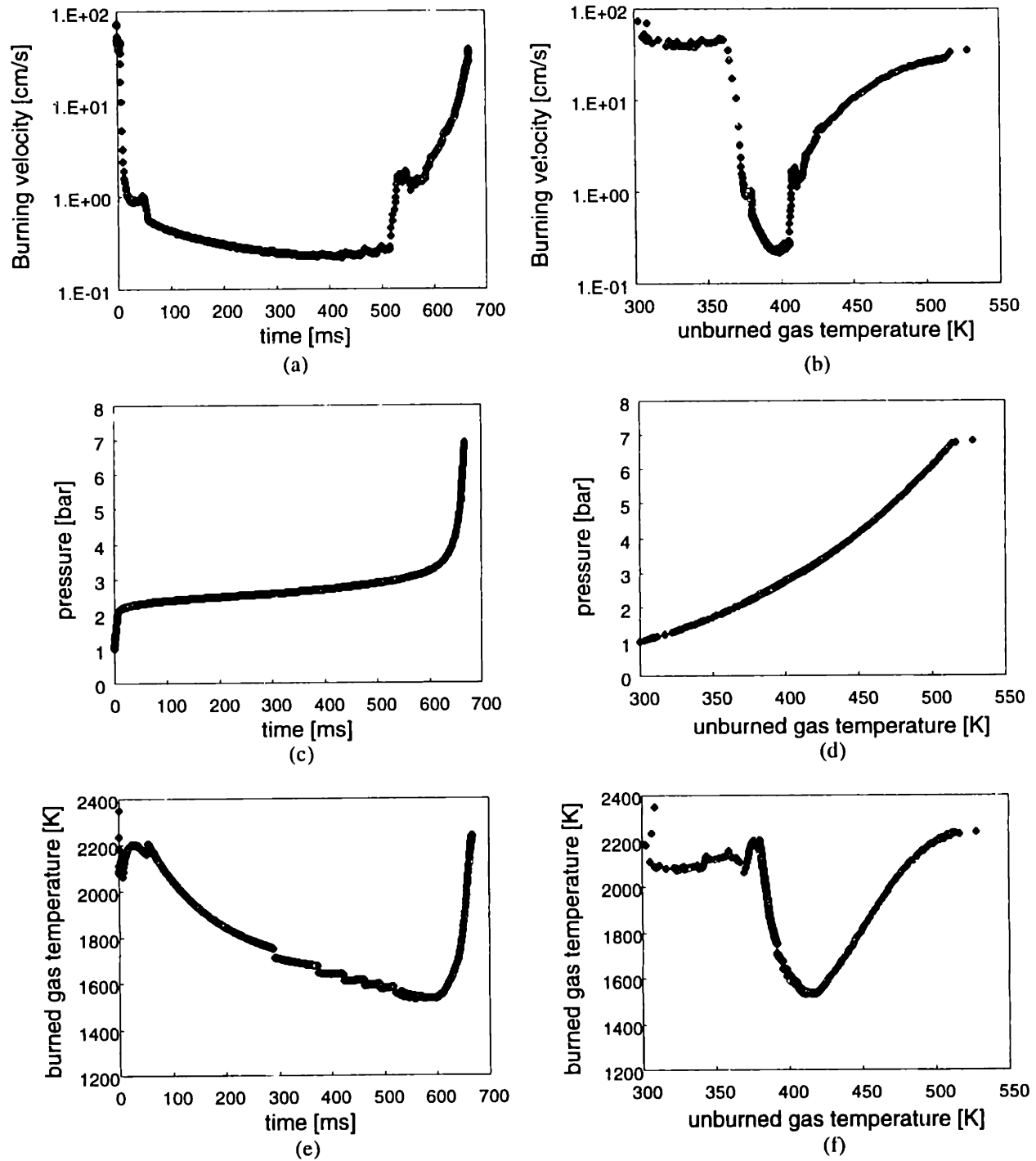


Fig. 4.41 Burning of lean pocket in stoichiometric mixture. The pocket starts 0.4 cm away from the left wall. Equivalence ratio of lean mixture = 0.1, Pocket width=1.2 cm. (a) burning velocity vs. time, (b) burning velocity vs. unburned gas temperature, (c) pressure vs. time, (d) pressure vs. unburned gas temperature, (e) burned gas temperature vs. time (f) burned gas temperature vs. unburned gas temperature.

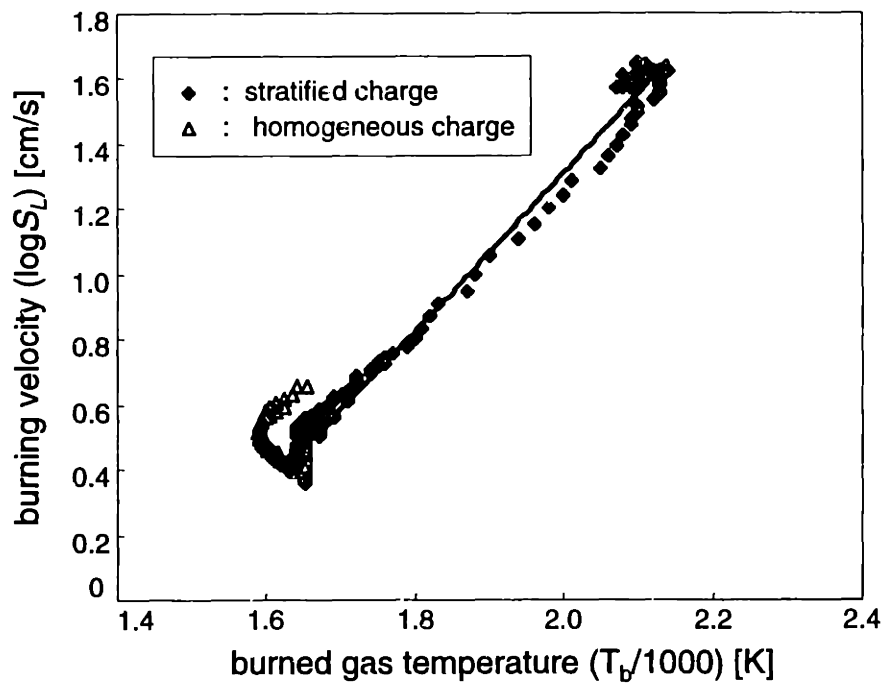


Fig. 4.42 Correlation of burning velocity with burned gas temperature for the burning of stratified charge burning. Equivalence ratio : rich mixture : stoichiometry, lean mixture: 0.5. Curve-fitted equation :  $\log(S_L) = 2.4149 T^* - 3.5161$ , where  $T^* = T_b/1000$ . The case of homogeneous mixture of  $\phi = 0.5$  is plotted for comparison.

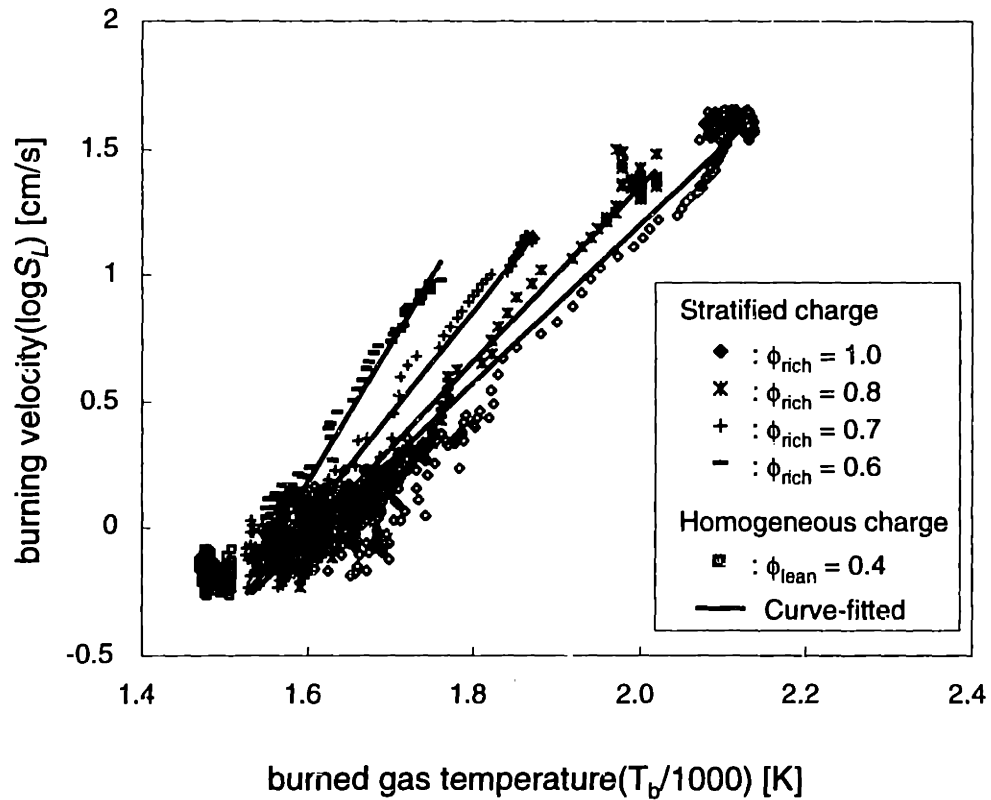


Fig. 4.43 Correlation of burning velocity with burned gas temperature for stratified charge burning. Equivalence ratio: rich mixture  $\phi_{rich}=0.6\sim 1.0$ , lean mixture  $\phi_{lean}=0.4$ . Data are curve-fitted with solid line. The plot of homogeneous burning case is included for comparison.